QUANTITATIVE APROACHES FOR ASSESSING GROUND MOTION IMPACT IN PERFORMANCE BASED EARTHQUAKE ENGINEERING

by

Peng Deng

A thesis submitted to the Faculty and the Board of Trustees of the Colorado School of Mines in partial fulfillment of the requirements for the degree of Doctor of Philosophy (Civil and Environmental Engineering).

Golden, Colorado

Date_____

Signed: _____

Peng Deng

Signed: _____

Dr. Shiling Pei
Thesis Advisor

Golden, Colorado

Date_____

Signed: _____

Dr. John McCray
Professor and
Department Head of Civil and Environmental Engineering

ABSTRACT

Over the past several decades, Performance Based Earthquake Engineering (PBEE) has evolved to become a major focus in earthquake engineering research. One of the most attractive features of this philosophy is the ability to account for response uncertainty in a more explicit manner. One of the cornerstones of modern PBEE is the ability to perform nonlinear time history analysis (NLTHA) on structural systems with the aid of fast computers. This advancement in tools made the use of incremental dynamic analysis (IDA) popular. Through IDA, curves describing the relationship between peak responses of structures and seismic intensity of earthquake ground motions can be obtained and can be used to derive uncertainty metrics of the seismic responses of interest. Many critical concepts in PBEE, such as fragility, response distribution, and seismic reliability, are linked heavily to IDA. As a result, the computation of most PBEE metrics must be done numerically (empirically) through NLTHA. The fundamental understanding of ground motion (GM) impact in PBEE is not clear.

In order to better understand the role of GMs in PBEE, an innovative approach was proposed in this study to quantify GM uncertainty and its impact on idealized structural system responses. The research work started at the quantification of IDA curves as a function of ground motion parameters, structural parameters and seismic intensity. This was done successfully for the elastoplastic single-degree-of-freedom (SDOF) system acceleration and then expanded to bilinear SDOF system displacement, which has direct implications for damage control in PBEE. The proposed formulas quantitatively illustrate (1) the changing of response uncertainty with seismic intensity; (2) the interaction of ground motion parameters and structural parameters on uncertainty propagation; (3) the relative contribution of ground motion uncertainty and structural parameter uncertainty with different seismic intensity. Additionally, the identified ground motion parameters in the uncertainty quantification framework can present the ground motion characteristics and then can be used to validate the ground motion

suite equivalency in the context of response uncertainty. The newly developed methodology challenges the existing simplified ways to calculate seismic uncertainty, such as the assumption of constant uncertainty contribution from GMs at different intensity levels. This was then tested through specially designed shake table tests that are focused on validating seismic uncertainty propagation. Through the probabilistic shake table tests, it was validated that the response uncertainty value is dependent on the seismic intensity, and the relative contribution of ground motion uncertainty and structural parameter uncertainty is closely correlated with seismic intensity. By using the experimental response data, square-root-sum-of-squares (SRSS) method used in many simplified uncertainty estimation procedures was verified to be not exact but conservative. Through collaboration with researchers at the US Geological Survey, the relationship between seismically induced structural damage and GM response spectrum was investigated. A vector-valued damage potential indicator (DPI) including seismic intensity and spectral shape component was proposed. Through correlation analyses, a circle rule was proposed to identify the most critical period regions of the response spectrum with regard to the bilinear SDOF system damage. This approach also provided a pathway to evaluate GM impact on structures without NLTHA.

TABLE OF CONTENTS

ABSTRACT……..……iii

LIST OF FIGURES……viii

LIST OF TABLES……xi

LIST OF SYMBOLS……...xii

LIST OF GLOSSARY……xiii

ACKNOWLEDGEMENTS……xiv

CHAPTER 1 INTRODUCTION……1

1.1 Background…….……1

1.2 Objectives of the Research……...5

1.3 Organization of Thesis……6

CHAPTER 2 UNCERTAINTY QUANTIFICATION ON ELASTOPLASTIC SDOF SYSTEM ACCELERATION……...9

2.1 Abstract……9

2.2 Introduction……..9

2.3 Multi-record Incremental Dynamic Analysis……12

2.4 Quantify GM-induced Uncertainty for Linear Systems……16

2.5 Quantify GM-induced Uncertainty for Elastoplastic SDOF System Acceleration……19

2.6 Validation of the GM-induced Uncertainty Propagation Characterization…28

2.7 Summary and Conclusions……32

CHAPTER 3 UNCERTAINTY QUANTIFICATION ON BILINEAR SDOF SYSTEM DISPLACEMENT……..33

3.1 Abstract……..33

3.2 Introduction……33

3.3 Methodology……..36

3.4 Bilinear SDOF System Characterizations……...37

3.5 Ground Motion Characterizations……..38

3.6 Modeling IDA Curves for Bilinear SDOF Systems……...39

3.7 Model Validation……49

3.8 PBEE Applications…….53

3.9 Summary and Conclusions…….55

CHAPTER 4 EXPERIMENTAL STUDY OF UNCERTAINTY PROPAGATION THROUGH SHAKE TABLE TESTS……...……57

4.1 Abstract……..57

4.2 Introduction……57

4.3 Probabilistic Shake Table Test Concept……60

4.4 Test Specimens……...61

4.5 Test Program……..62

4.6 Observed Uncertainty Propagation Characteristics……65

4.7 SRSS Method…….71

4.8 Summary and Conclusions…….73

CHAPTER 5 STRUCTURAL DAMAGE PREDICTION THROUGH SPECTRUM BASED DAMAGE POTENTIAL INDICATOR……..75

5.1 Abstract……..75

5.2 Introduction……75

5.3 Existing Study on Response Spectrum Based Damage Potential Indicator...77

5.4 A Vector-valued Damage Potential Indicator……79

5.5 Response Spectrum Similarity Index…….81

5.6 Bilinear SDOF Systems……..82

5.7 Earthquake Ground Motion Characteristics……...84

5.8 Maximizing Damage Correlations for Bilinear SDOF Systems……85

5.9 Numerical Validation…….92

5.10 Summary and Conclusions……..……...94

CHAPTER 6 CONCLUSIONS AND FUTURE WORK……95

6.1 Major Observations and Conclusion……..95

6.2 Future Work……...97

REFERENCE……...99

LIST OF FIGURES

Figure 1.1 Conceptual component of general PBEE……1

Figure 1.2 Qualitative inclusion of modeling uncertainty (FEMA P695)……....4

Figure 2.1 Flowchart for the framework of the proposed analyses……...…...12

Figure 2.2 Example IDA curves of a linear system and an elastoplastic SDOF system.….14

Figure 2.3 Examples of (a) IDA curve samples and (b) corresponding COV curve along with the intensity..…….……...……..……15

Figure 2.4 Illustration of (a) IDA curves and (b) the COV curve of an elastoplastic SDOF system under CUREE GM suite..……..……..16

Figure 2.5 COV spectra with (a) 1% damping ratio and (b) 5% damping ratio under CUREE and FEMA P695 GM suite, respectively..…….……...18

Figure 2.6 CDFs of peak displacement responses of linear 3 degree-of-freedom structures with (a) T=0.74s, ξ=5%, (b) T=1.0s, ξ=5%, (c) T=0.76s, ξ=1% and (d) T=1.31s, ξ=1% under CUREE and FEMA P695 suites..…...……...18

Figure 2.7 Relationship between k_2 and T……...…….22

Figure 2.8 Relationship between coefficient a and PGV/EPV……..……...23

Figure 2.9 Relationship between coefficient b and PGV/EPV……..……...24

Figure 2.10 Relationship between (a) C_y and λ, (b) C_y and β, (c) ξ and μ (c), (d) ξ and η….24

Figure 2.11 Comparisons between the real COV values and the predicted ones by the uncertainty propagation formulation for the elastoplastic SDOF systems with (a) T=0.5 s and (b) T=1.5 s …….……30

Figure 2.12 CDFs of (a) I_0/S_a(1s,5%) and (b) PGV/EPV for the CUREE suite and the Eq20 suite.……..…….30

Figure 2.13 COV_R trends of two different elastoplastic systems under the CUREE suite and the Eq20 suite……...……..…….……31

Figure 3.1 Acceleration response spectra of 102 earthquake records…..……39

Figure 3.2 Typical IDA curves of bilinear SDOF systems and their corresponding hysteretic characteristics……..……...41

Figure 3.3 (a) Comparison of two IDA curves with two values of C_y and (b) the relationship between IDA curves and C_y. …….43

Figure 3.4 IDA curves of bilinear systems with (a) T=0.5 s, (b) T=1.0 s and (c) T=1.5 s...44

Figure 3.5 Relationship between PGA/PGV and parameter c in different natural periods,

hardening ratios and damping ratios…….…….48

Figure 3.6 Relationship between α_{sq}/v_{sq} and parameter a in different natural periods, hardening ratios and damping ratios……..48

Figure 3.7 Values of a_1, a_2, c_1 and c_2 for different structural parameters…….……...49

Figure 3.8 Comparison results from uncertainty quantification formulas and NLTHA…..50

Figure 3.9 Validation of GM suite equivalence for bilinear systems with (a) T=0.5s, (b) T=1.0 s and (c) T=1.5 s.....53

Figure 3.10 IDA curves of bilinear systems with (a) T=0.5 s and (b) T=1.0 s via NLTHA and IDA curve quantification formulation Eq. (3-15)……...……..53

Figure 3.11 CDFs for the case (a) PGA=0.42g and (b) PGA=0.84……...……54

Figure 3.12 (a) Median and (b) logarithmic standard deviation of formula-calculated ductility vs. simulated ones…….54

Figure 3.13 Fragility curves of the systems with (a) T=0.5 s and (b) T=1.0 s..……..…...55

Figure 4.1 Concept of probabilistic shake table test……..……..60

Figure 4.2 Illustration of (a) a test specimen and (b) the dimension of dog bone plate…...61

Figure 4.3 Specimen collapse……...62

Figure 4.4 12 specimens fixed on the shake table……..……..62

Figure 4.5 Illustration of (a) acceleration and (b) displacement response spectra of the 7EQS suite…….…….....63

Figure 4.6 Transfer function samples of three specimens……..……..64

Figure 4.7 Natural period range of the specimen groups……..……...64

Figure 4.8 IDA curves of each group (a~g)……..……...65

Figure 4.9 Comparison of response uncertainties from response spectra and shake table test……..66

Figure 4.10 Response uncertainty caused by structural parameter uncertainty…….67

Figure 4.11 IDA curves of (a) T=0.50 s and (b) T=0.43 s and (c) (d) the corresponding response uncertainties……..69

Figure 4.12 Weight of two uncertainty contributions on response uncertainty……...…..71

Figure 4.13 Illustration of response uncertainty results by different values about β_{SU} and β_{GU}……...73

Figure 5.1 Hysteretic model of the bilinear SDOF system……..……84

Figure 5.2 5% damped response spectra of (a) original ground motions and (b) scaled ground motion……...…….85

Figure 5.3 R^2 contour results for the bilinear SDOF system with T_1=0.5 s, 1.0 s and 1.5 s……...87

Figure 5.4 Illustration of the circle rule of optimal period band…….…….88

Figure 5.5 Contours of R^2 for bilinear systems with C_y=0.1, 0.2, 0.3……..…89

Figure 5.6 Circle rule illustration of bilinear SDOF systems with different parameters.....90

Figure 5.7 Relationship between λ and the optimal starting period……..……...91

Figure 5.8 Relationship between SI_{DPI} and normalized ductility difference.....93
.

LIST OF TABLES

Table 2.1 Selected IMs to develop the intensity independent IMs (Riddell, 2007; Yang et al., 2009)…….23

Table 2.2 Eight ground motions used to validate uncertainty propagation formulation…..31

Table 2.3 Twenty ground motions (Eq20 GM suite) used to validate GM uncertainty equivalency…….……..31

Table 3.1 Values of C_y corresponding to bilinear systems with different natural periods...44

Table 3.2 Ten ground motions used to validate uncertainty quantification formulations....50

Table 3.3 Information about PEER8 GM suite ……..…….52

Table 3.4 Information about Equivalent EQs1 GM suite……...……..52

Table 3.5 Information about Equivalent EQs2 GM suite……...……..52

Table 3.6 Information about Equivalent EQs3 GM suite……...……..52

Table 4.1 Detailed information of the 7EQS suite……..…….62

Table 4.2 Response uncertainty results by the SRSS method using the suggested values from FEMA P695……...……..73

LIST OF SYMBOLS

Seismic Intensity……..……..I

Seismic Intensity at which a system yields……..……..I_y

Fundamental period……..…….T, T_1

Damping ratio……..….ξ

Normalized yield displacement……...….C_y

Elastic stiffness……..….k

Post-yield stiffness…….….k_p

Mass……..….m

Yield displacement……d_y

Gravity acceleration……..……..g

Initial natural frequency……...…….ω_n

Hardening ratio…….…..α

Spectral acceleration…….…….S_a

Coefficient of Determination……...……R^2

Response uncertainty……..β_{RU}

Ductility……..…..μ

Structural parameter uncertainty…… β_{SU}

Ground motion uncertainty…… β_{GU}

Starting period……...…T_s

Ending period……....T_e

Intensity component……...……λ, p_1

Spectral shape component…….……p_2

LIST OF GLOSSARY

PBEE: Performance Based Earthquake Engineering

GM: Ground Motion

COV: Coefficient of Variation

FEMA: Federal Emergency Management Agency

PSHA: Probabilistic Seismic Hazard Analysis

NLTHA: Nonlinear Time History Analysis

SDOF: Single-Degree-of-Freedom

IDA: Incremental Dynamic Analysis

SRSS: Square-Root-Sum-of-Squares

DPI: Damage Potential Indicator

CMS: Conditional Mean Spectrum

GCIM: Generalized Conditional Intensity Measure

MC: Monte-Carlo

PGV: Peak Ground Velocity

EDP: Engineering Demand Parameter

CUREE: Consortium of Universities for Research in Earthquake Engineering

CDF: Cumulative Distribution Function

PGD: Peak Ground Displacement

PDF: Probability Density Function

PGA: Peak Ground Acceleration

IM: Intensity Measure

SP: Structural Parameter

PBSD: Performance Based Seismic Design

FOSM: First-Order Second-Moment

FFT: Fast Fourier Transform

SI: Similarity Index

ACKNOWLEDGEMENTS

I would like to thank my advisor, Dr. Shiling Pei for all of his mentorship and help during my Ph.D. studies. I am also grateful to the help of our collaborator at Colorado State University, Dr. John W. van de Lindt and Mr. Omar Amini for setting up and arranging the shake table tests. Besides, I deeply appreciate the communications and advising from USGS collaborators Dr. Stephen Hartzell, Dr. Nicolas Luco and Dr. Sanaz Rezaeian. Most of work in Chapter 5 is inspired by these communications. Finally, I would like to express my gratitude to my Ph.D. committee members: Dr. D. V. Griffiths, Dr. Joseph P. Crocker and Dr. William C. Navidi.

The financial support from NSF and USGS are greatly appreciated. Without these support, I won't have a chance to finish this thesis.

CHAPTER 1

INTRODUCTION

1.1 Background

The ultimate goal of earthquake engineering is to ensure life safety and mitigation of economic loss to the built environment during earthquake events. Traditional seismic design approaches served the need of life safety in most of the cases through its conservative estimation of loads and dynamic effects, but have very limited use in controlling damage from earthquakes. Over the past a few decades, Performance Based Earthquake Engineering (PBEE) became very attractive in seismic engineering research because of its potential to consider performance objectives beyond life safety. One of the most attractive features of this philosophy is the ability to account for response uncertainty explicitly, essentially consider all major sources of uncertainty in its analysis, including (1) ground motion (GM) uncertainty, (2) structural parameter uncertainty (or aleatoric uncertainty), and (3) numerical modeling uncertainty. This provides PBEE the ability to directly address reliability of a design for any performance objectives of interest for stakeholders.

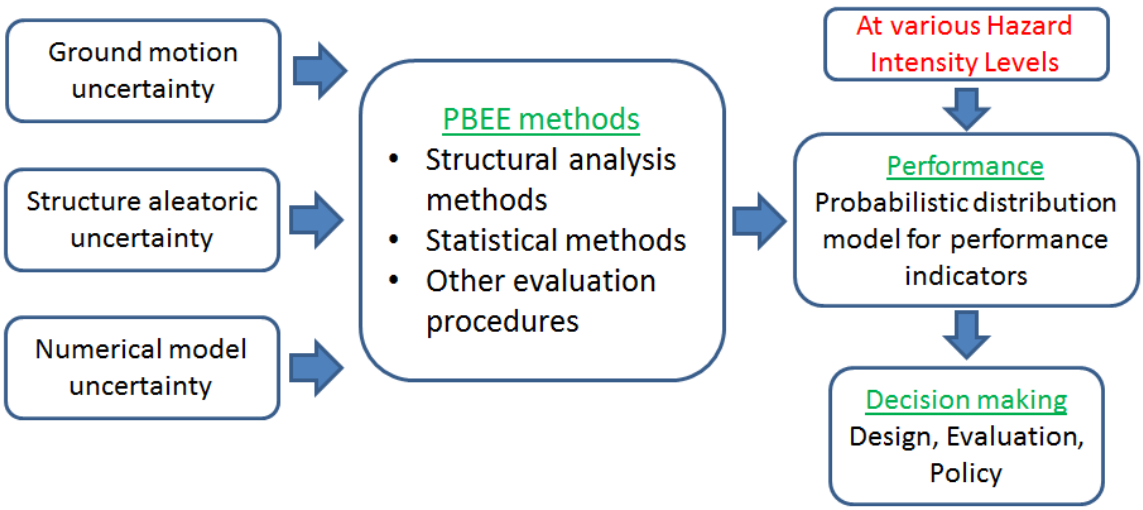

Figure 1.1 Conceptual component of general PBEE.

It can be seen from Figure 1.1 that the main "output" from PBEE methods is the probabilistic distribution of the performance indicators. Most of the time, the coefficient of variation (COV) and standard deviation values for the indicators will be sufficient for engineering purposes. While the structural analysis procedures can usually provide the mean or median of the seismic responses with reasonable accuracy, statistical methods are needed to determine the dispersion (e.g., standard deviation) of the seismic responses. This cannot be accomplished without accurate considerations of the uncertainty impacts from the three major sources, namely ground motion uncertainty, structural parameter uncertainty, and numerical modeling uncertainty. The following is a brief summary of commonly used modeling techniques for these uncertainty components.

1.1.1 Ground motion uncertainty

Ground motion uncertainty has been routinely considered in many PBEE studies through the use of a suite of earthquake records in numerical simulations. The ATC63 project (FEMA-P695 2009) used a suite of 22 ground motions mainly selected from California earthquakes, which have been adopted by many researchers on numerous projects. Another suite of 20 earthquake ground motions was suggested by Krawinkler et al. (2001) for the use in the wood frame structure seismic analysis. Nielson and Pang (2011) developed a procedure to randomly pick records from a ground motion data pool containing 160 records for a bridge structure fragility study. These ground motion suites, combined with specific techniques to scale them to the desired hazard level, are widely accepted by the seismic research community to be representative of the uncertainty in the ground motions. In many analyses, it is often the only uncertainty considered in the PBEE analysis (e.g., Kim and Rosowsky 2005) with the argument that the uncertainty contribution from ground motions dominates that from other sources. However, the limitation here is very apparent. There is no a generally-accepted approach for the selection of GM records to be included in the analysis. A more elaborate

framework of probabilistic seismic hazard analysis (PSHA) can be applied to special cases where a particular region with known faults and rupture mechanism can be considered, but it is far beyond what is practical for typical structural engineering applications. Even when some commonly-used GM suites are available for the use by the researchers, the incorporation of GM uncertainty is empirical in nature through NLTHA. The amount of GM records in a suite is far less than what will typically be considered as conducting Monte Carlo type simulations, such as the less-than 10 GM records required in the alternative design procedure of ASCE7. Thus, the consideration of the GM uncertainty is likely the weakest link in PBEE.

1.1.2 Structural parameter uncertainty

Structural parameter uncertainty of the structure is typically neglected in many studies with the belief that its impact will be overshadowed by uncertainty contribution from the GM source. In addition, the nature of this type of uncertainty makes it hard to be quantified in the first place, thus making this assumption even more appealing. However, there are techniques in PBEE that can be used to investigate the impact of structural parameter uncertainty. For example, in probabilistic finite element analysis, numerical model properties are randomized and subjected to the earthquake excitations. This type of method is typically very computationally intensive and building specific. Celik and Ellingwood (2010) investigated seismic fragilities for non-ductile reinforced concrete frames and concluded that aleatoric uncertainty can be neglected for the fragility analysis. However, the investigation conducted by Yin and Li (2010) on the probabilistic dynamic simulation of wood frame structures indicated that structural parameter uncertainty can greatly affect the collapse probability of such buildings. Other research efforts on steel and concrete structures can also be found. Based on the results observed from these studies, the contribution of the uncertainty to structural performance can be quite different depending on structural properties and hazard levels. An experimental investigation was conducted in this study to validate one of the simple

assumptions commonly used in PBEE regarding structural uncertainty contribution, which will be discussed in Chapter 4.

1.1.3 Numerical modeling uncertainty

Numerical modeling uncertainty reflects the fact that numerical models cannot simulate the structural behavior perfectly due to our lack of knowledge. In FEMA P695 procedure (FEMA-P695 2009), modeling uncertainty is related to the quality and capacity of the numerical model used, as shown in Figure 1.2 below. When there is no experimental data to support the evaluation of the model, this simplified procedure may be the only option to consider modeling uncertainty in PBEE. Although data from shake table tests can be used to quantify the model accuracy, the comparison is typically done in a deterministic fashion (e.g., Van de Lindt et al. 2010). Model accuracy is also correlated to particular structural responses and seismic intensity. Pei and van de Lindt (2011) developed a "grading" system for the numerical model accuracy on different structural responses and observed the variation of model accuracy with the increased earthquake intensity level. With very limited data points from experiments, it is difficult to distinguish modeling error, bias, and uncertainty. Although there is no doubt regarding the existence of numerical modeling uncertainty in PBEE, it remains one

Representation of Collapse Characteristics	Accuracy and Robustness of Models		
	High	Medium	Low
High. Index models capture the full range of the archetype design space and structural behavioral effects that contribute to collapse.	(A) Superior $\beta_{MDL} = 0.10$	(B) Good $\beta_{MDL} = 0.20$	(C) Fair $\beta_{MDL} = 0.35$
Medium. Index models are generally comprehensive and representative of the design space and behavioral effects that contribute to collapse.	(B) Good $\beta_{MDL} = 0.20$	(C) Fair $\beta_{MDL} = 0.35$	(D) Poor $\beta_{MDL} = 0.50$
Low. Significant aspects of the design space and/or collapse behavior are not captured in the index models.	(C) Fair $\beta_{MDL} = 0.35$	(D) Poor $\beta_{MDL} = 0.50$	--

Figure 1.2 Qualitative inclusion of modeling uncertainty (FEMA P695).

of the least investigated sources of uncertainty due to the difficulty in isolating it from modeling bias and input model parameter uncertainty. Note that the structures adopted in this thesis study are simple oscillator systems which help to minimize the modeling bias. Thus, this thesis is not focused on modeling uncertainty, which may need another comprehensive study on its own.

1.2 Objectives of the Research

Currently, there has not been an unanimously agreed upon procedure in PBEE to quantify and propagate uncertainty from different sources. Taking ground motion uncertainty as an example, an engineer may select a particular set of earthquake ground motions to conduct the analysis. It will be assumed that the selected suite of ground motions is "representative" of the seismic hazard for this building site. However, the outcome of the analysis might be different when a different set of ground motions are used (e.g., Nielson and Pang 2011; Ramanathan K. 2010) or even when the same ground motion suite with different hazard levels are conducted. The fundamental reason for the difficulty in representing earthquake GM uncertainty lies in the empirical nature of how the impact of GMs on response uncertainty was calculated. Since the majority of the applications in PBEE include structural response assessment beyond linear responses, most of the methods in PBEE very reliant on NLTHA to predict earthquake effects, resulting in that no direct derivation can be applied to address the problem of uncertainty propagation. Classic probabilistic approaches that worked well for functions cannot be easily applied to the "black box" of NLTHA. The only option is Monte Carlo type simulation. But due to the complexity of nonlinear structural models and the limitation in available earthquake ground motions, it is difficult to gain a comprehensive picture of response uncertainty with only a handful of simulations. One of the major objectives of this study is to go beyond NLTHA to explore alternative models for seismic responses of structural systems, which will enable a more rational approach to assess response uncertainty. This philosophy was also applied in a parallel study on GM damage potential, in which a

spectral similarity indicator was developed to compare the damage potential of two GMs without conducting NLTHA.

With regard to structural parameter uncertainty, past studies have pointed out (e.g., Yin and Li 2010) that although the impact of structural parameter uncertainty on system responses can be negligible for small earthquakes, it can become quite significant and comparable to ground motion uncertainty contribution when the system becomes highly nonlinear and near collapse. This statement implies that the uncertainty contribution from structural parameters (or ground motions) might vary with seismic intensity. The investigation of seismic intensity influence on uncertainty contribution of ground motions and structural parameters on structural responses can be conducted using theoretical and experimental methods. The experimental work conducted in this study shed lights on some fundamental assumptions regarding structural uncertainty.

In summary, the readily available NLTHA tools in modern PBEE have greatly increased the ability of researchers to explore advanced designs and systems. But at the same time, many research work in PBEE becomes empirical in nature and relies heavily on simulation techniques. This study is aimed at exploring alternative ways to assess the impact of earthquake excitations on structural system responses and damage. It is believed that the relationship between seismic inputs and response outputs can be simple, abstract, and tractable when the questions are appropriately formulated. Several related topics were explored in this thesis work, including GM uncertainty propagation and GM damage potentials.

1.3 Organization of Thesis

The thesis consists of 6 chapters. Chapter 1 is introducing the background and objective of the research in the thesis; Chapter 6 summarizes major findings and proposed future research work. Chapters 2-5 are modified from four technical manuscripts published in or submitted to

peer-reviewed journals. In the following section, the main content of Chapters 2-5 is summarized.

Chapter 2: A new closed form approach to quantify the GM uncertainty in uniform scaling process in multi-record IDA was proposed. This uncertainty quantification approach was applied to linear systems and elastoplastic SDOF system acceleration, and was validated using a variety of simplified structural models and ground motion suites. The GM uncertainty quantification was performed by developing a parametric IDA curve using intensity-independent GM parameters as inputs. Through regression analysis, IDA curves can be obtained without conducting NLTHA. This chapter is derived from the modification of "An approach to quantify the influence of ground motion uncertainty on elastoplastic system acceleration in incremental dynamic analysis" which was accepted by *Advances in Structural Engineering*. The authors are Peng Deng[1], Shiling Pei[2], John W. van de Lindt[3], Hongyan Liu[4] and Chao Zhang[5].

Chapter 3: Expanding from the idea presented in Chapter 2, an uncertainty quantification framework for seismic displacement response of bilinear SDOF systems was proposed. The framework considers the interaction of ground motions and structural parameters in the uncertainty propagation. Criteria about ground motion suite equivalency in the context of resulting response uncertainty were developed. Additionally, PBEE applications such as fragility analysis were conducted based on the proposed quantification framework. This extension puts this research one step closer to PBEE applications as the displacement of a bilinear system is a performance metrics that can be related to structural damage. This chapter is derived from the modification of "Uncertainty quantification for seismic responses of bilinear SDOF systems: A semi-closed-form estimation" which was published in *Soil Dynamics and Earthquake Engineering*. The authors are Peng Deng[1], Shiling Pei[2], John W. van de Lindt[3] and Chao Zhang[5].

Chapter 4: A special shake table test was designed to decouple the ground motion uncertainty and structural parameter uncertainty, which helps the researchers to experimentally investigate how each uncertainty source affects final response uncertainty. Through the tests, the relative contribution of ground motions and structural parameters on the response uncertainty was tracked to validate a fundamental assumption often used in PBEE. The commonly-used square-root-sum-of-squares (SRSS) method was also evaluated according to test data.

Chapter 5: A spectrum based approach was developed to compare different GMs with regard to their ability to induce damage on structural systems. A vector-valued damage potential indicator (DPI) derived from response spectrum magnitude and shape was proposed. A circle rule was proposed to identify the critical period band of the response spectrum which is used to calculate the DPI. The effectiveness of the DPI was validated and it is discovered that ground motions with similar DPIs for a given structure will have similar structural damage. This essentially enables the establishment of damage equivalency between GMs without conducting NLTHA.

---

[1]Ph.D. Candidate. Department of Civil and Environmental Engineering, Colorado School of Mines, Golden, CO 80401, USA.
[2]Assistant Professor. Department of Civil and Environmental Engineering, Colorado School of Mines, Golden, CO 80401, USA.
[3]George T. Abell Distinguished Professor in Infrastructure. Department of Civil and Environmental Engineering, Colorado State University, Fort Collins, CO 80523, USA.
[4]Teaching Associate Professor. Department of Civil and Environmental Engineering, Colorado School of Mines, Golden, CO 80401, USA.
[5]Ph.D. Candidate. Department of Civil and Environmental Engineering, Michigan Technological University, Houghton, MI 49931, USA.

CHAPTER 2

UNCERTAINTY QUANTIFICATION ON ELASTOPLASTIC SDOF SYSTEM ACCELERATION

Modified from a paper accepted by *Advances in Structural Engineering* (Deng et al. 2017)

Peng Deng, Shiling Pei, John W. van de Lindt, Hongyan Liu, and Chao Zhang

2.1 Abstract

The inclusion of ground motion (GM) induced uncertainty in structural response evaluation is an essential component of Performance Based Earthquake Engineering (PBEE). In current practice, GM uncertainty is often represented in PBEE analysis empirically through the use of one or more GM suites. How to quantitatively characterize GM-induced structural response uncertainty propagation at different seismic hazard levels has not been thoroughly studied to date. In this study, a procedure to quantify the influence of GM uncertainty on elastoplastic single-degree-of-freedom (SDOF) acceleration responses in an Incremental Dynamic Analysis (IDA) is proposed. By modeling the shape of the IDA curves, the formula to calculate the uncertainty in peak acceleration responses of linear systems and elastoplastic SDOF systems was constructed. This closed-form calculation provided a quantitative way to establish statistical equivalency for different GM suites with regard to the acceleration response in these simple systems. This equivalence was validated through a numerical experiment, in which an equivalent GM suite for an existing GM suite was constructed and shown to yield statistically similar acceleration responses to that of the existing GM suite at all intensity levels.

2.2 Introduction

Over the past several decades, Performance Based Earthquake Engineering (PBEE) has attracted a significant attention in both research development and engineering practice (FEMA356 2000; Ghobarah 2001; Günay and Mosalam 2013; Sfahani et al. 2015). One of the most attractive features of this philosophy is the ability to account for the response uncertainty

in a more explicit manner than traditional methods. PBEE requires accurate considerations of major sources of uncertainty in its analysis, including (1) ground motion (GM) uncertainty (record-to-record uncertainty), (2) structural parameter uncertainty, and (3) numerical modeling uncertainty. In most PBEE procedures (Baker and Cornell 2003; Hamburger et al. 2003; Pang et al. 2010; Porter 2003), the consideration of uncertainty sources and their propagation behavior is empirical. Typically, GM-induced uncertainty is considered to be the dominant contributor to the uncertainty of structural performance (Kwon and Elnashai 2006; Lee and Mosalam 2005; Liel et al. 2009; Yin and Li 2010), and is routinely included in the performance-based seismic analysis by using a suite of ground motion records. In most analyses where a GM suite is used, other uncertainty sources are neglected (Kim and Rosowsky 2005; Wong and Harris 2012). In terms of methods to select ground motions, Baker and Cornell (Baker 2011) proposed a conditional mean spectrum (CMS) to assess the difference of ground motions based on the parameter ε on the spectral shape. This is an assessment approach mainly focusing on the spectral acceleration without considering other characteristics of ground motions. Bradley (2010; 2012) proposed a generalized conditional intensity measure (GCIM) approach through comparing the distribution of the identified intensity measures of a GM suite with the target GCIM distribution. There are also research efforts towards selecting a GM suite to better represent uncertainty in scenario earthquakes (Wang 2011) with corresponding tools (Wang et al. 2015). As of now, there has not been a systematic way to quantitatively compare different GM suites with a focus on their impact on induced structural response uncertainty. Choosing one GM suite over another can sometimes be subjective and based on the discretion of researchers and engineers, which does not ensure the equivalence between different analyses regarding structural response uncertainty. This background provided the impetus for this study.

Among the commonly-used GM suites in the current seismic research, the FEMA P695 project (FEMA-P695 2009) identified a suite of 22 ground motions. Another suite of 20

earthquake ground motions was suggested by Krawinkler et al. (2001) for the nonlinear time history analysis of wood frame buildings. Nielson and Pang (2011) developed a procedure to randomly pick records from a ground motion data pool containing 160 records for a bridge structure fragility study. The rationale of using such a large GM suite is similar to conduct Monte-Carlo (MC) simulations or Latin hypercube sampling methods for approximating random variables (Dolsek 2009; Fragiadakis and Vamvatsikos 2010; Vamvatsikos and Fragiadakis 2010). Different from traditional MC simulations, the number of ground motions is quite limited (compared to a typical MC simulation in reliability analysis) due to the computational expense of time history analysis. In alternative design methods available in ASCE7-10 (2010), a minimum of three ground motions is required. The code specifies the scaling of these ground motions but does not address the uncertainty associated with these records explicitly. When a particular GM suite is selected for the analysis, it is implicitly assumed that the selected suite of ground motions is "representative" of the GM variability for the given structure site. However, many studies have indicated that the outcome of this analysis will be sensitive to the GM suite used (Nielson and Pang 2011; Ramanathan K. 2010). Even when one wishes to select among several potential GM suites, it is difficult to compare them rationally.

Furthermore, even for a given GM suite, the level of uncertainty it introduces to the structural response will vary with the hazard level (i.e., scaling of the GM suite). In this study, the mechanism of how the influence of GM uncertainty on response uncertainty can be affected by the GM suite scaling will be investigated for idealized linear and elastoplastic systems, and metrics to quantify the influence of GM uncertainty along with intensity will be proposed. The procedure for conducting the proposed analysis was summarized in Figure 2.1. This study consists of an investigation of two simple systems: linear elastic system and elastoplastic system. For the linear system, GM-induced uncertainty from a given GM suite can be

characterized by a COV spectrum of the GM suite, which will be introduced in detail later. For the elastoplastic system, the key to quantifying GM uncertainty is the development of a parametric model for IDA curves. The proposed models for the systems were validated with numerical examples.

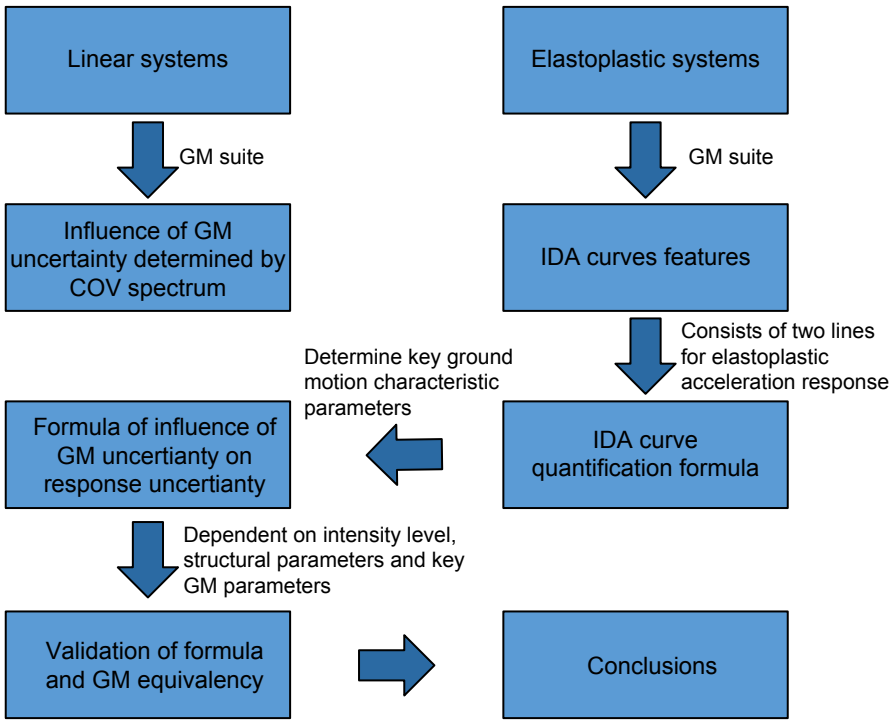

Figure 2.1. Flowchart for the framework of the proposed analyses.

2.3 Multi-record Incremental Dynamic Analysis

Incremental dynamic analysis (IDA) (Vamvatsikos and Cornell, 2002; Vamvatsikos and Cornell, 2004), which has been extensively used by researchers ever since its development, is a parametric analysis method used to provide insight into the performance of structures subjected to different levels of ground motion intensity. When combined with a GM suite scaled to different intensity levels, IDA can be used to develop many core components of PBEE, such as structural response distributions and fragility curves. Considering a uniform scaling (all GM records in a suite are scaled with the same factor), the intensity of the GM suite (not of the individual records) can be quantified by a single value I, which may be taken as the

average value of a user-selected intensity measure (e.g., spectral acceleration, peak ground velocity (PGV), etc.) for all the records in the GM suite. In this study, the focus is the uncertainty in engineering demand parameter (EDP) (e.g., peak drift, acceleration, damage, etc.) represented by its coefficient of variation (COV). The propagation of GM uncertainty in seismic responses of a certain structure can be formulated as:

$$COV_R = g\left(COV_{\mathrm{EQ}}, \mathbf{f}, I\right) \tag{2-1}$$

where COV_{R} is the coefficient of variation of the peak structural response of interest; COV_{EQ} represents the GM uncertainty of the GM suite selected, which can be quantified by the COV of the key GM parameters of records (the appropriate parameters will be discussed in later sections); **f** is a vector represents the structural characteristics of the dynamic systems. I is the intensity level of the GM suite defined earlier. $g()$ is a general function representing uncertainty propagation. The benefit of this uncertainty propagation formulation is two-fold: 1) the characterization of GM uncertainty can be quantified and independent of ground motion intensity (i.e., scaling), which means that once the ground motion records in a suite are selected, there will be a consistent representation of the underlying uncertainty for the GM suite regardless of the scaling; and 2) the influence of GM suite intensity on structural response uncertainty is decoupled from the GM uncertainty characterization. While Eq. (2-1) is conceptual and the viability of this formulation needs further proof, it will be shown in the following sections that such an uncertainty propagation formulation can be derived from simple dynamic system responses. It will also be shown that the key to achieving this formulation is to establish the relationship between the shape of the structure's IDA curves and intensity-independent GM parameters.

IDA curves have been routinely used to describe the change in peak structural response quantities as a function of ground motion intensity. Based on the shape of the IDA curve, there are two main categories as shown in Figure 2.2 (curves were generated from time history

simulation of elastic and elastoplastic SDOF systems). Note that the horizontal axis in Figure 2.2 is the peak acceleration of the SDOF system while the vertical axis indicates the PGV of the input ground motion. The Type I curve has a constant slope representing a linear system; The Type II curve represents the IDA curve of an elastoplastic SDOF system, for which the post-yield IDA curve can be approximated as a straight line.

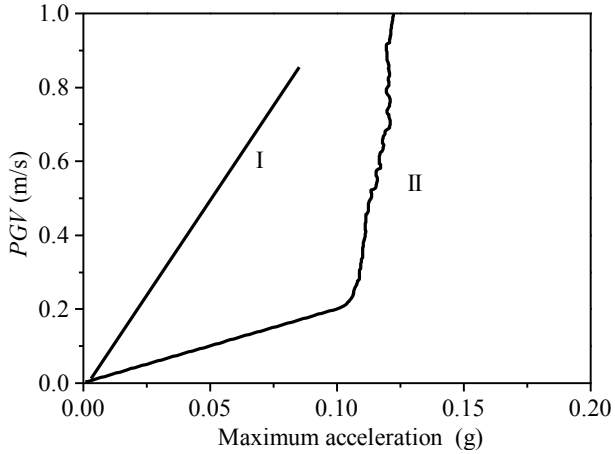

Figure 2.2 Example IDA curves of a linear system and an elastoplastic SDOF system.

The mechanism of GM-induced uncertainty propagation can be illustrated using a conceptual multi-record IDA scenario. Considering a GM suite containing N records, the corresponding IDA curves for a given structure will form a "band" shown conceptually in Figure 2.3. As there are more than one record, the intensity level in Figure 2.3 can be defined as the average intensity of the GM suite. Initially when the intensity is low, there will be a linear region in which the COV_R remains constant. Then, when the GM suite reaches a particular intensity level I_1, the first record within the suite will push the structure into a nonlinear region. As the intensity continues to increase, other records will start to "yield" the structure, until the intensity reaches I_2 at which the structure behaves nonlinearly for all records. When plotting the change of COV_R against the GM suite intensity, one should expect three distinct regions of GM intensity in which the GM uncertainty propagates differently in structural responses, namely the linear constant region (Region I, $I < I_1$), mixed transitional

region (Region II, $I_1 < I < I_2$), and nonlinear region (Region III, $I > I_2$). For a group of Type II IDA curves shown conceptually in Figure 2.3(a), a possible behavior of COV_R as a function of I is illustrated in Figure 2.3(b), which is not constant at different intensity levels. The phenomena of this changing about COV_R can be observed in real nonlinear systems, such as the data points shown in Figure 2.4, which were constructed using the peak accelerations of an elastoplastic oscillator under the CUREE GM suite (Krawinkler et al., 2001). The variable k_0, k_2 and I_y in Figure 2.4(a) will be discussed later.

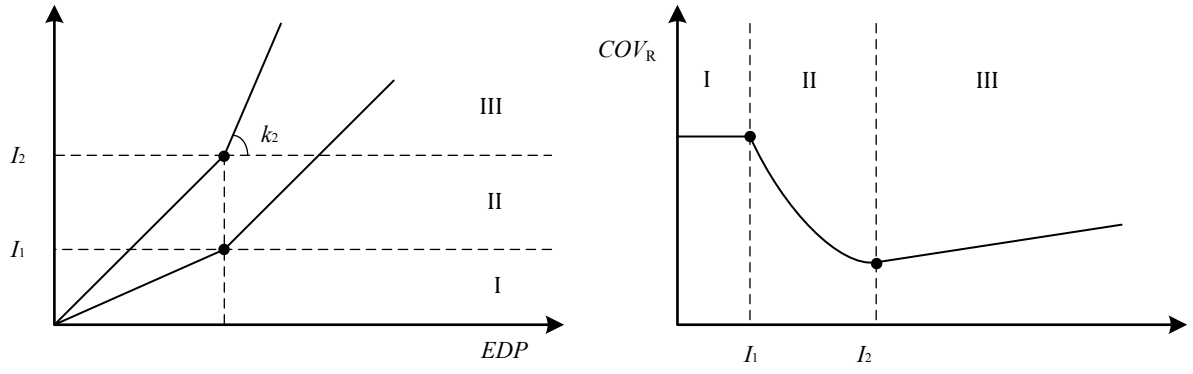

(a) (b)

Figure 2.3 Examples of (a) IDA curve samples and (b) corresponding COV curve along with the intensity.

From Figure 2.3 and Figure 2.4, we know that the key to quantifying the uncertainty propagation mechanism in multi-record IDA is the shape of IDA curves. In the following sections, the COV_R of the peak responses will be studied quantitatively as an example for simple linear and nonlinear oscillators. Key GM characteristics that control the shape of IDA curves for simple structural systems will be identified. It is intended to use these key GM characteristics to quantify GM uncertainty so that this uncertainty in different GM suites can be compared rationally.

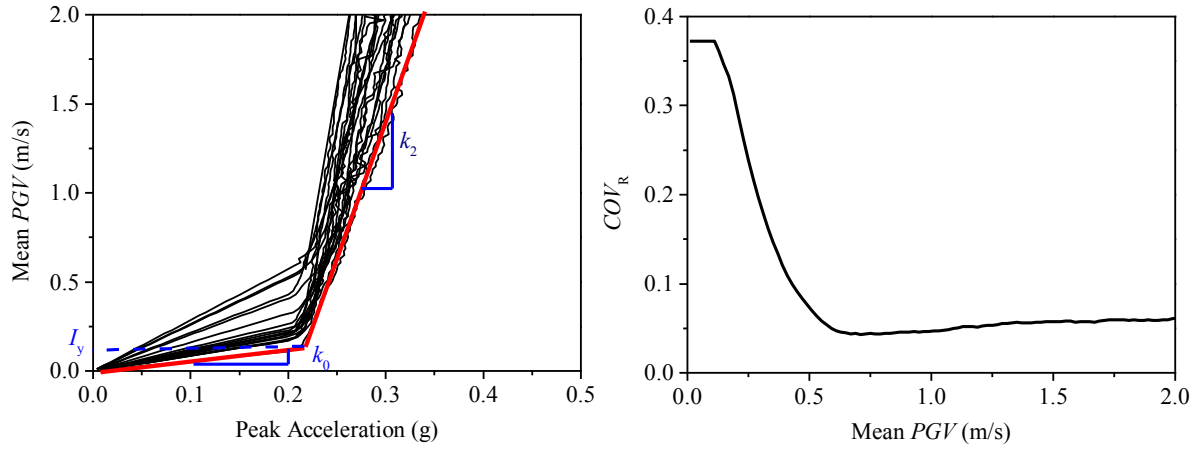

(a) (b)

Figure 2.4 Illustration of (a) IDA curves and (b) the COV curve of an elastoplastic SDOF system under CUREE GM suite.

2.4 Quantify GM-induced Uncertainty for Linear Systems

For linear systems, the peak structural responses are approximately proportional to the elastic response spectrum of the earthquake record at the structure's natural frequency. As a result, the IDA curve is a straight line and the GM uncertainty can be quantified by the uncertainty in the ground motion spectral acceleration. Figure 2.5 shows the coefficient of variation of the acceleration response spectrum (termed hereafter as the COV spectrum) for two commonly-used unscaled GM suites (i.e., the CUREE GM suite (Krawinkler et al., 2001) and the FEMA P695 GM suite (FEMA-P695, 2009)). Note that the COV spectrum is a scaling-independent characteristic of a given GM suite and can change for different damping ratios.

For linear systems, once the COV spectrum is established for each GM suite (as shown in Figure 2.5), a closed-form propagation rule for the response uncertainty caused by GM uncertainty could be derived as:

$$COV_{\mathrm{R}} = COV_{\mathrm{spe}}\left(T,\xi\right) \tag{2-2}$$

where $COV_{\mathrm{spe}}(T, \xi)$ is the COV spectrum of acceleration, displacement or velocity (note that the COV spectrum will be identical for the three types of responses.) for a GM suite as a

function of natural period T and damping ratio ξ. When comparing two GM suites for the purpose of using them in linear system analysis, two different GM suites can be considered equivalent if their $COV_{spe}(T, \xi)$ values at the system natural period match closely. For example, the CUREE and FEMA P695 suites can be considered equivalent to a 5% damped linear system with a natural period of 0.74 s, but are statistically different for structures with natural periods of 1.0 s (Figure 2.5(b)). The same condition is shown for a 1% damped linear system for T=0.76 s and T=1.31 s (Figure 2.5(a)). Figure 2.6 shows the Cumulative Distribution Function (CDF) of peak displacement responses of two three-degree-of-freedom linear shear building models excited by the CUREE and FEMA P695 suites. Note that the average PGV of CUREE suite is scaled to be same as the one of FEMA P695 suite for the comparison of displacement distributions. The two 5% damped shear buildings have the first mode periods equal to 0.74 s and 1.0 s, respectively. For the system with a natural period of 0.74 s, the CUREE and FEMA P695 suites almost yielded identical CDFs (Figure 2.6(a)), while this is not the case for the system with a natural period of 1.0 s (Figure 2.6(b)). Furthermore, the COVs of peak displacement responses in Figure 2.6(a) closely matched the corresponding GM suite COV spectrum at the natural period (COVs of structural responses for single or three-degree-of-freedom oscillators with 0.74 s natural period all almost equal to 0.5 in Figure 2.5(b)). In other words, for the application of linear system analysis, the influence of GM uncertainty on response uncertainty can be quantified by its COV spectrum. Figures 2.6(c) and (d) provided additional proof with 1% damping ratio case that response uncertainty of linear systems is dictated by COV spectrum of the GM suite used. Compared to the more general formulation in Eq. (2-1), the uncertainty propagation for linear systems is independent of the GM suite scaling.

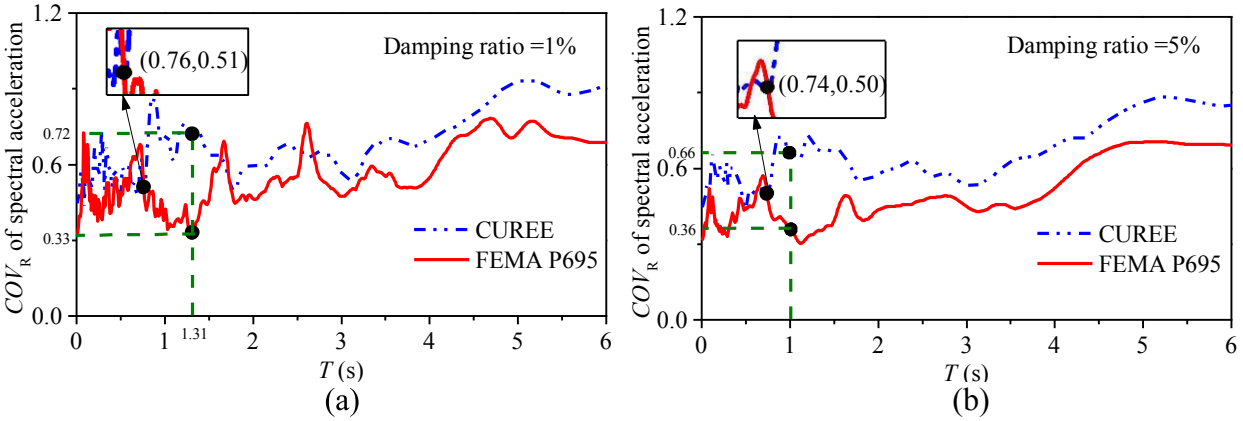

Figure 2.5 COV spectra with (a) 1% damping ratio and (b) 5% damping ratio under CUREE and FEMA P695 GM suite, respectively.

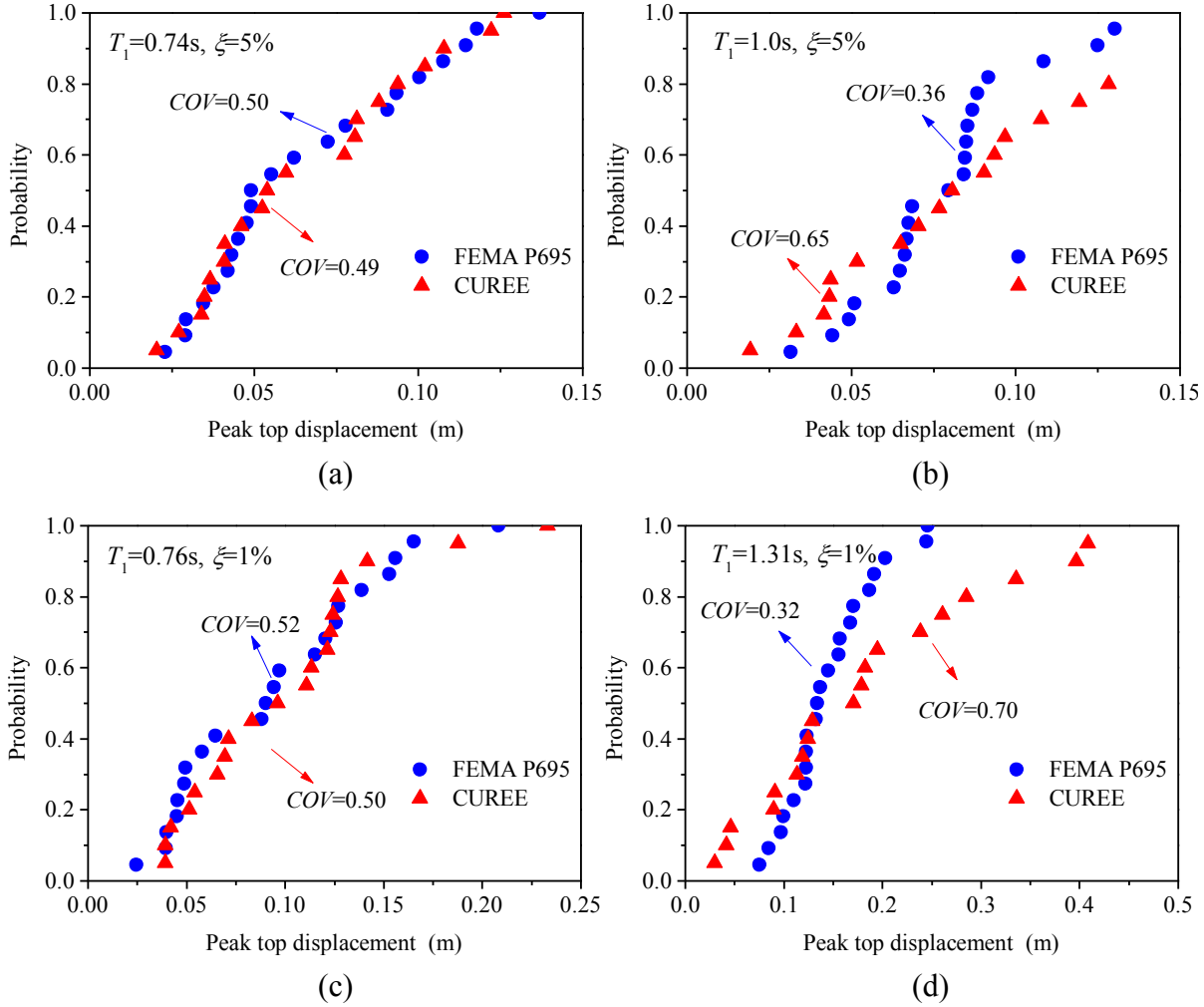

Figure 2.6 CDFs of peak displacement responses of linear 3 degree-of-freedom structures with (a) T=0.74s, ξ=5%, (b) T=1.0s, ξ=5%, (c) T=0.76s, ξ=1% and (d) T=1.31s, ξ=1% under CUREE and FEMA P695 suites.

2.5 Quantify GM-induced Uncertainty for Elastoplastic SDOF System Acceleration

Applying the proposed GM uncertainty propagation formulation (Eq. (2-1)) to the simplest nonlinear system, the peak acceleration of the elastoplastic SDOF system was considered in this study. The ground motion intensity is represented by the peak ground velocity (PGV). The simulation shows that the IDA curve of the elastoplastic system acceleration has a Type II shape with two segments separated by a yielding intensity point (the intensity at which the elastoplastic system yields). As shown in Figure 2.4(a), one can simplify the IDA curve as a bilinear function which has three control parameters. The parameter k_0 is the initial slope of the IDA curve; parameter I_y is the intensity level at which the system yields; and parameter k_2 is the slope of the curve after yielding. As a result of this change in the slope of the IDA curve, the uncertainty propagation becomes intensity dependent for even the simplest nonlinear system.

2.5.1 Defining Elastoplastic SDOF System Parameters

Since this study aims to decouple GM suite uncertainty, a simpler definition for elastoplastic systems is adopted here. An elastoplastic SDOF system can be defined with three physical structural parameters, namely initial stiffness, damping ratio and the yield displacement. In order to make the study results more generalized, initial stiffness and yield displacement were replaced with two dimensionless variables, namely the initial natural frequency w_n (equals to $\sqrt{k/m}$) and the normalized yield displacement C_y:

$$C_y = d_y / \left(mg / k\right) = \frac{d_y \omega_n^2}{g} \tag{2-3}$$

$$d_y = \frac{C_y g}{\omega_n^2} \tag{2-4}$$

where d_y is the yield displacement; m is the mass; k is the initial stiffness; g is the gravity acceleration.

2.5.2 Regression of the IDA Curves

With the structural system parameters defined, the shape of the IDA curve, defined by parameters k_0, k_2, and I_y shown in Figure 2.4(a), can then be calculated using C_y, ω_n (or T), damping ratio ξ, and key GM parameters (be identified later in this section) for any given ground motion record.

The initial IDA "slope" k_0 can be calculated as:

$$k_0 = \frac{I_0}{S_a(T,\xi)} \tag{2-5}$$

where $S_a(T,\xi)$ denotes the acceleration response spectrum of a GM record (Unit:g); I_0 is the corresponding intensity value of the unscaled GM record.

The yielding intensity I_y can also be calculated relatively easily because it has a physical meaning, which is the intensity level at which the system yields. Thus for an individual record, when the peak displacement of the elastoplastic SDOF system is equal to the yield displacement, the scaling can be expressed as:

$$I_y = \frac{I_0 \times d_y}{D(T,\xi)} \tag{2-6}$$

where $D(T, \xi)$ is the displacement response spectrum. The displacement response spectrum can be expressed by the pseudo-acceleration spectrum ($A(T, \xi)$) as:

$$D(T,\xi) = \frac{1}{\omega_n^2} A(T,\xi) \tag{2-7}$$

Then, substituting Eq. (2-7) into Eq. (2-6):

$$I_y = \frac{I_0 \omega_n^2 d_y}{A(T,\xi)} \tag{2-8}$$

For the case with a small damping ratio, the pseudo-acceleration spectrum can be assumed to be the same as the total acceleration spectrum (Chopra 2012). So, Eq. (2-8) can be formulated as:

$$I_{\mathrm{y}} = \frac{I_0 \omega_{\mathrm{n}}^2 d_{\mathrm{y}}}{S_{\mathrm{a}}\left(T,\xi\right) g} \tag{2-9}$$

Substituting Eq. (2-4) into Eq. (2-9):

$$I_{\mathrm{y}} = \frac{I_0 C_{\mathrm{y}}}{S_{\mathrm{a}}\left(T,\xi\right)} = k_0 C_{\mathrm{y}} \tag{2-10}$$

From Eq. (2-10), one can see that the seismic intensity at the yield point is determined by the C_{y} and k_0. For a given system subjected to a GM suite with multiple records, the intensity (I_1) (Figure 2.3(a)) is directly dependent on the record with the smallest k_0 in the suite while the I_2 is controlled by the record with the largest k_0.Thus, k_0 *and* C_{y} completely determine the elastic part of the IDA curves. Note that $k_0 = I_0/S_{\mathrm{a}}(T,\xi)$ can be seen as a key GM parameter.

In order to derive the post-yield trend of the IDA curve, the slope (k_2) needs to be quantified as well. This parameter is controlled by the nonlinear characteristics of the structure and cannot be derived in a closed form. Thus a series of nonlinear time history simulations were conducted using elastoplastic oscillators with different earthquake GMs to identify the trends. Using the PGV as the intensity measure, the simulations showed that there is a linear relationship between parameter k_2 and the natural period T of the oscillator in logarithmic scale (shown in Figure 2.7, the data are generated using records from CUREE GM suite for the elastoplastic system with 5% damping ratio and C_{y}=0.4):

$$\ln\left(k_2\right) = a \ln\left(T\right) + b \tag{2-11}$$

where the coefficients a and b are functions of key GM parameters and structural system parameters. Logically, because the coefficients a and b control the shape of the IDA curve,

the GM parameters that influence the value of a and b must be intensity-independent. In other words, the value of k_2 should not be a function of ground motion intensity.

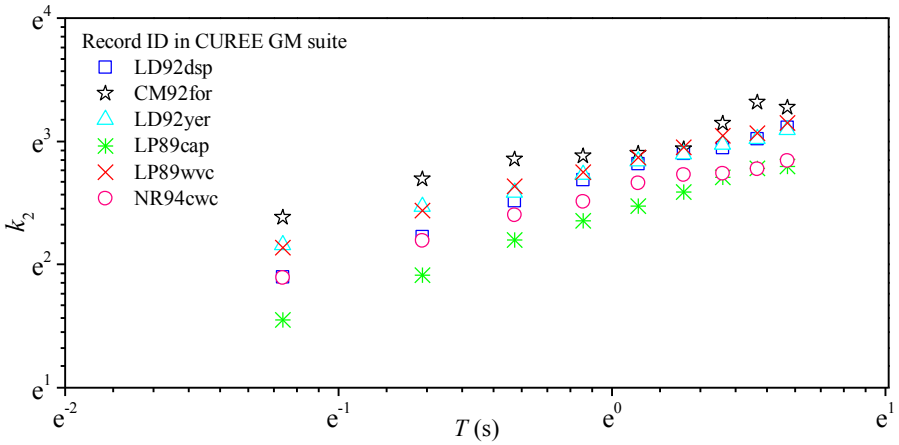

Figure 2.7 Relationship between k_2 and T.

Based on earlier studies (e.g, Riddell, 2007, Yang et al., 2009), there are a number of intensity-dependent measures that can be used to characterize a GM quantitatively. The ratio between these measures (e.g., *PGV*/*PGD*) is typically intensity-independent (or normalized) that they remain constant when the GM record is scaled. Table 2.1 shows some of the intensity measures selected in this study to construct the intensity-independent parameters. Further information about these measures can be found in the literature (Riddell, 2007; Yang et al., 2009).

A correlation analysis between normalized intensity measures and the coefficient a and b was conducted. Through a trial-and-error process, the normalized intensity measure which has the strongest correlation with coefficient a and b was identified in this study. In the analysis, the widely-used CUREE and FEMA P695 GM suites were used. The analysis considered a wide range of elastoplastic SDOF systems with different initial natural periods (from 0.3 s to 2.0 s), normalized yield displacements (from 0.1 to 0.4), and damping ratios (from 1% to 5%).

Table 2.1 Selected IMs to develop the intensity independent IMs (Riddell, 2007; Yang et al., 2009)

Intensity measure	Calculation method
PGA	Maximum of the absolute acceleration of GMs
PGV	Maximum of the absolute velocity of GMs
PGD	Maximum of the absolute displacement of GMs
EPA	$EPA = S_a\left[0.1s, 0.5s\right]/2.5$
S_I	$S_I = \int_{0.1}^{2.5} S_v(5\%, T)dT$
EPV	$EPV = S_v\left[0.8s, 1.2s\right]/2.5$
IEPV	$IEPA = S_v\left[T_{PV} - 0.2s, T_{PV} + 0.2s\right]/2.5$

Note: 1. $S_a[T_1, T_2]$ stands for the sum of 5% damped spectral acceleration from T_1 to T_2.

2. $S_v[T_1, T_2]$ stands for the sum of 5% damped spectral velocity from T_1 to T_2.

3. S_v (5%,T) is the spectral velocity value at period T.

4. T_{pv} is the period at which spectral velocity reaches maxima.

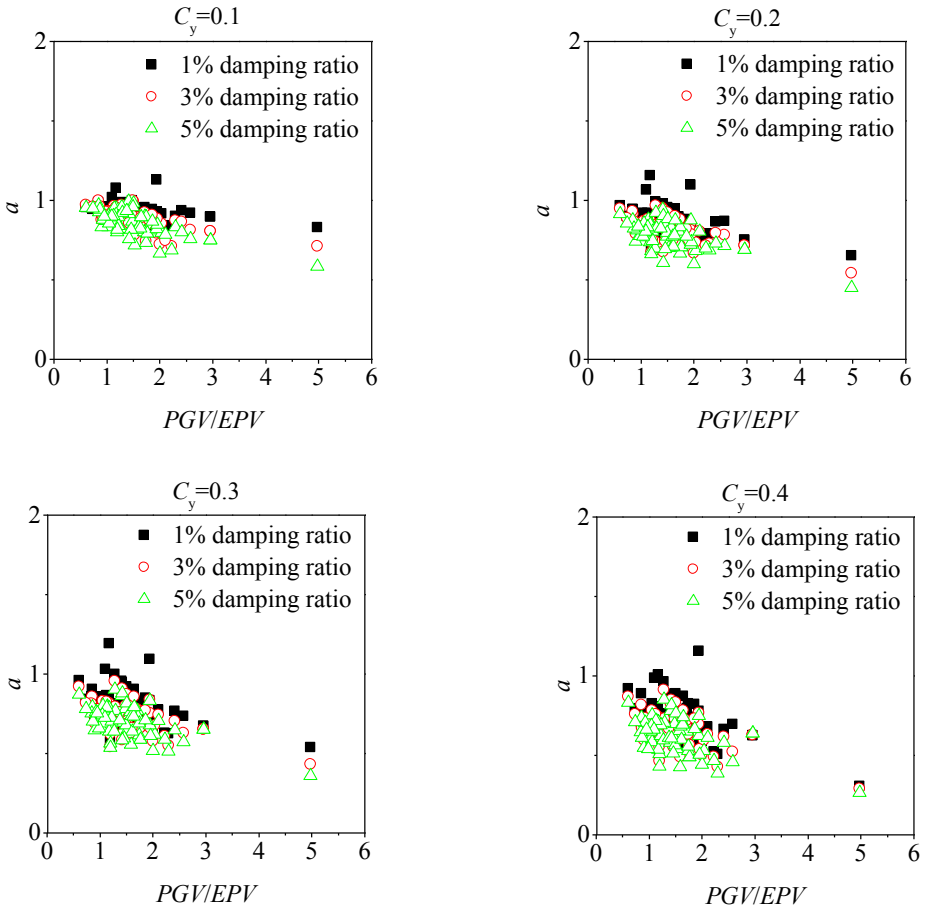

Figure 2.8 Relationship between coefficient *a* and *PGV*/*EPV*.

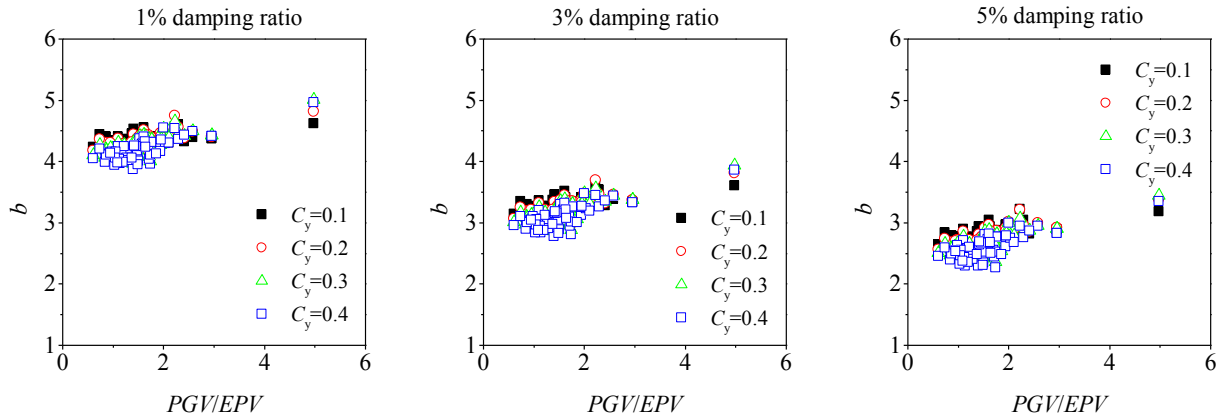

Figure 2.9 Relationship between coefficient *b* and *PGV/EPV*.

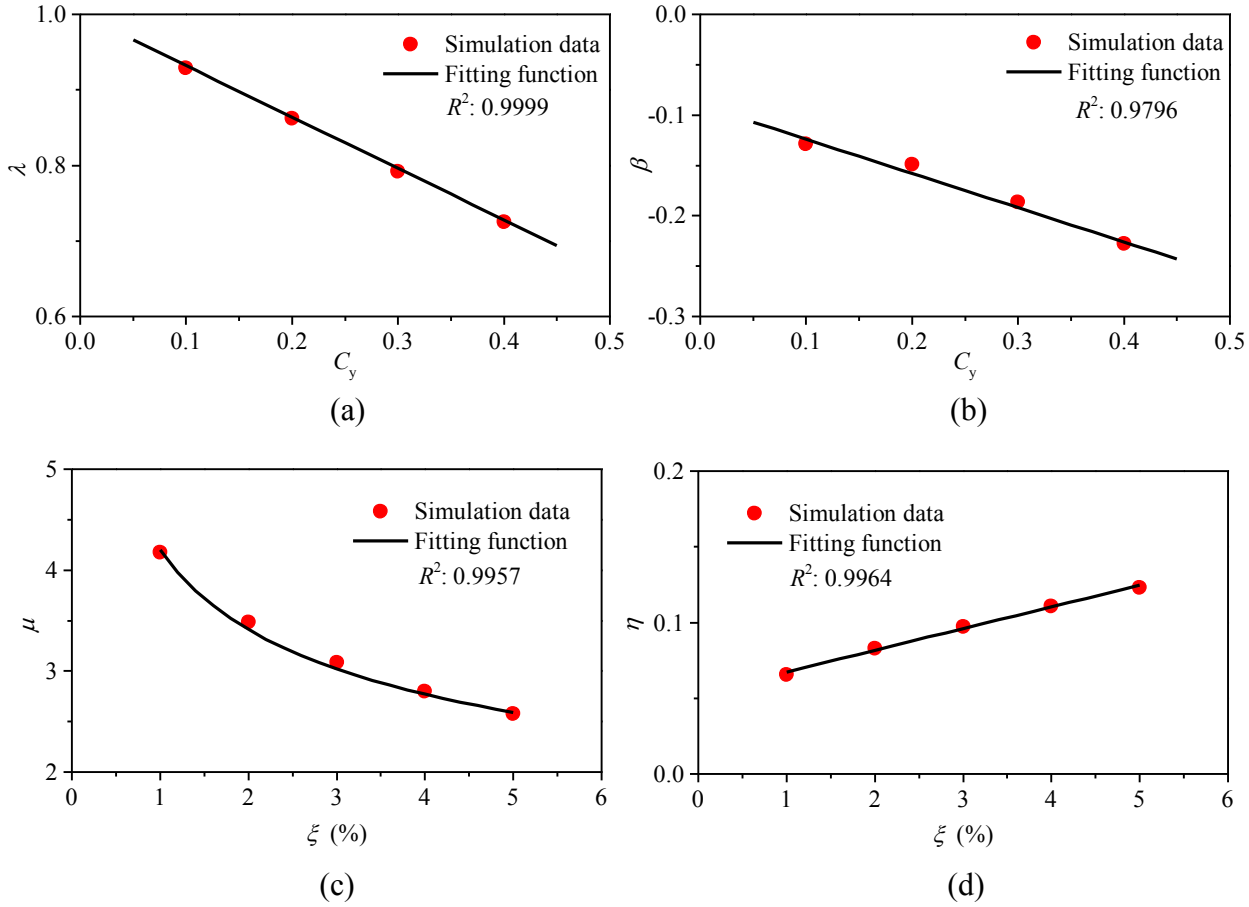

Figure 2.10 Relationship between (a) C_y and λ, (b) C_y and β, (c) ξ and μ (c), (d) ξ and η.

In the correlation analysis, *PGV/EPV* of the ground motions was found to have the strongest correlation with coefficient *a*. Figure 2.8 shows the relationship between coefficient *a* and *PGV/EPV*. The simulation also showed that the damping ratio ξ has little effect on *a*.

Thus, we can formulate coefficient a as a function of C_y and the velocity related ground motion measure as:

$$a = \lambda \left(PGV / EPV \right)^{\beta} \tag{2-12}$$

where λ and β can be modeled as linear functions of C_y (as it can be shown in Figure 2.10(a) and (b)). Thus, Eq. (2-12) can be expressed as follows:

$$a = \left(-0.682 C_y + 0.998 \right) \left(PGV / EPV \right)^{-0.335 C_y - 0.0892} \tag{2-13}$$

Figure 2.9 demonstrates that the coefficient b is also strongly related with the normalized intensity measure (PGV/EPV), and that the C_y does not affect the value of b. Thus, the normalized GM parameter PGV/EPV and the damping ratio are used as predictors of b, in the functional form as:

$$b = \mu \left(PGV / EPV \right)^{\eta} \tag{2-14}$$

where parameters (μ, η) are modeled based on the simulated data (through regression analysis) as functions of damping ratio ξ in percentage, as shown in Figure 2.10(c) and (d). Note that although the values of λ, β μ and η obtained from regression analysis of the data in Figures 2.8 and 2.9, it will be shown later in the validation example that the value of these parameters are quite general and can be applied to a completely different GM suite. Thus coefficient b can be calculated as:

$$b = 4.204 \xi^{-0.292} \left(PGV / EPV \right)^{0.0143 \xi + 0.0531} \tag{2-15}$$

It is worth noting that the IDA curve for the peak acceleration will be parallel to the vertical axis (PGV axis) after yielding for the undamped system (i.e., peak acceleration should be constant after yielding), which means the slope (k_2) should approach positive infinity. The formulation in Eq. (2-15) does ensure that the value of b approaches an infinite value when the damping ratio approaches zero.

2.5.3 Uncertainty Propagation Formulation

Through the regression and the derivation outlined above, the functional form of the IDA curve for the peak acceleration response of the elastoplastic oscillator was obtained for an individual ground motion record. In order to derive the uncertainty propagation of a GM suite that has multiple ground motion records, a simple linear transformation of the IDA curves can be performed. Recall that for an individual record, PGV was used as the ground motion intensity measure. For a GM suite, one can define the average peak ground velocity (mean of *PGVs*), i.e., $I = \sum_{1}^{n} PGV_i / n$ as the GM suite intensity measure. Note that other intensity measures such as peak ground acceleration (PGA) can also be used, and the results will only differ by a linear factor. In order to conduct uniform scaling of the suite, a normalized relative intensity vector $\mathbf{p} = \left[PGV_1, PGV_2 ... PGV_n\right] / I$ that represents the relative PGV magnitude of all records within the suite can be defined. This normalized relative intensity vector **p** will be kept unchanged during the scaling process. The PGV of the i^{th} individual ground motion can be calculated as $I \times p_i$ given the suite intensity I.

The IDA curve parameters k_0, k_2, and I_y (derived using the individual record PGV as the intensity measure) can be transformed into the suite IDA curve (the suite average PGV is used as the intensity measure). The formula is below:

$$k_0' = \frac{k_0}{p_i} \tag{2-16}$$

$$k_2' = \frac{k_2}{p_i} \tag{2-17}$$

$$I_y' = \frac{I_y}{p_i} \tag{2-18}$$

where k_0' , k_2' and I_y' are the IDA curve parameters when plotted using the suite average PGV as the intensity measure. After this transformation, the analytical function of individual IDA curve can be obtained for the uniform scaling of the GM suite. Then the COV of the peak acceleration can be calculated analytically. Following Eq. (2-1), the uncertainty of the elastoplastic SDOF system acceleration under a given GM suite can be calculated as:

$$COV_{\mathrm{R}} = \frac{std\left(A_{\max,i=1..n}(I)\right)}{mean\left(A_{\max,i=1..n}(I)\right)}$$

$$A_{\max,i}(I) = \begin{cases} \dfrac{I}{k_0'} & I < I_{\mathrm{y}}' \\ \dfrac{I_{\mathrm{y}}'}{k_0'} + \dfrac{\left(I - I_{\mathrm{y}}'\right)}{k_2'} & I \geq I_{\mathrm{y}}' \end{cases}$$

$$k_0' = \frac{I_i}{S_{\mathrm{a}}(T,\xi)_i\, p_i} \qquad I_{\mathrm{y}}' = \frac{I_i C_{\mathrm{y}}}{S_{\mathrm{a}}(T,\xi)_i\, p_i}$$

$$k_2' = \frac{1}{p_i}\exp\left[\begin{array}{l}\left(-0.682C_{\mathrm{y}} + 0.998\right)\left(PGV_i / EPV_i\right)^{-0.335C_{\mathrm{y}} - 0.0892}\ln(T) \\ +4.204\xi^{-0.292}\left(PGV_i / EPV_i\right)^{0.0143\xi + 0.0531}\end{array}\right] \tag{2-19}$$

where I_i indicates the intensity (such as PGV) of the i^{th} individual record; $S_{\mathrm{a}}(T,\xi)_i$, PGV_i and EPV_i indicate the spectral acceleration, PGV and EPV of i^{th} ground motion record, respectively; I is the GM suite intensity for the uniform scaling that is calculated as average of all individual intensity measures. $A_{\max,i}$ indicates the peak acceleration response function for i^{th} IDA curve.

Note that if the intensity is smaller than the smallest I_y' among a GM suite, this means the structure will behave linearly for all GMs, and the COV of structural responses is constant and equals to the ξ damped COV spectrum value at T (Figure 2.5). Through this formulation, the uncertainty of structural responses can be completely determined by the structural system (T, C_{y}, and ξ) and the intensity-independent GM suite parameters (PGV/EPV and $I_0/S_{\mathrm{a}}(T,\xi)$). Thus, for a given structure, the GM uncertainty can be represented by the PGV/EPV and

$I_0/S_a(T,\xi)$ statistics of the ground motions within the suite. This essentially decouples GM uncertainty from the scaling of the GM suite.

2.6 Validation of the GM-induced Uncertainty Propagation Characterization

In order to validate the effectiveness of the GM-induced uncertainty propagation characterization method proposed, two types of validation processes were adopted in this study. Firstly, the established uncertainty propagation formulation (Eq. (2-19)) was applied to a randomly selected GM suite. This validation is needed first because the formulation and the regression parameters (Eq. (2-13) and Eq. (2-15)) were obtained using the CUREE and FEMA P695 suites. Thus, it is necessary to show that the resulting regression parameters are robust enough for any GM suites. Secondly, the equivalency of the GM uncertainty was validated by generating a GM suite that approximately has the same $I_0/S_a(T,\xi)$ and *PGV*/*EPV* statistics as the CUREE GM suite. Then, nonlinear time history simulations were performed using both GM suites to show that by matching $I_0/S_a(T,\xi)$ and *PGV*/*EPV* distribution, a matching distribution of the elastoplastic system acceleration responses can be obtained at various intensity levels. In other words, if the EDP of interest is the peak acceleration for elastoplastic SDOF systems, the two GM suites are equivalent as long as they have similar $I_0/S_a(T,\xi)$ and *PGV*/*EPV* statistics.

2.6.1 Validation of Uncertainty Propagation Formulation

For validation of the uncertainty propagation formulation, eight ground motions randomly selected from the NGA ground motion database (Chiou et al., 2008) are listed in Table 2.2. Several different elastoplastic systems were examined, including those with natural periods of 0.5s and 1.5s, 1% and 5% damping ratio, and normalized yield displacements of 0.1 and 0.4. The COV of responses calculated using the proposed uncertainty propagation formulation is presented in Figure 2.11 as dashed lines, while the real COV values simulated from the time history analysis are represented as solid lines. From the comparison in Figure

2.11, one can see that the uncertainty propagation formulation can quantitatively characterize the change in COV_R with the increasing intensity level in all cases. This is especially true for the linear and transitional intensity regions (i.e., the formulation captures COV_R trends almost perfectly for all oscillators). However, after all the records in the GM suite produce yielding of the structure, the prediction formulation may underestimate COV_R values. This underestimation is likely due to the numerical fluctuation of the simulated IDA curves in the post-yielding region, which is not captured by the elastoplastic IDA shape approximation.

2.6.2 Validation of GM Uncertainty Equivalency

GM uncertainty equivalency in this study is defined as the situation in which different GM suites produce structural responses that have the same level of uncertainty (measured by COV) at different seismic intensity levels. According to Eq. (2-19), the $I_0/S_a(T,\xi)$ and PGV/EPV were identified as the main GM parameters that control elastoplastic system acceleration response uncertainty. As a result, if these two parameters of different GM suites are similar (having similar distributions), the equivalence of uncertainty in elastoplastic system acceleration responses is ensured. In order to validate this proposed GM uncertainty equivalency, 20 GM records (named as Eq20 GM suite and listed in Table 2.3) were selected from the 1600 earthquakes in NGA ground motion database (Chiou et al., 2008). The two key parameters (I_0/S_a(1s,5%) and PGV/EPV) of these 1600 earthquake records were calculated. Based on these key parameters, the ground motions which have almost same values of the two parameters of the ground motions in CUREE GM suite were selected (the CDFs of two key parameters of Eq20 GM suite and CUREE GM suite are shown in Figure 2.12). Two different elastoplastic systems (with different C_y) were subjected to both GM suites. The COV_R trends are plotted in Figure 2.13. It can be shown that these two GM suites are truly equivalent with regard to the acceleration response uncertainty at different intensities. This result validated that

it is possible to establish quantitative uncertainty equivalency between two different GM suite using the method proposed.

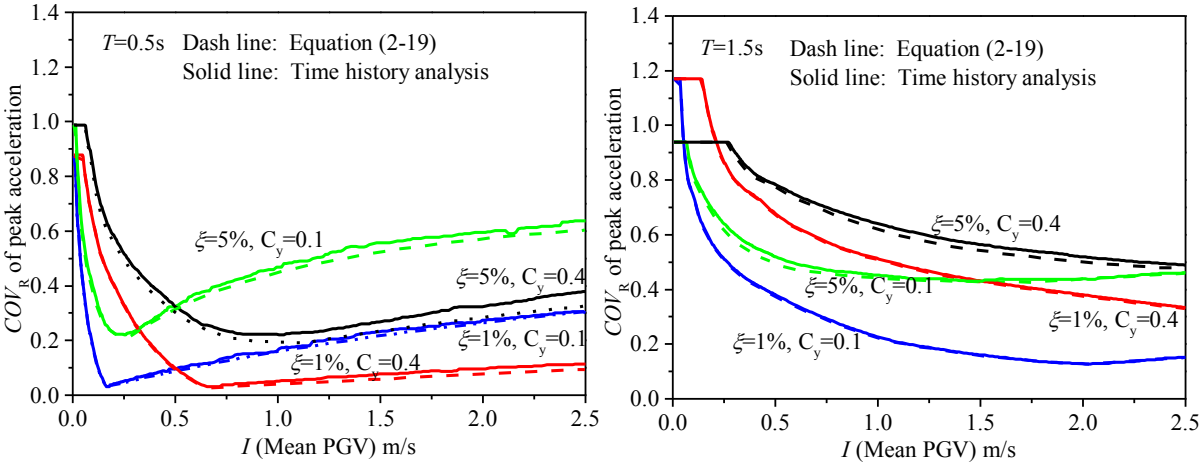

Figure 2.11 Comparisons between the real COV values and the predicted ones by the uncertainty propagation formulation for the elastoplastic SDOF systems with (a) T=0.5 s and (b) T=1.5 s.

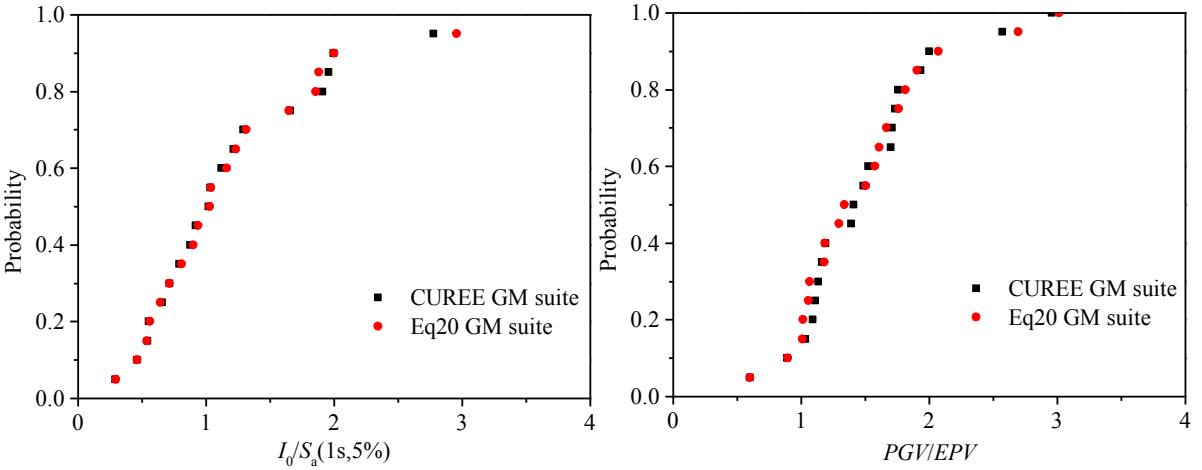

Figure 2.12 CDFs of (a) I_0/S_a(1s,5%) and (b) PGV/EPV for the CUREE suite and the Eq20 GM suite.

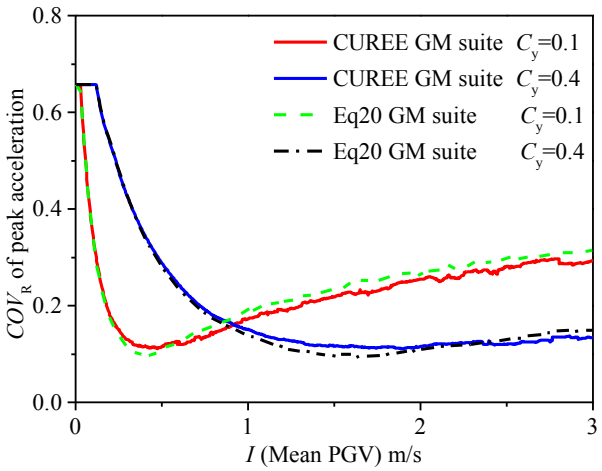

Figure 2.13 COV_R trends of two different elastoplastic systems under the CUREE suite and the Eq20 GM suite.

Table 2.2 Eight ground motions used to validate uncertainty propagation formulation

Earthquake	M	Fault	Station	Comp.
Kern County,1952	7.36	Reverse	LA - Hollywood Stor FF	090
Drama, Greece,1985	5.20	Normal Oblique	Drama	WE
Lytle Creek,1970	5.33	Reverse Oblique	Lake Hughes #1	021
Dinar Turke,1995	6.40	Normal	Cardak	076
Coalinga-01,1983	6.36	Reverse	Parkfield - Cholame 6W	000
Borrego Mtn,1968	6.63	Strike slip	LB - Terminal Island	249
Borah Peak, ID-01,1983	6.88	Normal	ANL-768 Power Plant (Bsmt)	SOU
Imperial Valley-07,1979	5.01	Strike slip	El Centro Array #6	140

Table 2.3 Twenty ground motions (Eq20 GM suite) used to validate GM uncertainty equivalency

Earthquake	M	Fault	Station	Comp.	Scaling factor
Chi-Chi Taiwan-03,1999	6.20	Reverse	TCU117	N	3.46
San Simeon CA,2003	6.52	Reverse	Buttonwillow - Hwy 58 & Wasco	H1	5.76
Loma Prieta,1989	6.93	Reverse Oblique	Emeryville; Pacific Park #2 Free Field	260	0.49
Chi-Chi Taiwan-06,1999	6.30	Reverse	CHY032	E	2.56
Kobe Japan,1995	6.90	Strike Slip	Amagasaki	090	0.78
Northridge-06,1994	5.28	Reverse	Tarzana - Cedar Hill A	090	2.91
Livermore-02,1980	5.42	Strike Slip	Antioch - 510 G St	270	5.60
Whittier Narrows-01,1987	5.99	Reverse Oblique	Beverly Hills - 14145 Mulhol	279	1.58
Kobe Japan,1995	6.90	Strike Slip	HIK	000	2.35
Superstition Hills-02,1987	6.54	Strike Slip	Westmorland Fire Sta	090	2.62
Kobe Japan,1995	6.90	Strike Slip	Fukushima	090	1.93
Chi-Chi Taiwan-06,1999	6.30	Reverse	CHY065	N	3.06
Niigata Japan, 2004	6.63	Reverse	FKS021	EW	1.91
Whittier Narrows-01,1987	5.99	Reverse Oblique	LA - 116th St School	270	0.95
Whittier Narrows-01,1987	5.99	Reverse Oblique	LA - 116th St School	360	0.85
Coalinga-01,1983	6.36	Reverse	Pleasant Valley P.P. - yard	045	0.37
Northridge-01,1994	6.69	Reverse	Sunland - Mt Gleason Ave	260	1.00
Chi-Chi Taiwan-05,1999	6.20	Reverse	CHY059	N	4.13
Superstition Hills-02,1987	6.54	Strike Slip	El Centro Imp. Co. Cent	090	0.98
Parkfield-02 CA,2004	6.00	Strike Slip	Parkfield – Joaquin Canyon	021	0.81

2.7 Summary and Conclusions

This study presented a new approach to quantify and decouple the GM uncertainty from the uniform scaling process in multi-record IDA. The uncertainty quantification approach was applied to linear system responses and elastoplastic SDOF system acceleration responses and validated using a variety of simplified structural models and GM suites. The GM-induced uncertainty propagation quantification for a given system was performed by establishing a functional relationship between the IDA curve shape and intensity-independent measures of the ground motion.

For a given linear system subjected to a GM suite, the COV_R of peak structural responses is a constant which is determined by the GM suite's COV spectrum at the linear system's dominant natural period. For elastoplastic SDOF systems, the trend of COV_R for peak acceleration responses will change with the GM suite intensity level. The uncertainty in the acceleration responses was controlled by $I_0/S_a(T,\xi)$and PGV/EPV of a GM suite and intensity-independent structural properties including the normalized yield displacement, natural period, and damping ratio. Using the formulation proposed, the GM uncertainty can be decoupled from the hazard intensity. This formulation also provides a quantitative way to establish equivalency between two GM suites with regard to structural responses.

The current study is limited in its scope that only linear system responses and the acceleration responses of elastoplastic SODF systems were considered. Although the formulation of GM-induced uncertainty is shown to be viable for simple systems, the application of the proposed approach to more complicated nonlinear systems needs to be explored in future studies. The regression formula derived in this study will need to be modified if the IDA curve is for other engineering demand parameters (such as displacement).

CHAPTER 3

UNCERTAINTY QUANTIFICATION ON BILINEAR SDOF SYSTEM DISPLACEMENT

Modified from a paper published in *Soil Dynamics and Earthquake Engineering* (Deng et al. 2017)

Peng Deng, Shiling Pei, John W. van de Lindt, and Chao Zhang

3.1 Abstract

The ability to accurately quantify uncertainty in structural system seismic responses is a critical component of performance-based earthquake engineering (PBEE). Currently, for nonlinear systems, this is achieved empirically using a large number of simulations with different excitation inputs (ground motion suites) and numerically randomized structural model samples. This study focused on one of the simplest nonlinear hysteretic systems, the bilinear single-degree-of-freedom (SDOF) oscillator, to develop a semi-closed-form solution for seismic displacement response uncertainty as a function of 1) intensity-independent ground motion characteristics, 2) structural parameters, and 3) ground motion intensity level. This approach included the development of a parametric model for bilinear system IDA curves with intensity independent ground motion parameters and structural parameters. The accuracy of the proposed model was validated through nonlinear time history analysis (NLTHA) simulations.

3.2 Introduction

As the implementation of performance-based earthquake engineering (PBEE) concepts continues to increase within the earthquake engineering community, significant emphasis has been placed on explicitly quantifying seismic response uncertainty caused by input uncertainties. There are three main sources of input uncertainty in a PBEE analysis, including (1) ground motion (GM) uncertainty (record-to-record variability), (2) structural parameter uncertainty and (3) numerical modeling uncertainty. Currently, there has not been a

unanimously agreed upon procedure in PBEE to quantify and propagate these uncertainties. Generally, the GM uncertainty, which is often assumed to be the dominant source of uncertainty (Kim and Rosowsky 2005; Kwon and Elnashai 2006; Lee and Mosalam 2005; Liel et al. 2009; Yin and Li 2010), is represented through time history analysis of structural models using a suite of site-representative ground motions (although not as many as for a typical Monte-Carlo simulation (Vamvatsikos and Fragiadakis 2010) due to high computational cost) or using simplified approximations. For example, first-order-second-moment (FOSM) approach has been used in uncertainty estimation for earthquake-induced losses (Baker and Cornell 2008; Bradley and Lee 2010); FEMA-P695 (2009) method represents GM uncertainty with a constant dispersion parameter. Most existing research studies assume that the seismic demand can be approximated as a linear function of seismic intensity in logarithmic scale, and thus the associated logarithmic standard deviation was often used to represent the GM uncertainty (Celik and Ellingwood 2010; Ellingwood and Kinali 2009; Padgett and DesRoches 2007). However, Ellingwood and Kinali (2009) found that the contribution to response uncertainty from selected GMs may depend on the hazard intensity. The mechanism of this dependence has not been studied comprehensively.

The uncertainty in structural parameters was often neglected in PBEE under the assumption that their impact is overshadowed by GM uncertainty. For example, Ellingwood and Kinali (2009) conducted a seismic risk analysis of steel frames and indicated that the randomness in structural properties can be ignored due to its insignificant influence (compared with the impact of GM suite uncertainty) on seismic demand. Celik and Ellingwood (2010) conducted seismic fragility analysis on non-ductile reinforced concrete frames using median (or mean) values of structural parameters. They found that the simulation approach is adequate for assessing the structural damage and loss estimation under moderate earthquakes. However, Yin and Li (2010) investigated the seismic collapse behavior of light-frame wood structures

and indicated that the variation in structural parameters (e.g., strength) can greatly affect the collapse probability of such structures. Dolsek (2009) conducted an incremental dynamic analysis of four-story-reinforced concrete frames and found that the uncertainty of structural parameters such as the damping and yield (or ultimate) rotation in columns has a remarkable influence on structural collapse demands. Bradley (2013) and Liel et al. (2009) reached a similar conclusion that the structural parameter uncertainty tends to have great impact if the uncertainty level is high.

Currently, there are mainly two approaches to incorporate both GM and structural parameter uncertainty for nonlinear system seismic responses. The first approach is to conduct a large number of time history simulations using nonlinear model samples representative of the structural parameter distributions. This approach is computationally intensive and atypical for design practice. The second approach is to combine GM and structural parameter uncertainty with the assumption that their impacts on response demands are independent and uncorrelated. For example, they can be combined based on classical statistics methods such as the square-root-sum-of-squares (SRSS) (FEMA-P695 2009; Fragiadakis and Vamvatsikos 2010; Vamvatsikos and Fragiadakis 2010). Although it is true that the sources of these uncertainties are independent and have no correlation, their contributions to the structural response uncertainty will interact and influence each other (i.e., coupled).

Incremental dynamic analysis (IDA) (Vamvatsikos and Cornell 2002; Vamvatsikos and Cornell 2004) is a commonly-used procedure to obtain the seismic demands as a function of seismic intensity (i.e., the IDA curve). IDA with a ground motion suite was often used to obtain the seismic demand distribution under a certain intensity (Huo and Zhang 2013) or the distribution of intensity to achieve target structural performances (i.e., fragility analysis) (Baker 2015). In this study, we investigated the relationship between structural parameters, intensity-independent GM characteristics, and the shape of the IDA curve. Then, based on this

relationship, an uncertainty propagation quantification model of bilinear SDOF system displacement was established. This model provides a semi-closed-form calculation of bilinear SDOF system displacement response uncertainty, and can potentially simplify PBEE calculations by avoiding NLTHA.

3.3 Methodology

As indicated earlier, seismic demand analysis in PBEE is often conducted by generating IDA curves that explicitly describe the relationship between the ground motion intensity and the structural response of interest. The shape of an IDA curve is determined by structural parameters and the earthquake ground motion input used. Generally, IDA curves for nonlinear systems are derived through repetitive nonlinear time history simulations which can be very computationally intensive. In this study, we seek to obtain IDA curves in a functional form as

$$R = D(\mathbf{p},\mathbf{g},I) \tag{3-1}$$

where R is the structural response of interest; I is the intensity measure; $\mathbf{p}$ is the vector consisting of influential structural parameters, $\mathbf{g}$ is the vector consisting of key GM parameters which have a significant influence on the seismic responses. Note that GM parameters in this formulation will be intensity-independent, since seismic intensity is considered as an independent parameter. Once this structural response function is constructed, the impact of structural and GM uncertainties on the response uncertainty (i.e., uncertainty propagation) can be conveniently derived based on the basic statistics theory. For example, given the known distribution (probability density function, PDF) of a structural parameter p_i (e.g., strength, stiffness, yielding point, etc.) as $PDF_{\mathrm{p}}(p_i)$, the PDF of the seismic response PDF_{R} at a given intensity I_0 (assuming GM parameters remain constant) can be calculated as

$$PDF_{\mathrm{R}} = \frac{\partial f}{\partial p_i} PDF_{\mathrm{p}}\left(p_i\right) \tag{3-2}$$

Similarly, the fragility for a given response performance target can also be calculated as

$$P\left(R \geq \text{target} \middle| I = x\right) = \int_{\text{target}}^{\infty} PDF_{\text{R}}\, dR \tag{3-3}$$

Evidently, these estimations can be done without running NLTHA once Eq. (3-1) can be expressed as a closed-form function for a given family of systems. However, as it will be shown in the next section, the IDA curve for a nonlinear system (even as simple as a bilinear system) does not have a convenient closed-form format, and will need to be approximated through the regression analysis. Thus Eqs. (3-2) and (3-3) will need to be evaluated numerically. In spite of this, the parametric study of the IDA curves will provide insights into uncertainty propagation in PBEE. In this study, the bilinear SDOF system was selected because it can be used to represent a wide range of nonlinear systems, while still simple enough to illustrate the core concept proposed in this study. The ultimate objective of this study is to enable the calculation of a bilinear system fragility and displacement response distributions conditional on the seismic intensity level in a semi-closed-form way relying only on a few key parameters related to the structure and the suite of ground motions used, without performing nonlinear time history analysis.

3.4 Bilinear SDOF System Characterizations

A bilinear SDOF system without strength deterioration is one of the simplest nonlinear systems in structural dynamics. A bilinear SDOF oscillator is generally defined by its initial stiffness, yield displacement, post-yield stiffness, mass, and damping ratio. For this study, the uncertainty quantification formulation requires the input parameters for Eq. (3-1) to be independent of each other. Thus it is beneficial to define the structural systems through ground motion-independent and dimensionless structural parameters. Four structural parameters were selected in this study, namely the initial elastic period (T), the damping ratio (ξ), the hardening

ratio (α) (defined as the post-yielding stiffness divided by the initial stiffness) and a yield displacement coefficient (C_y) defined as

$$C_y = \frac{d_y}{mg/k} = \frac{(2\pi)^2}{g}\frac{d_y}{T^2} \tag{3-4}$$

where d_y is the yielding displacement; m is the mass of the system; k is the initial stiffness. As shown in Eq. (3-4), C_y is a dimensionless parameter only dependent on d_y and T. Thus for the bilinear system discussed in this study, the structural parameter vector **p** conceptually presented in Eq. (3-1) is simply (T, ξ, α, C_y).

3.5 Ground Motion Characterizations

Because ground motions are non-stationary time series, it is very challenging to fully characterize them with a limited number of parameters. Considering the formulation of an IDA curve as shown in Eq. (3-1), the key GM parameter vector **g** in that formulation must be decoupled from the seismic intensity. Traditionally, GM characteristic indicators such as peak ground acceleration (PGA) and spectral acceleration (S_a) were used to characterize ground motion excitations. But these indicators are also measures of ground motion intensity, which means that fundamentally they cannot be the control parameters for the shape of the IDA curve. A common approach to constructing intensity-independent GM parameters is to use the ratio between two GM intensity measures, such as PGA/PGV. A large group of potential GM intensity measures worthy to be considered can be found in existing studies (Riddell 2007; Yang et al. 2009).

Initially, a closed-form expression of Eq. (3-1) was proposed (which will be presented in detail in the next section) to quantitatively describe the shape of IDA curves. Then a series of trial-and-error correlation analyses for a given system between the GM parameters (from the large pool of potential parameters from existing studies) and proposed IDA curve quantification function were conducted. The key GM parameters were then selected based on

the coefficient of determination (R^2), which represents the statistical measure of the goodness-of-fit. The objective of this process is to identify a group of key GM parameters that have significant influences on the shape of the IDA curves.

In order to conduct the needed regression analysis for identification of the controlling GM parameters, a GM suite of 102 ground motions (80 far-field (ordinary) ground motions from an existing study (Medina and Krawinkler 2004) combined with 22 far-field records in FEMA-P695 (2009)) was adopted in this study (original unscaled spectral accelerations of these ground motions are shown in Figure 3.1). It is important that the formulation proposed in Eq. (3-1) has the generality against GM selection, which means that if the controlling GM parameters were identified using the regression analysis from this 102-record suite, the obtained regression formula should also work for IDA curves generated with other GM records. This "portability" of the GM parameters will be validated in the example case study later where a different GM suite was used.

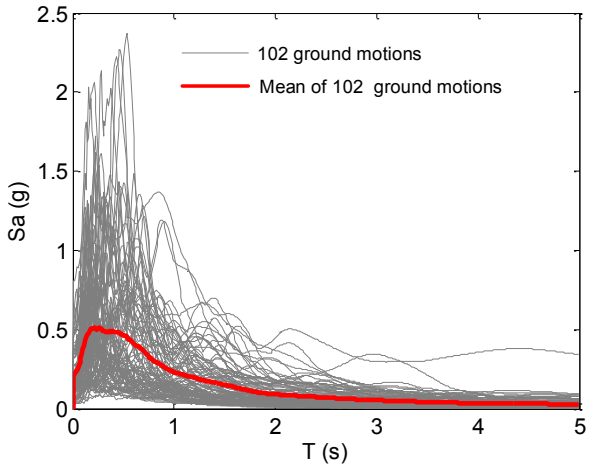

Figure 3.1. Acceleration response spectra of 102 earthquake records.

3.6 Modeling IDA Curves for Bilinear SDOF Systems

As mentioned earlier, the shape of the IDA curve is determined by structural parameters **p** and the key GM parameter vector **g**. In IDA, a wide range of intensity measures (IM) can be

used, including Peak Ground Acceleration (PGA), Peak Ground Velocity (PGV), and $S_a(T,5\%)$ (the 5% damped spectral acceleration value at the first period of the structure) (Vamvatsikos and Cornell 2002). For this study, an intensity measure independent of structural parameters will be ideal so that $S_a(T,5\%)$ was not selected as the intensity measure. For a given ground motion record, PGA and other intensity measures (such as PGV) can be related by a constant factor as the ground motion scales. The selection of a particular intensity measure does not affect the analysis process and results. Thus, PGA was used as the intensity measure for the subsequent analysis. For the structural response, the peak displacement is considered here because it is often correlated with structural damages (e.g., performance levels defined by building drift in FEMA356 (2000)) and has a wide application in PBEE.

The IDA curves of bilinear systems consist of two segments: a linear segment and a nonlinear segment. The curve transits from the linear to the nonlinear segment when the intensity increases to the point at which the system yields. Real structural systems will reach their ultimate strength after yielding and then collapse. This can be captured if the numerical model used to generate IDA curves has a collapse mechanism incorporated. In most PBEE studies, the collapse is only numerically approximated by having a non-convergence situation, resulting in IDA curves pointing towards very large deformation in a small intensity increment (Baker 2015; Christovasilis et al. 2009; Vamvatsikos and Cornell 2002; Vamvatsikos and Cornell 2004). For the ideal bilinear systems considered in this study, NLTHA will always converge and the IDA curve will asymptotically approach a straight line. The mechanism behind this phenomenon is that when the earthquake intensity approaches a very large value, the post-yield stiffness of the system will dominate the behavior of the system. The bilinear system under extremely large ground motions can be viewed as a linear system with the post-yield stiffness as its elastic stiffness and certain level of hysteretic damping (Hadjian 1982; Iwan 1980). Figure 3.2 shows IDA curves for a bilinear SDOF system under different ground

motion excitations. The hysteretic responses of the system at different points on the IDA curves (representing different stages of the oscillator) are also shown. It can be seen from the selected hysteresis plots at different intensity levels that the shape of bilinear system hysteresis will approach a narrow parallelogram as intensity increases, eventually resulting in a response similar to a linear system with the post-yield stiffness as its elastic stiffness and additional hysteretic damping.

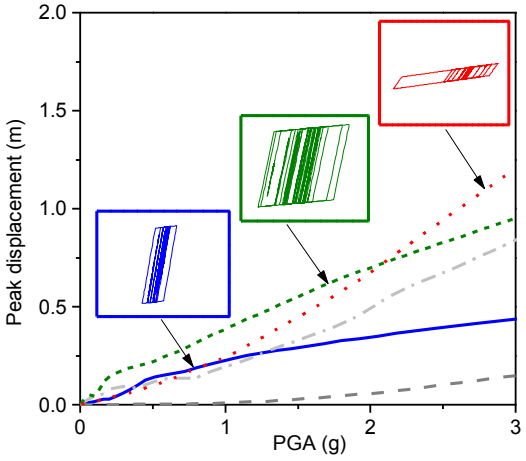

Figure 3.2 Typical IDA curves of bilinear SDOF systems and their corresponding hysteretic characteristics.

Based on these observations, a formulation for the bilinear system IDA curve was proposed as:

$$D(\mathbf{p},\mathbf{g},I)=\begin{cases} k_1 I & I<I_y \\ a\left(b^{-I+I_y}-1\right)+c\left(I-I_y\right)+k_1 I_y & I\geq I_y \end{cases} \tag{3-5}$$

where D ($\mathbf{p}$,$\mathbf{g}$,I) is the peak displacement demand of bilinear systems given the seismic intensity I , structural parameter vector **p,** and key GM parameter vector **g**. The parameters a, b, c are the undetermined coefficients which would be controlled by **p** and **g** (the functional relationship will be developed in the later section). This formula consists of the exponential part and linear part, separated by the yielding intensity level. k_1 is the slope of the linear portion of the IDA curve (showed in Eq. (3-6)), which is dependent on the structural parameter T and ξ and GMs.

Thus, with a known bilinear system, k_1 can be seen as a key GM parameter in **g** vector for linear part of IDA curves.

$$k_1 = \frac{S_{\mathrm{d}}\left(T,\xi\right)}{I_0} \tag{3-6}$$

where I_0 indicates the intensity value of the original (unscaled) ground motion. $S_{\mathrm{d}}(T,\xi)$ is the ξ damped spectral displacement value of the original (unscaled) ground motion at the linear period of the system (its unit is m, which is corresponding to peak displacement response). The corresponding I_{y} (the seismic intensity value under which the system reaches the yield condition) can be formulated as

$$I_{\mathrm{y}} = \frac{d_{\mathrm{y}}}{S_{\mathrm{D}}\left(T,\xi\right)} I_0 = \frac{\omega^2 d_{\mathrm{y}} I_0}{g S_{\mathrm{a}}\left(T,\xi\right)} = \frac{I_0 C_{\mathrm{y}}}{S_{\mathrm{a}}\left(T,\xi\right)} \tag{3-7}$$

d_{y} is the yield displacement of the bilinear systems. $S_{\mathrm{a}}(T,\xi)$ is the ξ damped spectral acceleration value of the original (unscaled) ground motion at the linear period of the structure (unit g), which can be obtained by multiplying ω^2 by $S_{\mathrm{d}}(T, \xi)$ (Chopra 2012). ω is the natural circular frequency, g is the acceleration of gravity, C_{y} is the yield displacement coefficient. From Eqs. (3-6) and (3-7), one can learn that both k_1 and I_{y} can be calculated using the unscaled ground motion

For the nonlinear segment of bilinear system IDA curves, the quantitative formulation is generalized with several modeling coefficients (a, b, and c) that need to be determined based on true bilinear system IDA responses. In this section, the influences of GM parameters on these model coefficients were investigated through the correlation analysis for different structural variables. The formula for the bilinear system IDA curves was obtained through regression of the correlation analysis simulation results. For bilinear system characteristics, the damping ratio (ξ) varied from 1% to 5% for the analysis, which covers the damping ratio values

of most real buildings. The hardening ratio (α) took values at 0.01, 0.05 and 0.1. The elastic periods (T) ranged from 0.1s to 1.5s, with an interval of 0.1s.

3.6.1 Impact of Bilinear System Parameters on the IDA Curve Modeling Coefficients

Structural parameters of a bilinear system include the damping ratio (ξ), hardening ratio (α), yield displacement coefficient (C_y), and initial elastic period (T). Changes in these parameters will affect the shape of the IDA curve. Interestingly, C_y did not affect the shape of the IDA curve, but simply stretched or compressed the IDA curve relative to seismic intensity (if other structural parameters remain unchanged). For example, Figure 3.3(a) shows two IDA curves generated using the same ground motion input but different systems with the structure parameter C_y=0.2 and 0.4 (T=1s, α=0.05, ξ =3%). The shapes of the two curves look different at first glance. But when the curve with C_y=0.4 was compressed along the both axes with a factor of 2, it overlapped the IDA curve with C_y=0.2 completely (Figure 3.3(b)). It can further be derived that the IDA curve with C_y=0.4 is identical to the IDA curve with C_y=0.2 stretched. The reason is that two bilinear systems that only differ in C_y value are proportional to each other in their load-displacement relationship. Thus, a "scalable" relationship exists between their corresponding IDA curves as it is shown in Figure 3.3.

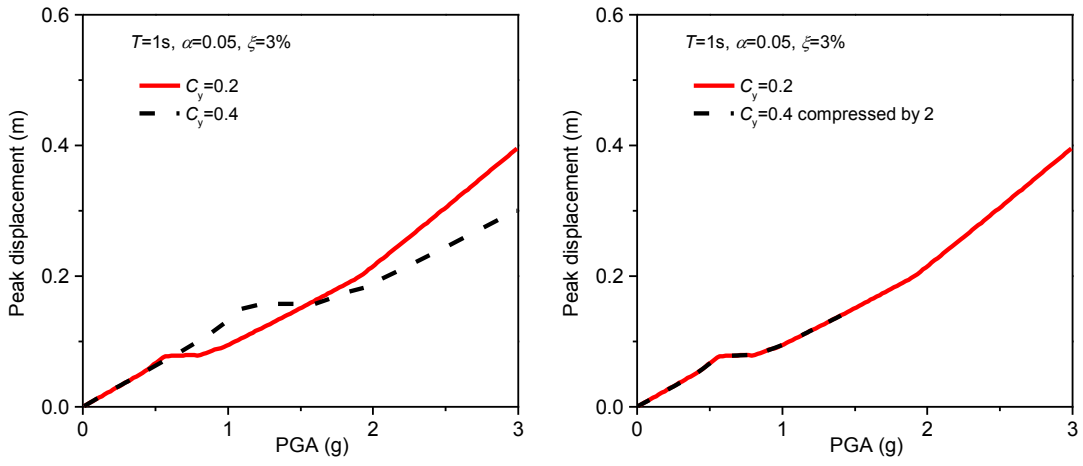

(a) (b)

Figure 3.3 (a) Comparison of two IDA curves with two values of C_y and (b) the relationship between IDA curves and C_y.

Thus, the yield displacement coefficient can be decoupled from the IDA curve quantification formulation, deducing it as

$$D'\left(\mathbf{p}',\mathbf{g},I\right)=\lambda\times D\left(\mathbf{p},\mathbf{g},\frac{I}{\lambda}\right) \tag{3-8}$$

$$\lambda=\frac{C_{\mathrm{y}}'}{C_{\mathrm{y}}} \tag{3-9}$$

where λ means the ratio of C_{y}' and C_{y}. *D'* is the bilinear IDA curve with structural parameter vector **p'** (C_{y}' is in **p'** while C_{y} is in **p**). Thus, the structural parameter of yield displacement coefficient can be regarded as a constant in the later regression analysis. Any other cases with different yield displacement coefficients can be calculated in the initial case. Table 3.1 summarizes the values of the yield displacement coefficient used in the analysis.

Table 3.1 Values of C_{y} corresponding to bilinear systems with different natural periods

T(s)	0.1	0.2	0.3	0.4	0.5	0.6	0.7	0.8	0.9	1	1.1	1.2	1.3	1.4	1.5
C_{y}	0.80	0.40	0.27	0.20	0.16	0.13	0.16	0.13	0.10	0.08	0.07	0.06	0.05	0.04	0.04

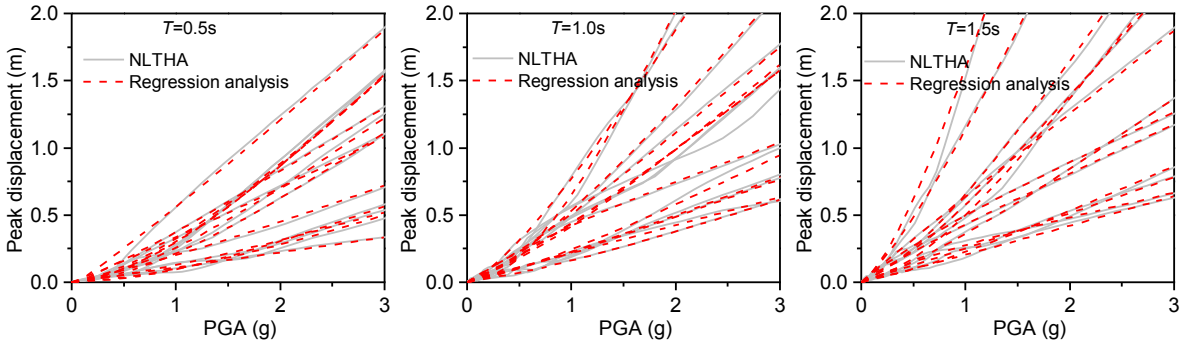

(a) (b) (c)

Figure 3.4 IDA curves of bilinear systems with (a) *T*=0.5 s, (b) *T*=1.0 s and (c) *T*=1.5 s.

Regarding the nonlinear segment of an IDA curve, the elastic period of the system has a notable influence on the curvature. Figure 3.4 illustrates the change of the degree of curvature of IDA curves for a bilinear system with three different natural periods. It can be seen that the degree of curvature for the IDA curves is positively correlated with the natural period of the system. Furthermore, through a large number of trial-and-error regression analyses, a relatively

simple relationship between coefficient b and natural period T was determined, yielding reasonable prediction accuracy (as shown in Figure 3.4):

$$b = T + 2 \tag{3-10}$$

3.6.2 Impact of GM Parameters on the IDA Curve Modeling Coefficients

Similar to structural parameters, the ground motion parameters also affect the shape of the IDA curves. As described earlier, these parameters are not as readily defined as the structural parameters did and must be sought through correlation analyses. Specifically to the bilinear system IDA curve formulation in Eq. (3-5), there are still two undetermined modeling coefficients, namely a and c, that can be formulated as functions of structural and GM parameters. It is assumed that a and c are power functions of GM parameters g_1 and g_2, respectively

$$a = a_1 \left(g_1 \right)^{a_2} \tag{3-11}$$

$$c = c_1 \left(g_2 \right)^{c_2} \tag{3-12}$$

where a_1, a_2, c_1 and c_2 are the coefficients which are only dependent on the specific structural parameters regardless of GMs. This type of formulations has the advantage that it can decouple the influence of the GM parameters and structural parameters on the IDA curves, which means that the impact of GM and structural parameters on the structural response is explicitly expressed. When a bilinear system is given, different ground motions with the same value of these two GM parameters (g_1 and g_2) as well as the k_1 parameter will generate very similar IDA curves. Thus, the GM parameter vector **g,** namely (g_1, g_2, k_1), is sufficient to characterize seismically-induced response uncertainty for bilinear SDOF systems.

A series of correlation analyses were conducted using the 102 GM suite with different intensity-independent GM parameters (the ratios of two intensity measures). The final GM parameters were selected from a group of (93 combinations of intensity measures from Riddell

(2007) and Yang et al. (2009)) intensity-independent GM parameters through a series of trial-and-error regression analyses. The one showing the strongest correlation based on the formulation was chosen. It was discovered that the coefficient a and c can be correlated with α_{sq}/v_{sq} and PGA/PGV respectively, where α_{sq} and v_{sq} are the integral values of the square of ground motion acceleration (unit: g) and velocity (unit: m/s) in the whole earthquake duration respectively. Figures 3.5 and 3.6 illustrate the correlation between two coefficients and identified GM parameters for an array of bilinear systems based on the statistical measure of the goodness-of-fit (R^2).

Based on observations from Figures 3.5 and 3.6, regression formulations for a and c can be proposed as:

$$a = a_1 \left(\frac{\alpha_{sq}}{v_{sq}} \right)^{a_2} \tag{3-13}$$

$$c = c_1 \left(\frac{PGA}{PGV} \right)^{c_2} \tag{3-14}$$

where a_1, a_2, c_1, c_2 are the coefficients which can be linked with structural parameters, namely natural period, damping ratio and hardening ratio. Note that because the impact of C_y was determined earlier, these four coefficients were independent of C_y. Figure 3.7 shows trends of these four coefficients with respect to structural parameters. All these correlations and trends were generated based on simulation data using the 102 GM suite.

From Figure 3.7, one can see that the value of a_1 is affected by the damping ratio and hardening ratio. However, the value of a_1 remains mostly constant for longer-than-0.2s structures with 0.05 to 0.1 hardening ratio while a_1 is decreasing with T increasing for the cases with σ=0.01. The value of a_2 tends to be closely related to the hardening ratio instead of

damping ratio. Apparently, c_1 increases with T increasing and is affected by both damping ratio and hardening ratio. Compared with a_2, c_2 has a similar trend with T but is more disperse.

Through the regression results and observations of the trends, the final parametric model for bilinear system IDA curves is

$$D_i\left(\mathbf{p},\mathbf{g},I\right)=\begin{cases} k_1 I & I<I_{\mathrm{y}} \\ a_1\left(\dfrac{\alpha_{\mathrm{sq}}}{v_{\mathrm{sq}}}\right)^{a_2}\left(\left(T+2\right)^{\left(-I+I_{\mathrm{y}}\right)}-1\right)+c_1\left(\dfrac{PGA}{PGV}\right)^{c_2}\left(I-I_{\mathrm{y}}\right)+k_1 I_{\mathrm{y}} & I\geq I_{\mathrm{y}} \end{cases} \tag{3-15}$$

where D_i means the peak displacement response formulation of the i^{th} individual record. k_1 and I_{y} can be derived from Eqs. (3-6) and (3-7), respectively. Structural parameter vector $\mathbf{p}$ is (T, ξ, α, C_{y}) while GM parameter vector $\mathbf{g}$ is ($\alpha_{\mathrm{sq}}/v_{\mathrm{sq}}$, PGA/PGV, k_1). The value of coefficients a_1, a_2, c_1 and c_2 were obtained based on Figure 3.7 and linear interpolation can be used for other values of the structural parameters. With this semi-closed-form formulation, multi-record IDA curves can be generated easily if the structural and GM parameters are known. These parametric IDA curves can form the basis for further PBEE evaluations such as fragility analysis. Response uncertainty is often quantified by the logarithmic standard deviation of the structural responses at a certain hazard level. This quantification assumes that the responses under a ground motion suite in which records have been scaled to a hazard level are lognormally distributed. Thus, response uncertainty can be calculated in closed-form as:

$$\beta=f\left(D_{i=1..n}\left(\mathbf{p},\mathbf{g},I\right)\middle|I=x\right) \tag{3-16}$$

where $f()$ indicates the lognormal standard deviation of the responses for n records at intensity $I=x$. This quantification of the seismic response uncertainty will be used in this study to validate the accuracy of the proposed formulations in uncertainty estimation when compared to the traditional NLTHA approach.

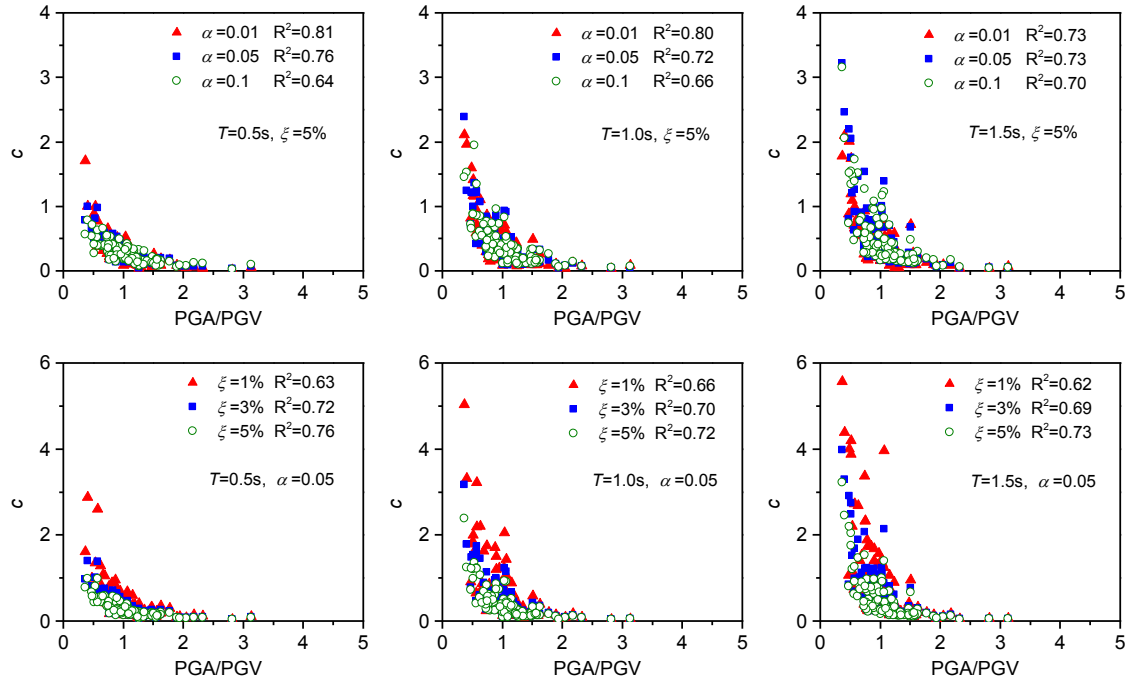

Figure 3.5 Relationship between *PGA*/*PGV* and parameter *c* in different natural periods, hardening ratios and damping ratios.

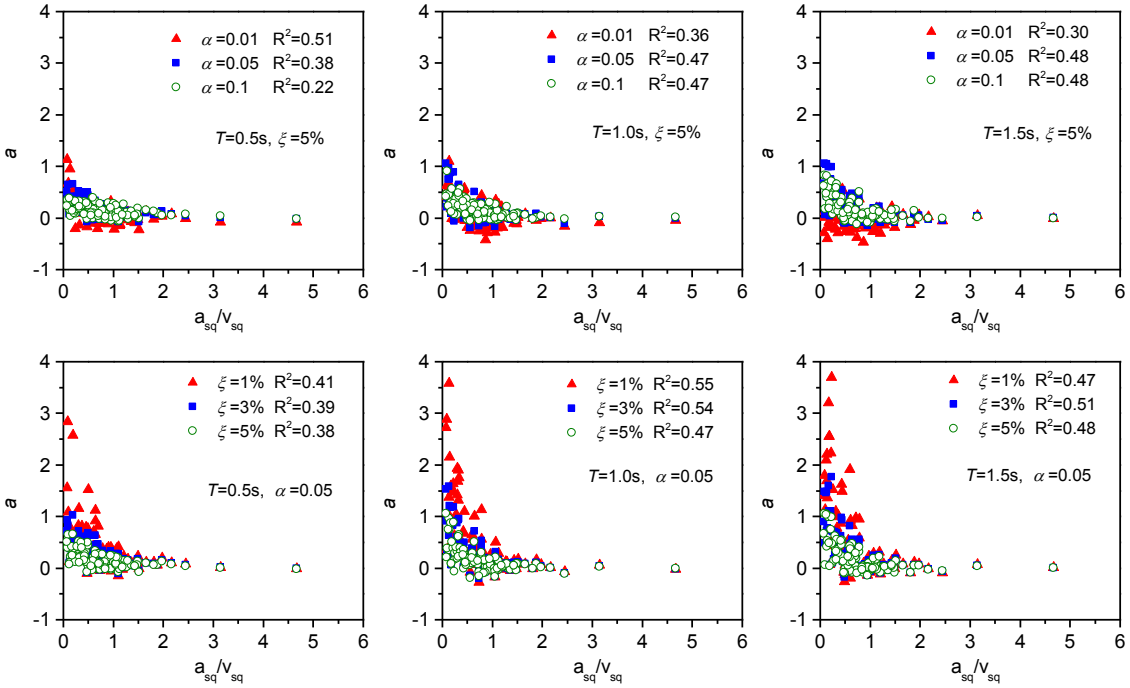

Figure 3.6 Relationship between α_{sq}/v_{sq} and parameter *a* in different natural periods, hardening ratios and damping ratios.

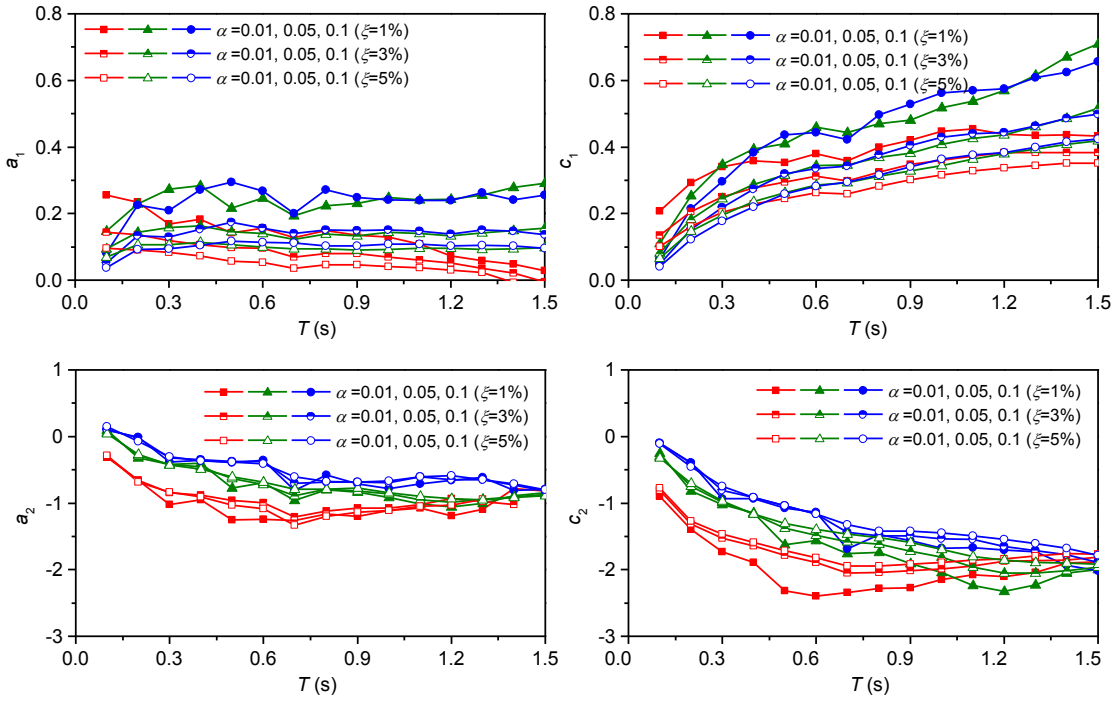

Figure 3.7 Values of a_1, a_2, c_1 and c_2 for different structural parameters.

3.7 Model Validation

3.7.1 Validation of Uncertainty Quantification Formulations

The concept of formulating a semi-closed-form IDA curve formulation outlined in Eq. (3-15) needs to be general so that the formulation will yield accurate results for any given ground motion suites. Since the calibration of the formula was conducted using a specific GM suite containing 102 GMs, the first step of model validation is to test the accuracy of the proposed formulation using other ground motion suites. Because the ultimate objective of the proposed formulation is to help quantify the uncertainty in PBEE with the satisfactory accuracy compared to NLTHA, the response uncertainty values derived using Eqs. (3-15) and (3-16) were compared to the results generated using NLTHA simulations. In this validation example, ten new ground motions (referred to here as PEER10, list on Table 3.2) were randomly selected from the NGA ground motion database (Chiou et al. 2008), and are not part of the original 102 ground motions used to derive the formulation. Multiple bilinear systems with different structural parameter values were used in the validation analysis. Figure 3.8 shows the

comparison results from the proposed formula and NLTHA. It is clear that the response uncertainty changes with intensity levels, which is captured by both the formulation and simulation. The response uncertainty (β_{RU}) initially remains constant when the seismic response demands are all linear, and then decreases after the system yields. As the intensity increases to a certain value, the uncertainty starts gradually increasing to a constant value and remains approximately at that level. From these observations, one can conclude that the response uncertainty will change with intensity levels. Results in Figure 3.8 also demonstrate that the proposed uncertainty quantification formulations can reasonably capture the change in response uncertainty with the seismic intensity increasing.

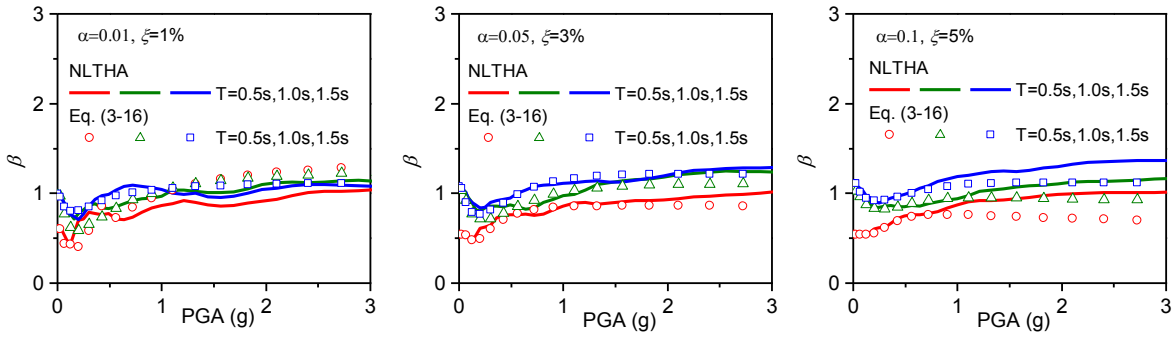

(a) (b) (c)

Figure 3.8 Comparison results from uncertainty quantification formulas and NLTHA.

Table 3.2 Ten ground motions used to validate uncertainty quantification formulations

Earthquake	Year	M	Fault	Station	Comp.
Northridge-01	1994	6.69	Reverse	Tarzana - Cedar Hill A	360
Kobe, Japan	1995	6.90	Strike slip	Yae	090
9154141	2000	4.51	Normal	Salton Sea Wildlife Refuge	HHE
Gazli, USSR	1976	6.80	Reverse	Karakyr	000
10321561	2008	4.19	Strike slip	Salton Sea Wildlife Refuge	HLN
10321561	2008	4.19	Strike slip	Meloland E Holton Rd.	HHN
14295380	2007	4.06	Strike slip	Meloland E Holton Rd.	HHN
Chi-Chi Taiwan-02	1999	5.90	Reverse	ILA003	03W
Taiwan SMART1(5)	1981	5.90	Reverse	SMART1 M03	3NS
14383980	2008	5.39	Reverse Oblique	Hemet - Acacia & Stanford	090

3.7.2 Validation of GM Suite Equivalency

The second step for validation is to test the GM suite equivalency, which can be used as the criteria for ground motion selection in PBEE analyses. The basic premise from the proposed formulation is that if two GM suites have similar distributions of GM parameters identified in the formulation, they should be able to produce similar levels of uncertainty in the given structural responses. In terms of ground motion selection, Baker (2011) proposed a conditional mean spectrum (CMS) to assess the difference of ground motions based on the parameter ε on spectral shape. This is an assessment approach mainly focusing on the spectral acceleration. Bradley (2010; 2012) proposed a generalized conditional intensity measure (GCIM) approach through comparing the distribution of the identified intensity measures of ground motion suite with the target GCIM distribution. Currently, there is a lack of quantitative criteria to compare different GM suites in the context of uncertainty of nonlinear structural responses. Recall that the key GM parameters $\mathbf{g} = (\alpha_{sq}/v_{sq}, PGA/PGV, k_1)$ for bilinear SODF systems were identified in the formulation earlier, thus one can establish equivalency in the GM uncertainty by comparing the distributions of these key GM parameters in different ground motion suites. If these key parameters are similar between two GM suites, the response uncertainties from these GM suites will be equivalent based on the formulation prediction.

In order to validate this assumption, eight GM records (named as PEER8) were randomly selected from the NGA ground motion database (Chiou et al. 2008) (see Table 3.3) to be the prototype GM suite. Again, these records are not part of the 102 ground motion records used to derive the formulation. Based on matching the distribution of the three key GM parameters of PEER8, three different GM suites (list on Table 3.4, 3.5 and 3.6) were selected from NGA ground motion database for three different bilinear SDOF systems (see Figure 3.9). Figure 3.9 illustrates that PEER8 GM suite and corresponding GM suite for each system did impose an equivalent level of the seismic response uncertainty across all intensity levels. It is

worth noting that the initial uncertainties which are calculated from elastic seismic responses in Figure 3.9(b) do not completely overlap. The reason is that the CDFs of GM parameter k_1 which determines the slope of the elastic part of the IDA curves have a small deviation. We can also conclude that for linear SDOF systems, the equivalency of GM suites is strictly satisfied if the distributions of k_1 are identical.

Table 3.3 Information about PEER8 GM suite

Earthquake	Year	M	Fault	Station	Comp.
Kern County	1952	7.36	Reverse	LA - Hollywood Stor FF	090
Drama, Greece	1985	5.20	Normal Oblique	Drama	WE
Lytle Creek	1970	5.33	Reverse Oblique	Lake Hughes #1	021
Dinar Turke	1995	6.40	Normal	Cardak	076
Coalinga-01	1983	6.36	Reverse	Parkfield - Cholame 6W	000
Borrego Mtn	1968	6.63	Strike slip	LB - Terminal Island	249
Borah Peak, ID-01	1983	6.88	Normal	ANL-768 Power Plant (Bsmt)	SOU
Imperial Valley-07	1979	5.01	Strike slip	El Centro Array #6	140

Table 3.4 Information about Equivalent EQs1 GM suite

Earthquakes	Year	M	Fault	Station	Comp.
Taiwan SMART1(33)	1985	5.80	Normal	SMART1 I08	8DN
Chi-Chi Taiwan-04	1999	6.20	strike slip	CHY034	34N
Yorba Linda	2002	4.27	strike slip	Compton - Long Beach & Palmer	H2
14095628	2004	5.03	strike slip	Mammoth	HLN
Chi-Chi Taiwan-03	1999	6.20	Reverse	TTN048	48W
Whittier Narrows-01	1987	5.99	Reverse Oblique	Tarzana - Cedar Hill	090
Northwest China-02	1997	5.93	Normal	Jiashi	000
Tottori Japan	2000	6.61	strike slip	HYG016	6NS

Table 3.5 Information about Equivalent EQs2 GM suite

Earthquakes	Year	M	Fault	Station	Comp.
Yorba Linda	2002	4.27	strike slip	Los Angeles - 7th & San Julian	H2
Chi-Chi Taiwan-04	1999	6.20	strike slip	CHY034	34N
Imperial Valley-06	1979	6.53	strike slip	Aeropuerto Mexicali	315
Taiwan SMART1(5)	1981	5.90	Reverse	SMART1 M03	3NS
Tottori Japan	2000	6.61	strike slip	OIT015	5EW
Lytle Creek	1970	5.33	Reverse Oblique	Colton - So Cal Edison	180
Imperial Valley-07	1979	5.01	strike slip	El Centro Array #1	140
Chi-Chi Taiwan-02	1999	5.90	Reverse	CHY078	78N

Table 3.6 Information about Equivalent EQs3 GM suite

Earthquakes	Year	M	Fault	Station	Comp.
14151344	2005	5.2	strike slip	North Shore Salton Sea 2	HHN
Chuetsu-oki Japan	2007	6.8	Reverse	IBR016	6NS
Big Bear-02	2001	4.53	strike slip	Indio - Monroe & Carreon	011
Gazli USSR	1976	6.8	Reverse	Karakyr	090
San Fernando	1971	6.61	Reverse	Cholame - Shandon Array #8	321
10410337	2009	4.7	strike slip	Laguna Bell	HNE
Yountville	2000	5	strike slip	Benicia Fire Station #1	180
14519780	2009	5.19	strike slip	Lone Juniper Ranch	HNE

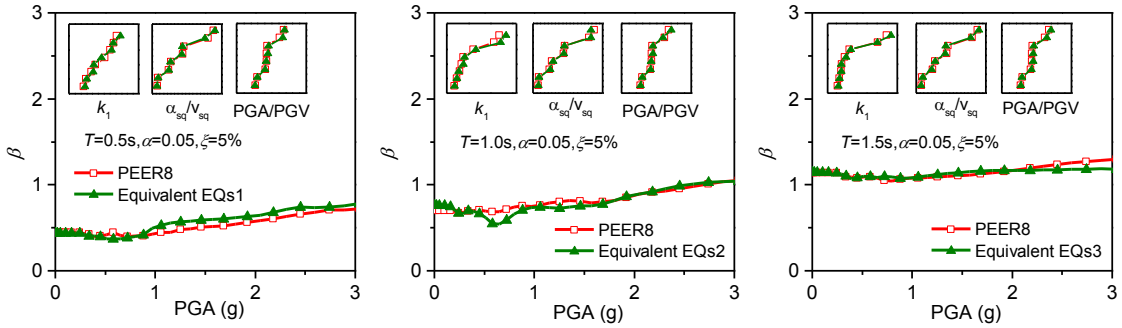

(a) (b) (c)

Figure 3.9 Validation of GM suite equivalence for bilinear systems with (a) T=0.5s, (b) T=1.0 s and (c) T=1.5 s.

3.8 PBEE Applications

The proposed uncertainty quantification formulations can be useful in several typical applications of PBEE to help generate accurate uncertainty estimations without conducting NLTHA. The following examples will illustrate some of these applications and the comparison of results between the formulations and NLTHA. The PEER10 GM suite (mentioned in section 3.7.1) was used for the example study and a bilinear system with 0.05 hardening ratio and 5% damping was used. Firstly, the shape of the IDA curves was compared in Figure 3.10, which lays the foundation for the subsequent derivation of seismic demand analyses given intensity level, and fragility analyses.

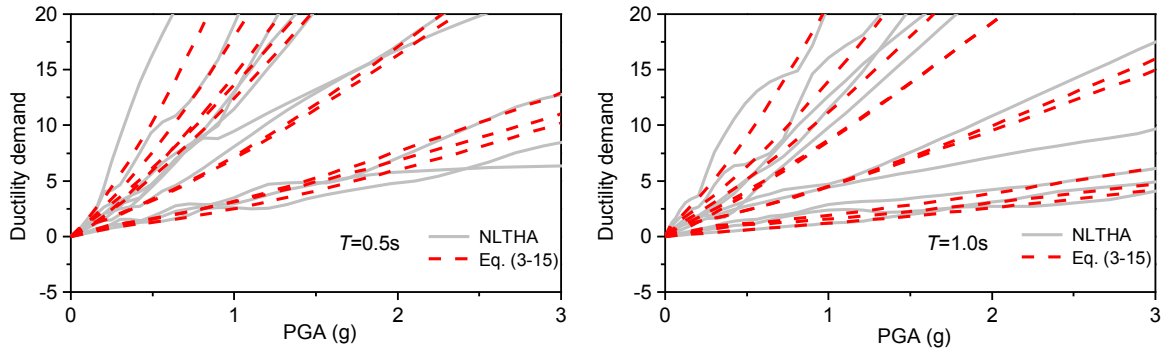

(a) (b)

Figure 3.10 IDA curves of bilinear systems with (a) T=0.5 s and (b) T=1.0 s via NLTHA and IDA curve quantification formulation Eq. (3-15).

3.8.1 Seismic Demands at Given Hazard Levels

Through the IDA curves, it is relatively straight forward to obtain the response distributions of the system under any prescribed seismic intensity levels. Take Los Angeles in California as an example, the USGS seismic hazard data (2014) indicates PGA=0.42 g for earthquakes of 10% in 50 years and PGA=0.84 g for earthquakes of 2% in 50 years. Figure 3.11 shows the response distributions (cumulative distribution function, CDF) for the two cases. It can be seen that the CDFs simulated through NLTHA and Eq. (3-15) are similar. Furthermore, Figure 3.12 shows the comparison of the median and logarithmic standard deviation of the calculated demands vs. simulated at all intensity levels (Responses are assumed to be lognormally distributed at a given seismic intensity level). The same accuracy is achieved for the two cases.

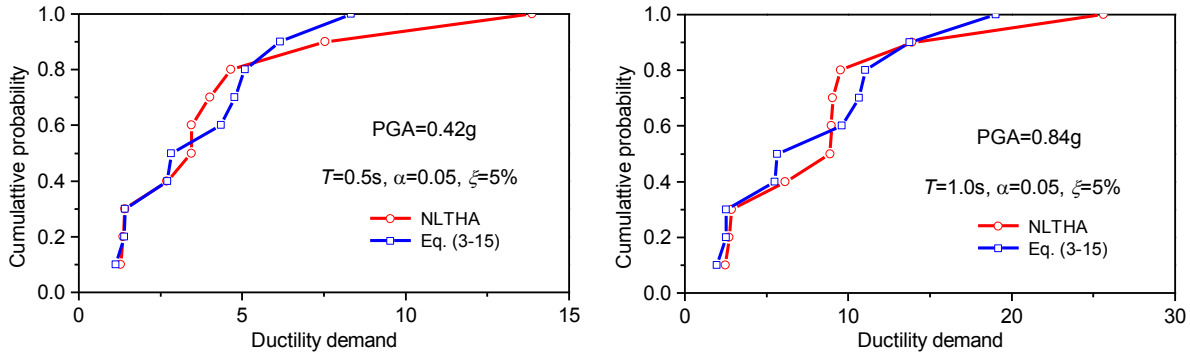

Figure 3.11 CDFs for the case (a) PGA=0.42 g and (b) PGA=0.84 g.

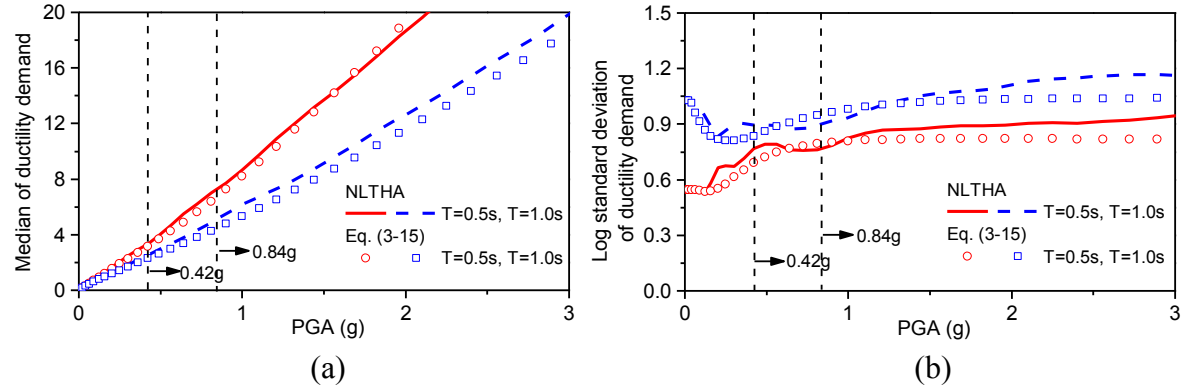

Figure 3.12 (a) Median and (b) logarithmic standard deviation of formula-calculated ductility vs. simulated ones.

3.8.2 Fragility Curves for a Given Performance Target

Fragility analysis is another important example component in PBEE. When IDA curves are quantified, one can obtain the response distribution under intensity I of a given GM suite. Generally, the response data are assumed to be lognormally distributed and the exceeding probability for a given performance target under intensity I can be calculated (Eq. (3-3)). Thus, Eq. (3-15) can also help derive fragility curves without NLTHA. Figure 3.13 demonstrates the comparison of fragilities of two bilinear systems with T=0.5s and T=1.0s under the PEER10 GM suite using NLTHA and Eq. (3-15). Three different ductility (u) levels were used in this example as the target performance levels (u=1, u=4 and u=8). From Figure 3.13, we can observe that the estimations using the semi-closed form formulation (Eq. (3-15)) can also accurately capture the fragility curves generated from NLTHA.

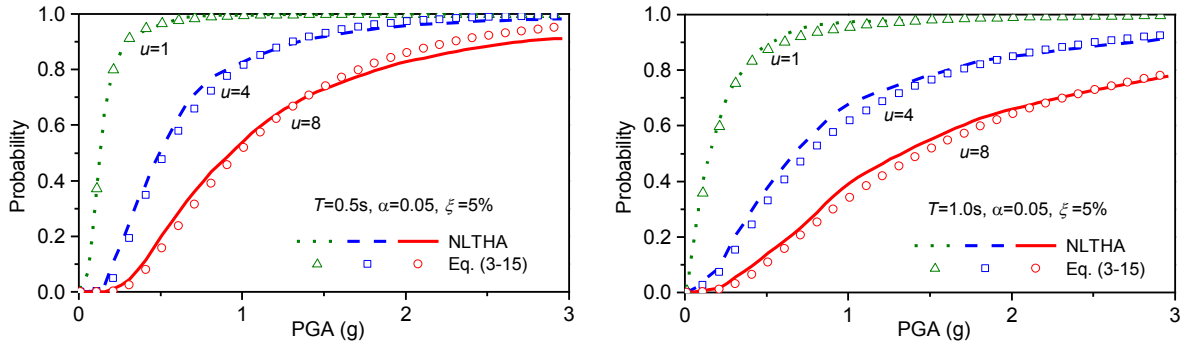

(a) (b)

Figure 3.13 Fragility curves of the systems with (a) T=0.5 s and (b) T=1.0 s.

3.9 Summary and Conclusions

A semi-closed-form solution concept was proposed to estimate uncertainty in the seismic displacement response of bilinear SDOF systems. The uncertainty quantification framework decoupled the impact on the IDA curves from different influential parameters including bilinear system structural properties and ground motion characteristics. A parametric IDA curve formulation was obtained through the regression using a large number of ground motion records, and was later validated with another set of ground motions different from the

suite used for regression analyses. With the help of the parametric IDA curves, the semi-closed-form uncertainty estimation approach was applied to typical PBEE calculations (e.g., the fragility development) and was proven to be accurate and effective in predicting system response uncertainty when compared to the traditional simulation-based method. However, it should be pointed out that the consideration of GM uncertainty in this study was limited by the use of a sub-set of GM motions from the PEER NGA database. Although the conceptual methodology can be applied to more GM motion records, it is expected that the regression results and parameters may change if a GM suite significantly different from the ones used in this study was adopted. Also, the current study only illustrated the applicability of this approach to simple bilinear systems. The application of the proposed approach to realistic structures with more complicated nonlinear response characteristics should be investigated further in future studies.

CHAPTER 4

EXPERIMENTAL STUDY OF UNCERTAINTY PROPAGATION THROUGH SHAKE TABLE TESTS

4.1 Abstract

The propagation of uncertainty in seismic response analysis, is the mechanism through which ground motion (GM) uncertainty and structural parameter (SP) uncertainty contribute to response variability, and is critical for accurately quantifying seismic risk in performance-based earthquake engineering (PBEE). Response uncertainty in existing PBEE analyses is estimated either through statistical variance combination approaches or through computationally intensive time history simulations. In general, experimental exploration of the uncertainty propagation is cost prohibitive and impractical. In this study, a series of shake table test were conducted to generate statistical seismic response data of 12 nominally identical simple specimens subjected to a suite of seven earthquakes at different seismic intensity levels. The test data were analyzed in order to decouple the contributions of GM uncertainty and structural parameter uncertainty on response uncertainty with different intensity levels and verify several basic characteristics about uncertainty propagation. In addition, the accuracy of the square-root-sum-of-squares (SRSS), which is used for combining different input uncertainties to quantify the total uncertainty, was evaluated through the comparison with test data.

4.2 Introduction

Shake table tests are typically conducted to obtain realistic structural responses in order to validate and calibrate models for the seismic design and seismic risk assessment. Generally, full-scale or small-scale structures are built on a shake table and subjected to representative earthquakes scaled to target seismic hazard levels. Due to a limitation of resources, most shake table tests have a limited number of specimens (often a single specimen in the case of full-scale

or large tests) and ground motion inputs (Ji et al. 2009; Martinelli and Filippou 2009), making it impossible to experimentally examine the statistical characteristics of the responses. On the other hand, the core concept of PBEE is to explicitly consider the uncertainty in the seismic responses of systems. In the past, this has been accomplished indirectly through numerical simulations using models that were validated by shake table tests. For example, in order to validate a performance-based seismic design (PBSD) methodology targeted at achieving a predefined non-exceedance probability, a combination of full-scale shake table test (Van de Lindt et al. 2010), numerical model validation (Pei and van de Lindt 2011), and PBSD methodology validation through numerical simulations (Pang et al. 2010) was employed. Thus, direct investigation of how the uncertainties propagate through data analysis of statistical data from shake table tests provides a useful insight into better understand this problem.

There is a rich variety of approaches to estimate or simulate seismic uncertainty. Among commonly-used methods to consider the uncertainty contribution from the ground motions (record-to-record variability) and structural parameter variability, one method (Celik and Ellingwood 2010; Ellingwood and Kinali 2009; Li and Ellingwood 2007; Li and Ellingwood 2009; Yin and Li 2010) assumes that the structural responses have a linear relationship with spectral acceleration values of the ground motions in logarithmic scale. This assumption provides a means to quantify ground motion induced uncertainty using the residuals when doing the linear regression analysis. A more robust but computationally intensive approach to simulate response uncertainty is the time history simulation with randomized structural model samples and ground motion suites. Specifically, Monte Carlo simulation or Latin Hypercube sampling method is usually used to generate enough representative sample cases (Dolsek 2009; Gokkaya et al. 2016; Liel et al. 2009; Vamvatsikos 2014). In this case, GM uncertainty is generally considered by selecting a ground motion suite from natural ground motion databases (e.g., Dolsek 2009) or synthetic ground motion models

(e.g., Celik and Ellingwood 2010). The accuracy of this approach is highly dependent on the quality of the numerical model used and due to its complexity, it is mainly used in research studies. In terms of simplified approaches, the first-order second-moment (FOSM) method can be used in uncertainty estimation for earthquake-induced losses (e.g., Baker and Cornell 2008; Bradley and Lee 2010). In addition, a more simplified method SRSS (FEMA-P695 2009) is usually adopted in fragility analysis and seismic risk assessment (Bradley 2010; Cornell et al. 2002; Ellingwood et al. 2007; Vamvatsikos and Fragiadakis 2010; Yun et al. 2002) that combines different sources of uncertainties by assuming a constant uncertainty contribution. With most of the methods discussed above, they do not explore situations where the contributions to response uncertainty may vary depending on the hazard intensity. Additionally, the accuracy of the estimation methods for the uncertainty estimation in seismic responses has not been explicitly validated using shake table tests.

In this study, a series of specially designed shake table tests were carried out to generate a data pool that enables explicit uncertainty propagation validation. This test procedure utilized a group of simple and nominally identical specimens that carry measurable input uncertainty, subjected them to a ground motion suite scaled to different intensity levels, and then obtained the peak displacement responses from the specimen population to generate representative distributions of the structural responses of interest. This test procedure is hereby termed in this study as a "probabilistic shake table test". Through analysis of the test data, the influence of GM uncertainty and structural parameter uncertainty can be explicitly decoupled to examine their individual and relative contribution on response uncertainty with the seismic intensity. Then, this data were used to assess the commonly-used SRSS approach with the suggested values of input uncertainties from FEMA p695.

4.3 Probabilistic Shake Table Test Concept

To date, the study of uncertainty propagation in earthquake engineering has been conducted primarily through numerical simulations. The objective of the probabilistic shake table test designed and conducted in this study was to obtain experimental data to enable the direct investigation of seismic response uncertainty. The test was designed to generate data representing the decoupled influence of the structural parameter and the GM uncertainty on the seismic response uncertainty under different seismic intensities. This concept is shown in Figure 4.1, where each shake table test contains multiple specimen samples representative of a statistical distribution for a certain structural parameter. For each shake table test, the GM uncertainty is not present in the responses, thus the response uncertainty is only affected by the structural parameter uncertainty. At the same time, the response data from the same specimens (with the same values of structural parameters) under different earthquake record inputs can be

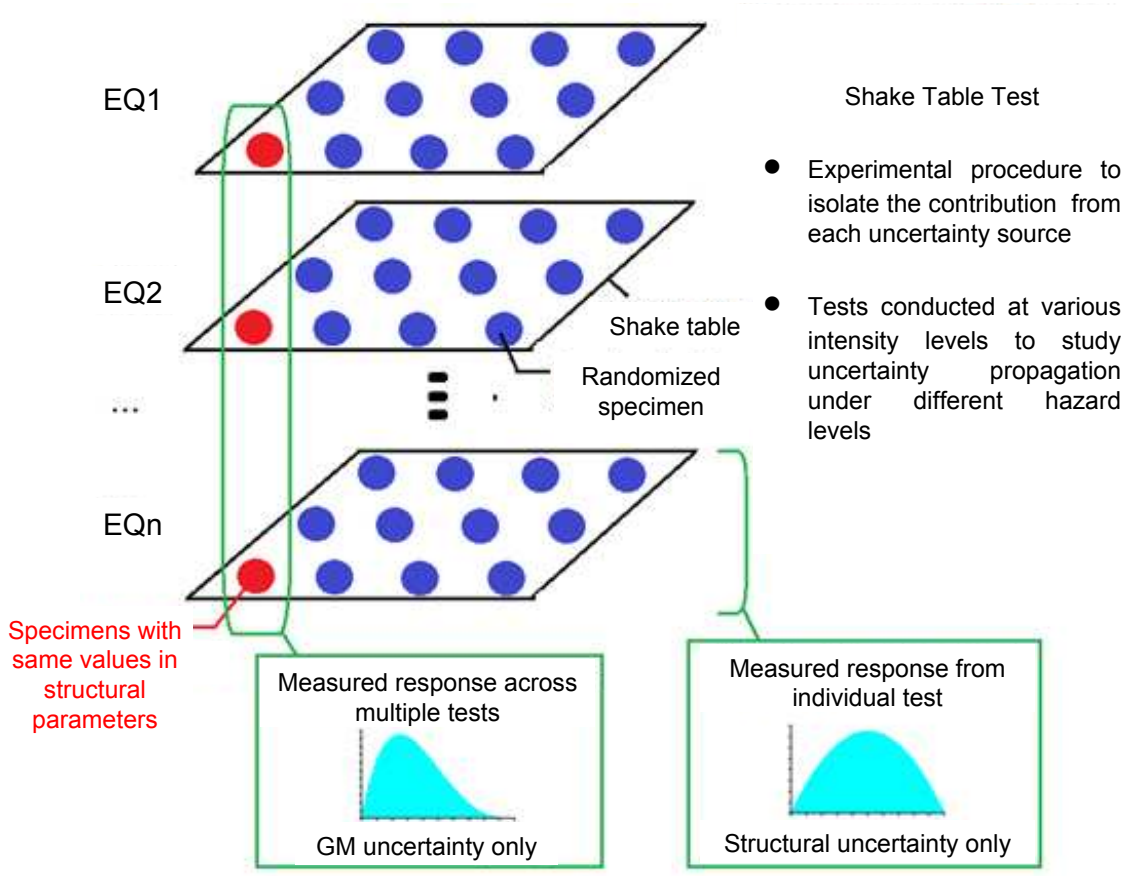

Figure 4.1 Concept of probabilistic shake table test.

grouped to represent the contribution of GM uncertainty, which is independent of structural parameter uncertainty. This process was repeated for an array of seismic intensity levels in order to identify the influence of GM intensity levels on response uncertainty.

4.4 Test Specimens

The objective of the probabilistic shake table test is to generate realistic probabilistic data set of seismic responses. A simple test specimen was designed to represent a nonlinear oscillator. Because the test program involves a large number of tests at different seismic intensity levels, the test specimens need to be repairable when they are damaged during the test. Also, multiple nominally identical specimens are needed to represent samples of a randomized structural system and represent the input structural parameter uncertainty. The specimen used in this study is shown in Figure 4.2. It consists of four square steel plates pin-connected to form a box-like structure that has no lateral stiffness. A thin steel plate (shaped like a dog bone, showed in Figure 4.2(b)) was connected to the top and bottom plates by bolts, providing the lateral stiffness for the system. If a ground motion is large enough, the specimen can experience collapse as shown in Figure 4.3. In this test, 12 specimens were used as shown in Figure 4.4. Displacement string potentiometers were used to measure the displacement responses of all specimens.

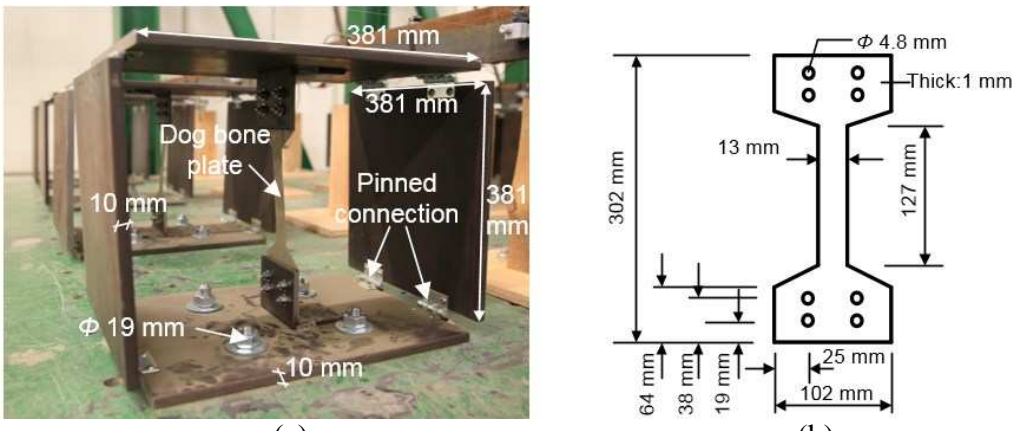

(a) (b)

Figure 4.2 Illustration of (a) a test specimen and (b) the dimension of dog bone plate.

Figure 4.3 Specimen collapse.

Figure 4.4 12 specimens fixed on the shake table.

4.5 Test Program

In the probabilistic shake table test, a group of ground motion records were used to represent GM uncertainty. Considering the scope of the test, seven earthquakes, via NGA ground motion database (Chiou et al. 2008), were selected for this study. Information about these earthquake records (named herein as 7EQS suite) is listed in Table 4. 1. Their 5% damped spectral acceleration and spectral displacement are shown in Figure 4.5.

Table 4.1 Detailed information of the 7EQS suite

ID	Earthquake	Year	Station	Mag.	Faults	Rjb (km)	Rrup (km)	Vs30 (m/s)
1	Northridge-01	1994	Tarzana - Cedar Hill A	6.7	Reverse	0.37	15.60	257.21
2	Imperial Valley-06	1979	Aeropuerto Mexicali	6.5	strike slip	0.00	0.34	259.86
3	Northwest China-02	1997	Jiashi	6.0	Normal	17.90	37.26	240.09
4	Chi-Chi Taiwan-05	1999	KAU020	6.2	Reverse	106.03	109.07	373.33
5	Taiwan SMART1(5)	1981	SMART1 M01	5.9	Reverse	26.31	27.36	268.37
6	Westmorland	1981	Westmorland Fire Sta	5.9	strike slip	6.18	6.50	193.67
7	Parkfield-02 CA	2004	Parkfield - Vineyard Cany 3W	6.0	strike slip	4.43	5.21	308.87

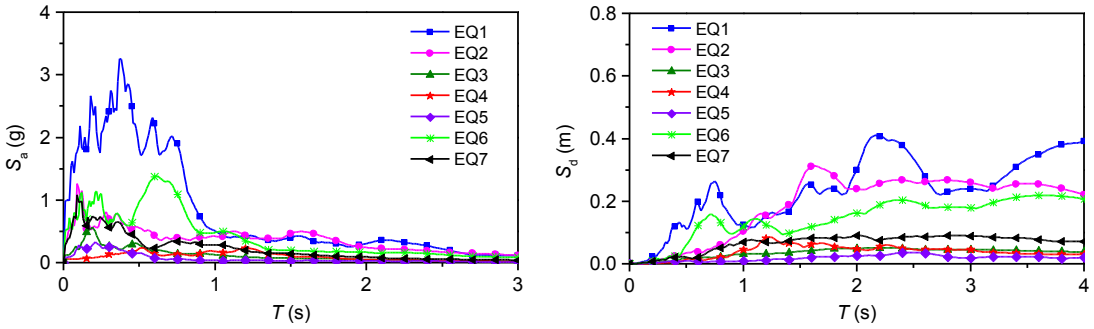

(a) (b)

Figure 4.5 Illustration of (a) acceleration and (b) displacement response spectra of the 7EQS suite.

The ground motion suite was scaled to four different intensity levels, which were selected with the intention of achieving different levels of nonlinearity in the specimens. Peak ground acceleration (PGA) was selected in this study as the intensity measure for scaling. The lowest intensity level (PGA_1=0.02 g) was selected to keep all test specimens in the linear range, while the highest level (PGA_4=0.7 g) was expected to push all test specimens past yielding. Two other intermediate levels (PGA_2=0.2 g, PGA_3=0.4 g) were included to provide additional points on the experimental incremental dynamic analysis (IDA) curves (Vamvatsikos and Cornell 2002; Vamvatsikos and Cornell 2004). Before the seismic testing, white noise tests were conducted to obtain the natural periods for the 12 specimens. After the white noise excitation, an earthquake record from the 7EQS suite was used as the excitation, starting from the lowest intensity level to the highest one (four ground motion intensity levels). Then, the dog bone plates of 12 specimens were replaced by brand new ones for the next set of earthquake records and this process was repeated. Thus, there are a total of 7×12=84 specimens used for the entire test program. The 12 specimens used for the i^{th} earthquake record are referred to as $Group_i$, where i indicates the earthquake record ID. Even though the specimens were manufactured from the same design, there is a large level of dispersion in their natural periods measured through white noise excitations. Figure 4.6 shows the fast Fourier transform (FFT)

functions of the examples of the specimen time history displacement responses obtained from white noise excitation. When one treats the specimen as a single-degree-of-freedom (SDOF) system and identifies the peak in the FFT function as the natural period of the specimen, the distributions of the natural periods of the 12 specimens in different groups are illustrated in Figure 4.7. Based on the 12 data points of natural periods within each group, the logarithmic standard deviation of them (β_{SU}) was calculated as shown in Figure 4.7. This dispersion, to a certain degree, represents the level of inherent structural property uncertainty for each group. This inherent structural uncertainty is introduced by the manufacturing precision of the specimens and the installation process.

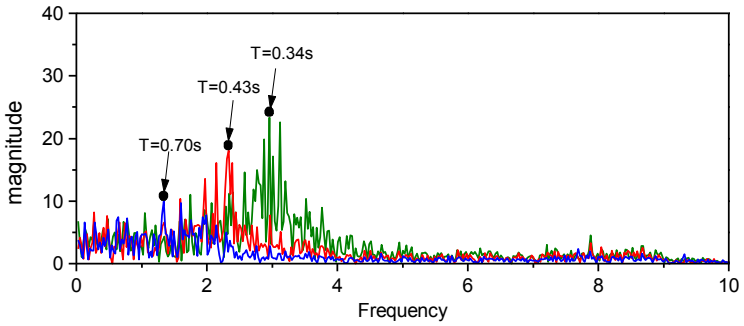

Figure 4.6 Transfer function samples of three specimens.

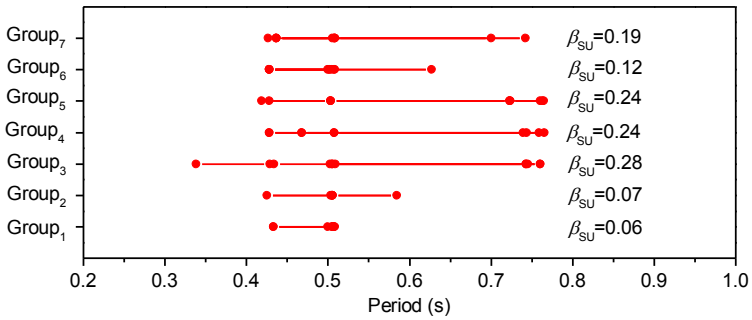

Figure 4.7 Natural period range of the specimen groups.

By subjecting test specimen groups to four seismic intensity levels, an experimental incremental dynamic analysis (IDA) process was realized, resulting in peak displacement response data to construct experimental IDA curves. Since a total of seven earthquake records were used, seven groups of IDA curves were obtained as shown in Figure 4.8. The dispersion

within each group represents only the influence of structural parameter uncertainty on IDA curves. These curves provide a unique data set that can be used to investigate uncertainty propagation with the seismic intensity, which will be discussed in the following sections.

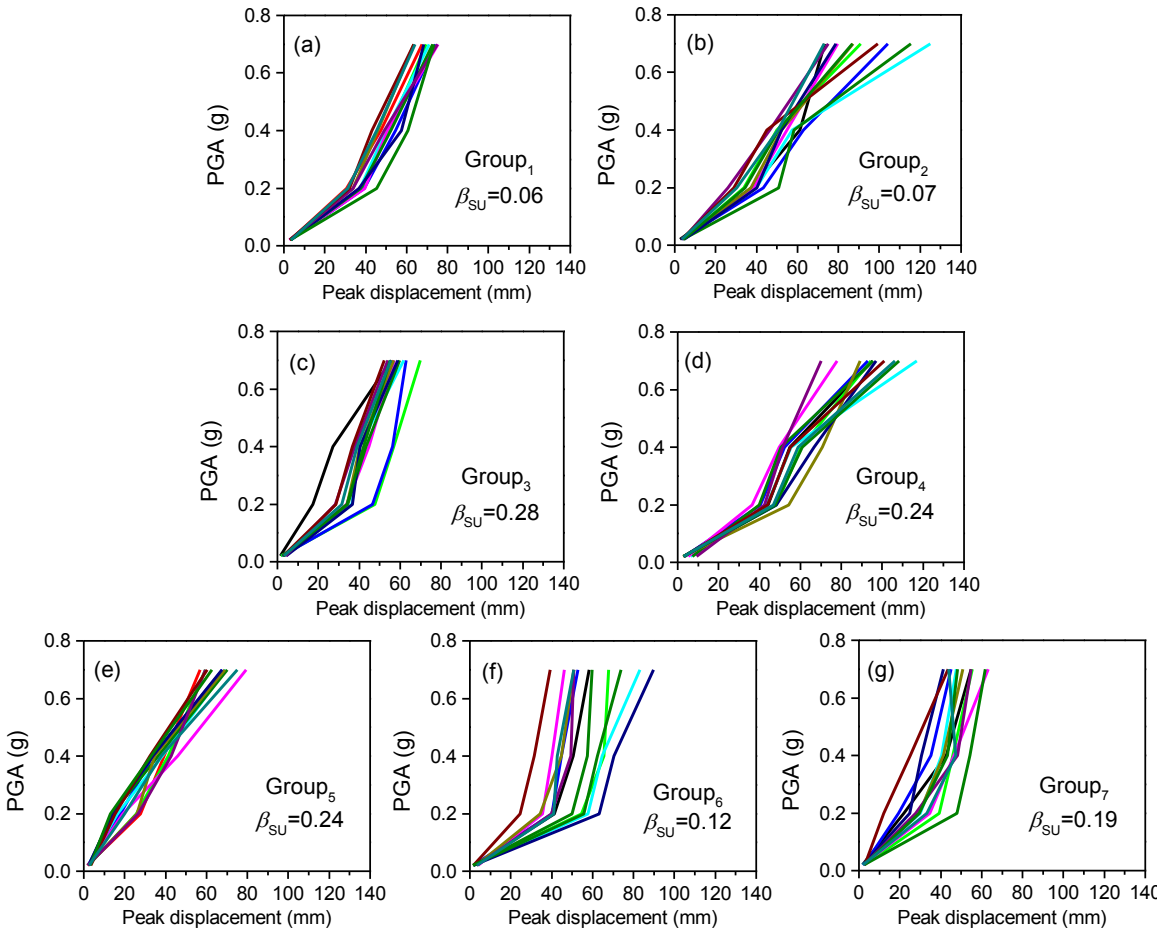

Figure 4.8 IDA curves of each group (a~g).

4.6 Observed Uncertainty Propagation Characteristics

Using experimental data on seismic response uncertainty obtained from the test program, four aspects of uncertainty propagation can be examined, namely the 1) relationship between response spectrum uncertainty and linear structural response uncertainty; 2) impact of seismic intensity level on structural parameter induced response uncertainty; 3) impact of seismic intensity level on ground motion induced response uncertainty; and 4) relative contributions of GM and structural parameter uncertainty on the total response uncertainty.

4.4.1 Relationship between Response Spectrum and Linear Response Uncertainty

By definition, a response spectrum describes the peak response of linear SDOF systems with different natural periods for a given ground motion excitation and damping ratio. Thus, once the natural period of a structure is known, the uncertainty of the linear seismic responses for a given earthquake suite can be directly calculated based on the ground motion response spectrum. Through the white noise excitation, the natural periods of the specimen samples were obtained (Figure 4.7). Using this information and an assumed 5% damping ratio, the uncertainty of displacement response spectrum values of each earthquake in the 7EQS suite can be calculated and represented using logarithmic standard deviation (β_{RU}). The actual peak displacement responses measured during the tests were also used to calculate the observed displacement response uncertainty (also represented by logarithmic standard deviation β_{RU}). Note that only the data from level one excitation (PGA_1=0.02g) for each group was used to ensure the responses are linear and each response spectrum of GMs has to scale to make the GM PGA=0.02 g. Figure 4.9 shows the comparison between the calculated and experimentally obtained displacement response uncertainty from all seven groups. It can be seen that the linear system response uncertainty can be adequately estimated through the uncertainty of the spectral response values for a known earthquake ground motion suite.

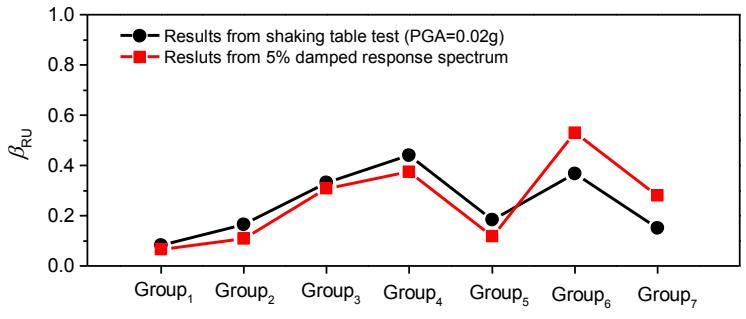

Figure 4.9 Comparison of response uncertainties from response spectra and shake table test.

4.4.2 Is Structural Parameter Induced Uncertainty Invariant with Intensity Levels?

Structural parameter uncertainty can be represented by the statistic distribution (e.g., logarithmic standard deviation) of structural parameters, such as the natural period. Structural parameter uncertainty tends to have an impact on the seismic response uncertainty, and its influence may change as the seismic intensity changes. Through the white noise excitation, the distributions of natural periods for specimens were obtained and the logarithmic standard deviation of the periods was adopted to represent the structural parameter uncertainty (β_{SU}) of the specimens in this study (showed in Figure 4.7). Recall that the IDA curves obtained in this study (shown in Figure 4.8) were resulted from seven different earthquakes. For any one of the earthquake records, the resulting 12 IDA curves are similar but not identical because the 12 specimens on the shake table have different natural periods (i.e., structural parameter uncertainty). If one only looks at the samples within each earthquake (namely, specimens in Group$_i$), the GM uncertainty (independent of intensity) was eliminated. All of the response uncertainties displayed in the IDA curves shown in each subplot of Figure 4.8 are resulted from the structural parameter uncertainty alone. Figure 4.10 shows the seismic response uncertainties of the system under different earthquakes and different intensity levels. The assumption of the invariant influence of structural parameter uncertainty on response uncertainty (in term of logarithmic standard deviation) does not appear to hold. There is no apparent trend on how the structural parameter uncertainty contribution changes with seismic intensity.

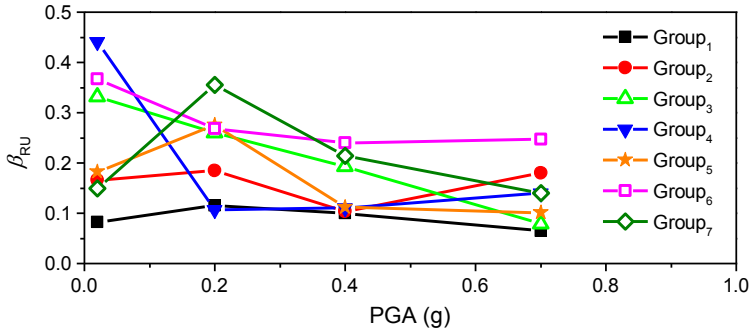

Figure 4.10 Response uncertainty caused by structural parameter uncertainty.

4.4.3 Is Ground Motion Induced Uncertainty Invariant with Intensity Levels?

GM uncertainty is difficult to quantify with a single parameter and is typically represented in analyses through the use of a ground motion suite. For linear systems, as shown earlier, GM uncertainty can be represented by the response spectra (Section 2.4). Because logarithmic standard deviation is invariant to proportional scaling (i.e., all records in a GM suite are scaled by the same factor), the influence of GM uncertainty to a linear system is invariant with intensity level. For nonlinear systems, this invariance does not hold. With the data obtained from the probabilistic shake table test, the ground motion induced uncertainty (quantified by β_{RU}) can be isolated to study its changing trend with respect to intensity levels. Across tests conducted with different earthquake records (ground motion induced uncertainty exists because of the variability of these records), response data from specimens with the same natural period were grouped together (thus getting rid out of the influence of structural parameter uncertainty) to calculate β_{RU} at different intensity levels. Two specimen groups with 0.5 s and 0.43 s natural periods were selected and their IDA curves were shown in Figure 4.11(a) and (b). The logarithmic standard deviations of the peak displacement responses under 7EQS suite with four PGA intensities were plotted in Figure 4.11(c) and (d). It can be seen that ground motion induced uncertainty changes with the intensity level for nonlinear systems. Although experimental data collected in this study is not comprehensive to show the an apparent or a consistent trend of how the response uncertainties change with intensity level, GM-induced uncertainty in terms of logarithmic standard deviation does appear to vary with the seismic intensity level.

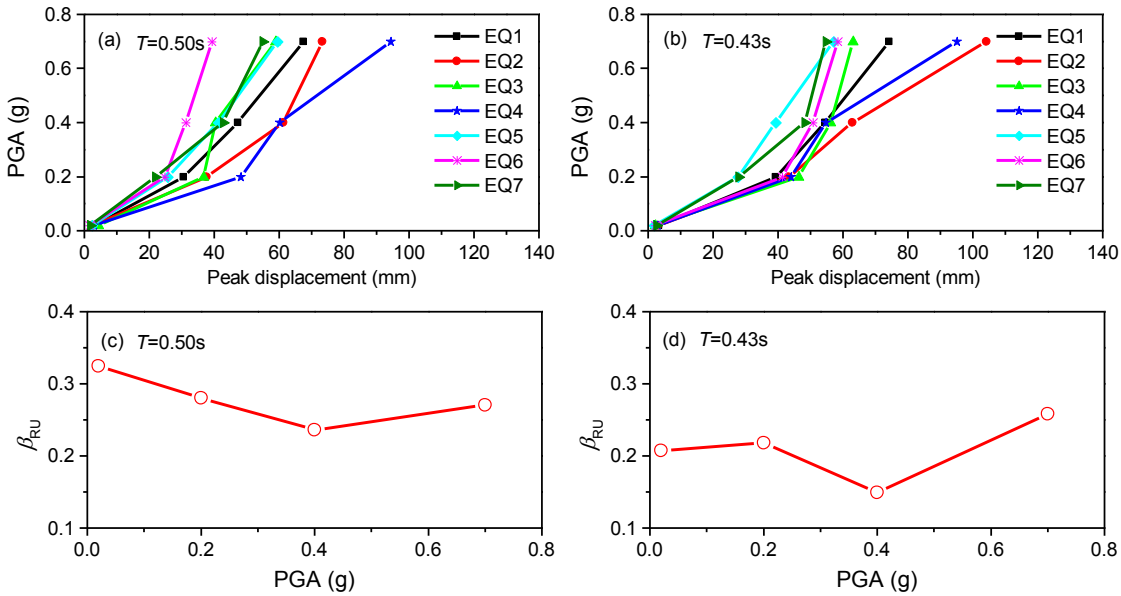

Figure 4.11 IDA curves of (a) T=0.50 s and (b) T=0.43 s and (c) (d) the corresponding response uncertainties.

4.4.4 Are GM and Structural Parameter Uncertainty Contributions Invariant with Intensity Levels?

Generally, GM uncertainty is considered as the most dominant source of uncertainty (Kim and Rosowsky 2005; Kwon and Elnashai 2006; Lee and Mosalam 2005; Liel et al. 2009; Yin and Li 2010). As to structural parameter uncertainty, there has not been a unanimously agreed upon value for its contribution in uncertainty propagation. Celik and Ellingwood (2010) investigated seismic fragilities for non-ductile reinforced concrete frames and concluded that it is adequate to use median (or mean) values of structural parameters in numeral simulation for evaluating the structural damage and loss estimation under moderate earthquakes. However, Yin and Li's investigation (Yin and Li 2010) on probabilistic dynamic simulation of wood frame structures indicated that the uncertainty in structural parameters such as strength can greatly affect the collapse probability of such buildings. Based on the results observed from these studies, the contribution of structural parameter uncertainty to structural performances can be quite different depending on the type of structure. Thus, it is worth investigating the relative contributions of GM uncertainty and structural parameter uncertainty in the total

uncertainty of the structural responses. The unique data from the probabilistic shake table test presented herein provides an opportunity to do this experimentally.

For each intensity level, there are a total of 7x12=84 samples representing both the GM and structural parameter uncertainty contributions. Firstly, one can calculate the total response uncertainty (logarithmic standard deviation of responses was used here) using all 84 samples. This logarithmic standard deviation value is termed here as $\beta_{\text{RU\_total}}$. Then, the mean peak response value from 12 samples under the same GM excitation was calculated. This mean value can be viewed as the average response under that earthquake with structural parameter uncertainty removed. Then a new logarithmic standard deviation with the seven mean values can be calculated (namely $\beta_{\text{RU\_GM}}$) which represents only the uncertainty contribution from ground motions. Mathematically, $\beta_{\text{RU\_total}}$ will always be greater than $\beta_{\text{RU\_GM}}$ and one can calculate the contribution from structural parameter uncertainty based on an assumed SRSS formulation ($\beta_{RU\_SU} = \sqrt{\beta^2_{RU\_total} - \beta^2_{RU\_GM}}$). Figure 4.12 illustrates the ratio of the two different source of uncertainty contributions to the total uncertainty at different intensity levels. One can see that the contribution from these two sources to the total response uncertainty varies with the seismic intensity. The simplified assumption of constant uncertainty contribution from GM and structural properties is not valid. More importantly, one can see from Figure 4.12 that GM-induced uncertainty does not always dominate response uncertainty (i.e., overshadows structural parameter uncertainty). At two intensity levels in the experiment (PGA_1=0.02 g and PGA_3=0.4 g), the uncertainty contributions from the GM and the structure are almost at the same level.

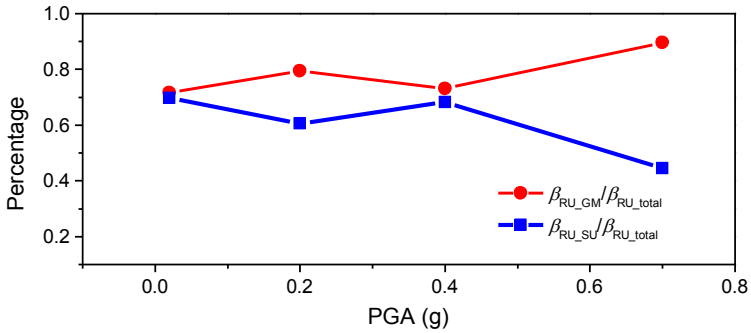

Figure 4.12 Weight of two uncertainty contributions on response uncertainty.

4.7 SRSS Method

With the data obtained from the probabilistic shake table test, commonly-used uncertainty estimation techniques for PBEE can be evaluated. There are currently two main approaches to consider both structural parameter and GM uncertainty in PBEE applications. The first approach is through nonlinear time history analysis (NLTHA), which is computationally intensive and is as accurate as the structural model used in the NLTHA. Another simplified method is to combine different sources of uncertainty that are to be represented by their logarithmic standard deviation through the square-root-sum-of-squares approach. This method is easy to apply in the seismic design, but requires assumed levels of uncertainty for different uncertainty sources and the assumption of independence among these uncertainty sources. Typically, the ground motion uncertainty, structural uncertainty, and modeling uncertainty are considered in PBEE. In the case of shake table tests, only two main uncertainty sources are present. The formulation of total peak displacement response uncertainty by the SRSS method to combine uncertainties from two sources can be expressed as following

$$\beta_{RU} = \sqrt{\beta_{GU}^2 + \beta_{SU}^2} \tag{4-1}$$

where β_{RU} is the logarithmic standard deviation of system peak displacement responses (total system response uncertainty). β_{GU} indicates the record-to-record variability (GM uncertainty)

while β_{SU} is referred as the uncertainty from structure properties (structural parameter uncertainty). There are no clearly defined procedures in the existing literature on how to calculate β_{GU} and β_{SU}. FEMA-P695 (2009) recommended ranges of estimated values for each. β_{GU} represents the influence caused by characteristic variability of selected ground motions which is from 0.2 to 0.45 while β_{SU} can be divided into four values depending on the accuracy of the structural model which is 0.1, 0.2, 0.35 and 0.5. According to the suggested value range in terms of two uncertainty sources, the range of uncertainty estimation results from Eq. (4-1) was calculated and listed in Table 4.2. Note that the SRSS method is intensity independent, resulting in the same logarithmic standard deviation of the responses at all intensity levels. For the comparison, the response uncertainties derived from tests with different PGA intensities are 0.34, 0.36, 0.22, and 0.26, respectively (shown in Figure 4.13). Apparently, if the lower bound for input uncertainties in FEMA P695 (β_{SU}=0.1, β_{GU}=0.20) is taken, the SRSS result (β_{RU}=0.22) will underestimate actual response uncertainty at some intensity levels (showed in Figure 4.13). When the peak values from FEMA P695 recommendation are selected (β_{SU}=0.5, β_{GU}=0.45), the result comes to 0.67 which is overly conservative at all intensities (shown in Figure 4.13). Using uncertainty value at the middle of the ranges leads to the predicted β_{RU}=0.44 (β_{SU}=0.3, β_{GU}=0.33). This result is actually fairly good for the test conducted here (showed in Figure 4.13). Recommended uncertainty levels in FEMA P695 document appear to have provided a sufficient interval to capture the uncertainty levels obtained from this experiment.

The above comparison considers only the arbitrary levels of estimated uncertainty from FEMA P695. Considering the information known in this test including the GMs used and the white noise tests of the specimens, a more refined SRSS analysis can be conducted. Instead of assuming values for β_{GU} and β_{SU}, the β_{GU} can be defined as the logarithmic standard deviation of 5% damped acceleration response spectrum values at average natural period 0.53s

(β_{GU}=0.45), while β_{SU} can be calculated from the measured natural periods of all specimens (β_{SU}=0.2). If this "known" set of information is used, the SRSS approach will result in a total logarithmic standard deviation of 0.49 (also shown in Figure 4.13) which is conservative (larger than observed) but not necessarily better than using the average uncertainty values from FEMA P695 recommendations.

Table 4.2 Response uncertainty results by the SRSS method using the suggested values from FEMA P695

β_{GU}	β_{SU}			
	0.1	0.2	0.35	0.5
0.2	0.22	0.28	0.40	0.54
0.45	0.46	0.49	0.57	0.67

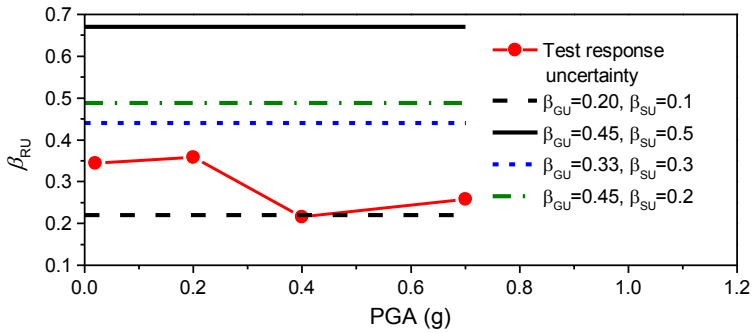

Figure 4.13 Illustration of response uncertainty results by different values about β_{SU} and β_{GU}

4.8 Summary and Conclusions

A probabilistic shake table test was conducted in this study to generate sample structural response data for investigating uncertainty propagation in PBEE. With a custom specimen design intended to represent a simple nonlinear oscillator, seven groups of 12 specimens were subjected to seven different earthquake records at different seismic intensity levels. This test resulted in a unique data set that was used to construct a suite of experimental multi-record IDA curves including both the ground motion and structural parameter induced uncertainty. Using the data, several conclusions can be drawn for the tests:

1. For linear systems, the uncertainty induced by ground motions and structural properties can be captured adequately based on scaled GM spectral values at the system natural period. This conclusion is well-known based on structural dynamics and was experimentally validated in this study.

2. In uncertainty propagation, the contributions of GM uncertainty and structural parameter uncertainty tend to change with the intensity level (ground motion scaling). With the limited data generated in this study, no apparent trend can be identified. This is a topic that deserves further investigation.

3. The relative contribution of GM and structural parameter uncertainty on the seismic response uncertainty is not constant over all intensities. It is experimentally validated that the GM uncertainty is not always the dominant uncertainty source at all intensity levels.

4. Although there is no seismic intensity dependence, adopting the SRSS approach with recommended uncertainty ranges by FEMA P695 seems to provide a reasonable and conservative estimation of the actual response uncertainty for the specimens tested as long as one does not use the lower bound values of the recommended ranges of input uncertainties. Even though NLTHA with an accurate structural model and adequate sample numbers will still be a more reliable way to estimate response uncertainty, this study reinforces that a simple approach such as the SRSS method proposed in FEMA P695 is viable and reasonable.

CHAPTER 5

STRUCTURAL DAMAGE PREDICTION THROUGH SPECTRUM-BASED DAMAGE POTENTIAL INDICATOR

5.1 Abstract

Improving predictive relationships between strong ground shaking and damage in buildings is an important topic in research on earthquake effects. Intensity measures (such as spectral acceleration at fundamental period $S_a(T)$) are often used as the damage potential indicator (DPI) of structures. However, this point-wise DPI captures only very limited information about response spectrum corresponding to the elastic behavior of a structure. In a severely damaged state, structural nonlinearity lengthens the effective period which makes other parts of the response spectrum relevant to damage. In this study, a vector-valued DPI including an intensity component and a spectral shape component was proposed. By comparing the DPI from two different ground motion records, a similarity index (SI) was constructed to quantify how similar two records are with respect to the structural damage. The optimal period range in the response spectrum that should be used to develop the similarity indicator was determined by a new circle rule for bilinear single-degree-of-freedom (SDOF) systems. Through a numerical validation, the vector-valued SI can be capable to predict the structural damages.

5.2 Introduction

Response spectrum is a commonly-used characterization metric for ground motions (GM) in both seismological and earthquake engineering communities. By definition, response spectrum reflects the peak acceleration or displacement responses of a series of linear elastic SDOF systems under a given ground motion's excitation, essentially quantifying the frequency contents of the given ground motion. In spite of some research efforts towards nonlinear response spectrum (e.g., Iwan 1980; Riddell 2008; Aydinoğlu 2003), linear response spectrum

is still widely-used by researchers and engineers to evaluate ground motion impact on structural systems (e.g., Loth and Baker 2015). Response spectrum does not explicitly include time domain information about the ground motions, which may be important for the damage assessment in nonlinear structural systems. But it has been, to some degree, used by researchers as a key metric for evaluating the characteristic difference of two ground motions, especially when earthquake engineering researchers want to identify the effect of main features of a ground motion on the structural damage.

In structural engineering, structural damage to earthquake excitation is more of a practical concern. Nowadays there is a need for performance based seismic design (PBSD) using advanced structural models, as damage is more of a concern when the design diagram is shifting towards resilience. For GMs with a small intensity that does not cause damage (i.e., structures behave linearly), it is safe to reach the conclusion that the structural responses under the GMs will match closely if their spectrum values at the structural fundamental period are closely matched. For the GMs that are large enough to cause damage, it will still be ideal if a ground motion "damage potential indicator" (DPI) can be derived from elastic response spectrum that can provide a reasonable correlation to structural damage. But, the nonlinear responses are affected by the structural nonlinearity and higher modes, which lengthen and shorten the structural effective period, respectively (Baker and Allin Cornell 2005). Thus, the DPI based on a response spectrum cannot only focus on the fundamental period. Spectral acceleration at other periods such as the periods longer-than fundamental period should be adopted.

In this study, a vector-valued DPI based on an elastic response spectrum was proposed including a seismic intensity component and a spectral shape component. The decoupling of the two components is expected to provide more clear understanding on their correlations with structural damages. In order to study the influence of the DPI vector on structural damages, a

correlation analysis on the difference of the DPI vector among ground motions and structural damage difference under these ground motions were conducted. According to the proposed circle rule, the method to determinate the optimal period region for the spectral shape component (that strongly correlates with nonlinear system damage under a given seismic intensity) was identified for GMs. Finally a group of other 1600 ground motions were used to validate the effectiveness of the method.

5.3 Existing Study on Response Spectrum Based Damage Potential Indicator

The basic objective of DPI is to develop a quantitative parameter of a ground motion history that correlates strongly with the damage it will induce on a structure. In the past, many researchers have investigated various ground motion parameters that can potentially be used as DPIs. These parameters can be divided into two categories, namely structure-independent and structure-dependent DPIs. Structure-independent DPI is derived only from the ground motion itself without considering structural properties. The common structure-independent DPIs can be peak values during the time history such as peak ground velocity, peak ground acceleration and peak ground displacement (Akkar and Özen 2005; Makris and Black 2004) as well as the time history-related characteristics such as Arias intensity (Arias 1970) and earthquake power index P_a (Housner 1975). The compound DPIs combing the peak quantity and time history-related quantity were also used (e.g., Fajfar intensity I_F (Fajfar et al. 1990), Rafael and Jaime I_a, I_v and I_d intensity to consider structural energy dissipation (Riddell and Garcia 2001), Park characteristic intensity I_C (Park et al. 1985), I_D index (Iervolino et al. 2006)). These structure-independent DPIs did show a reasonable level of correlation with structural system responses and damages. However, since the structural damage is heavily influenced by structural parameters, this type of DPIs is not very robust in predicting structural damages. On the other hand, most of the structure-dependent DPIs are mostly the indices derived using target structure's natural frequency information and response spectrum of the GM. The mostly-used

one is the 5% damped spectral acceleration ($S_a(T,5\%)$) at the fundamental period of a structure (e.g., Vamvatsikos and Cornell 2002; Yin and Li 2010; Bradley and Lee 2010; Ellingwood and Kinali 2009). However, when a structure vibrates into inelastic behavior, the period of the structure would be lengthened due to the fact that the structure softens under stiffness degradation (Baker and Allin Cornell 2005). In order to incorporate effect of the period elongation of the structure subjected to earthquakes, a parameter about the response spectrum value at the lengthened period should be added in a DPI to predict the nonlinear responses of interest. For example, Cordova et al. (2000) combined the spectral values at the fundamental period (T_1) and the lengthened period (T_L) as:

$$DPI = S_a\left(T_1\right)\left(\frac{S_a\left(T_L\right)}{S_a\left(T_1\right)}\right)^{\alpha} = S_a\left(T_1\right)^{1-\alpha} S_a\left(T_L\right)^{\alpha} \tag{5-1}$$

where $T_L = C \times T_1$ is the lengthened period; $C > 1$ is the coefficient about the period softening, quantifying the degree of the structure softening (namely, nonlinearity) under earthquakes. Thus, the value of C should be related with the intensity level of earthquakes. α is an undetermined coefficient to reflect the spectral shape which can be seen as the weighting of the two spectral values at T_1 and T_L (Mehanny 2009). According to the idea of constructing the DPI, Vamvatsikos and Cornell (2005) upgraded the DPI as:

$$DPI = S_a\left(T_s\right)^{1-\alpha} S_a\left(T_L\right)^{\alpha} \tag{5-2}$$

where the spectral value at the fundamental period (T_1) is replaced by the one at T_s. The value of T_s can be smaller than T_1 to consider for the effects of higher modes or larger than T_1 according to structural nonlinearity under earthquakes. Such definitions of T_s and T_L make the DPI more applicable to the tall, long-period structure dominated by higher modes of vibration or the structure controlled by strong nonlinearity under earthquakes. However, these DPIs only use the information of two points in the response spectrum, resulting in a lack of the

information of spectral shape over a period band that the structure will transit through as it softens. In order to incorporate the information of spectral shape over a period band, Bojorquez and Iervolino (2011) introduced a new DPI as:

$$DPI = \frac{1}{e}\sum_{i=1}^{e}\frac{S_{\mathrm{a}}\left(T_i\right)}{S_{\mathrm{a}}\left(T_1\right)} \tag{5-3}$$

Note that this DPI is dimensionless (without seismic intensity information) and only captures the shape of the elastic response spectra. It is a spectral shape indicator between T_1 and T_e. The response spectrum in this period band is expected to exhibit an averagely positive slope for DPI>1 while negative for DPI<1. But since this particular DPI does not have the intensity information, two GMs with very different intensity can have very close DPI values as long as their shapes are similar. The limitation of the DPI presents a challenge to compare the main spectral characteristics between two GMs.

5.4 A Vector-valued Damage Potential Indicator

As discussed, a DPI should be recommended to include both the seismic intensity and spectral shape information. Baker and Cornell (2005; 2006) proposed a vector-valued DPI consisting of spectral acceleration and epsilon to predict structural seismic performance. Although both the spectral magnitude and spectral shape are reflected in this DPI, the spectral shape information is very limited that only the shape information at one point is included. Herein, a spectral shape component over a period band was proposed to be similar as Eq. (5-3). It is starting at T_s instead of T_1, which can make the shape component involve in the effects of higher modes and nonlinearity. Thus, the proposed spectral shape component can be formulated as:

$$p_2 = \frac{1}{e-s}\sum_{i=s}^{e}\frac{S_{\mathrm{a}}\left(T_i\right)}{S_{\mathrm{a}}\left(T_1\right)} \tag{5-4}$$

It is evident that p_2 includes the spectral shape information over the period band from the starting period T_s and the ending period T_e. s means the point number at starting period while e indicates the point number at ending period. The period band needs to be carefully calibrated to make that p_2 has the strongest correlation with structural damages (referred to as optimal period band). The optimal period band should be intrinsically a counterbalance between effective period shortening via the higher mode effects (Chopra 2012) and effective period lengthening via the structural response nonlinearity (Bianchini et al. 2009; Iwan 1980). Higher mode effects are expected to the structural property and Katsanos et al. (2014) postulated that the degree of period lengthening (nonlinearity of structural performance) varies with the seismic intensity. Apparently, p_2 does not include information about GM intensity. But it is expected that the optimal period band will be dependent on the GM intensity. To better quantify the interplay between structural nonlinearity and seismic intensity, an indicator λ was formulated to reflect intensity information by normalizing the spectral acceleration value at the system fundamental period to the yielding intensity:

$$\lambda = \frac{I}{S_{a0}(T_1)} = \frac{S_a(T_1)}{S_{a0}(T_1)} \tag{5-5}$$

where $S_a(T_1)$ is the spectral acceleration at the fundamental period; $S_{a0}(T_1)$ indicates the spectral acceleration at which the ground motion starts to yield the structure.. When $\lambda \leq 1$, the structure remains linear and elastic during the GM excitation. The structure will only experience the damage if $\lambda > 1$. λ was used as the intensity component of the DPI vector as:

$$p_1 = \lambda \tag{5-6}$$

Thus, the vector-valued DPI can be constructed by the GM intensity component and the spectral shape component as:

$$DPI = [p_1, p_2] = \left[\lambda, \frac{1}{e-s} \sum_{i=s}^{e} \frac{S_a(T_i)}{S_a(T_1)} \right] \tag{5-7}$$

5.5 Response Spectrum Similarity Index

It is generally believed that similarity in response spectrum between the two GMs will result in the similar response in structures. One could argue that if we find a DPI that is good enough, matching that DPI will be a good starting point. It is logical except DPI itself (especially the spectral value based DPI) does not map to the structural damages functionally. In another word, none of the existing DPIs corresponds to structural damages in a deterministic fashion. As a result, there will be a range of performance by using different DPIs to predict structural damage. Nonetheless, DPI provided a way for us to construct a quantitative indicator that compares two response spectra. In this study, we define a Similarity Index (SI) based on the proposed vector-valued DPI. Because the DPI vector has two components, the evaluation of the SI becomes complicated. Certainly if both the components are close, we can conclude that the two GMs are very similar. Consider the situation where the intensity components of the GMs are close, but the spectral shape components are different, or verse visa. It is difficult to quantify the SI. One way to accomplish this is to add a constraint to one of the DPI components when comparing two GMs. For example, instead of comparing two GMs that have different intensity and shape component, one can scale both GMs (*i* and *j*) to have the same intensity component (p_1=x) and study the shape component similarity.

$$SI_{DPI} = p_{2,i}\Big|_{p_1=x} - p_{2,j}\Big|_{p_1=x} \tag{5-8}$$

It can be hypothesized that the resulting SI will show a strong correlation with the structural damage difference, which can be calculated using structural models through nonlinear time history analysis (NLTHA). For any two GMs, one can apply them to a structure and calculate the resulting damage difference using time history integration, and at the same time extract an SI value based on their response spectra. The SI and the difference in structural

damages can be paired up to seek a correlation. A "good" SI will be able to help maximize this correlation. The damage difference (Δ_{DD}) brought by two ground motions (i and j) can be formulated as:

$$\Delta_{DD} = u_i - u_j \tag{5-9}$$

where u_i is the structural damage such as ductility demand under i^{th} ground motion while u_j is under j^{th} ground motion.

In this study, bilinear SDOF systems were selected to maximize the correlation between similarity index of vector-valued DPI (SI_{DPI}) and difference of their seismic ductility demands (Δ_{DD}) through finding out the optimal period band in their response spectra for the shape component. In the following sections, 1) bilinear SDOF systems and ground motion selections were introduced. Besides, 2) we investigated the rule of the optimal period band that makes the strongest correlation between SI_{DPI} and Δ_{DD}, and 3) the influence of intensity component λ (namely, intensity level) on the determination of the optimal period band. At last, 4) a validation of the proposed framework through other ground motions was conducted.

5.6 Bilinear SDOF Systems

A bilinear SDOF system without strength degradation is one of simplest nonlinear systems that can be related with more complicated structures. It can be defined through four parameters: the initial elastic period (T_1), the damping ratio (ξ), the hardening ratio (α, defined as the post-yielding stiffness divided by the initial stiffness) and a yield displacement coefficient (C_y). C_y is a normalized parameter related with the yield displacement and elastic period (Deng et al. 2017):

$$C_y = \frac{d_y}{mg/k} \tag{5-10}$$

where d_y is the yield displacement; m is the mass; k is the elastic stiffness; g is the gravity acceleration. The hysteretic model of bilinear SDOF system can be seen in Figure 5.1. If the seismic intensity is not large enough to exceed the yielding point, a bilinear SDOF system with a given damping ratio will behave linearly, and then the corresponding spectral acceleration at fundamental period $S_a(T_1)$ can precisely capture the seismic responses of the system. Inversely, when the bilinear SDOF system is subjected to very strong earthquakes, loosely speaking, its response can be viewed as a linear system that has an elastic stiffness of k_p (post-yield stiffness of the bilinear system) and a certain level of hysteretic damping (Hadjian 1982; Iwan 1980). This is attributable to the fact that the post-yield stiffness of the bilinear system has dominated the structural response under high intensity earthquakes. Thus, it can be speculated that the spectral acceleration $S_a(T_p)$ at the period $T_p=\alpha^{-0.5}T_1$ (calculated by the post-yield stiffness) might have a strong correlation with the damage of the bilinear SDOF system under high intensity earthquakes. Additionally, since the bilinear SDOF system is considered, the structural nonlinearity is the only source shifting the effective period. Thus, the starting period T_s of the optimal period band is supposed to be equal to or larger than T_1 if we use this DPI vector to predict bilinear system damages. Note that the spectral acceleration to make a bilinear SDOF system start to yield can be calculated below. It can be learn that the yield intensity is completely dominated by the structural parameter C_y for bilinear SDOF systems.

$$S_{a0}\left(T_1\right) = d_y \omega_n^2 / g = C_y \tag{5-11}$$

where $S_{a0}(T_1)$ is in g unit; d_y is the yield displacement (unit: m); SDOF total acceleration can be assumed to be same as the pseudo-acceleration (equal to $d_y \times \omega^2$ in m/s^2 unit for the yielding condition of the bilinear SDOF system) (Chopra 2012).

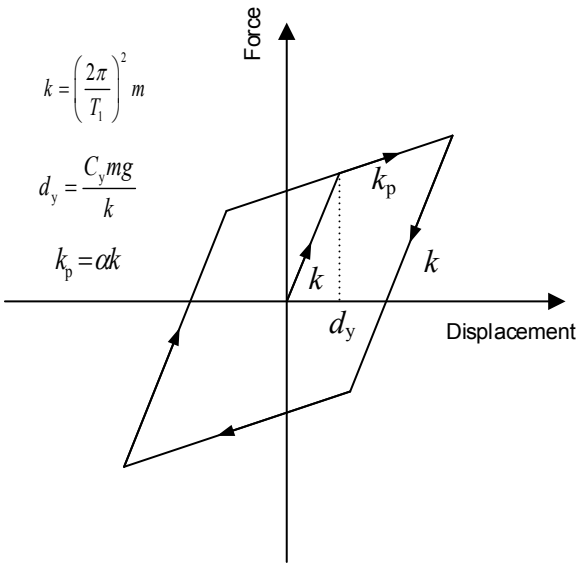

Figure 5.1 Hysteretic model of the bilinear SDOF system

5.7 Earthquake Ground Motion Characteristics

A wide-range of earthquake ground motions need to be selected for obtaining the statistical responses of the system through NLTHA. In this study, 102 far-fault earthquake records were selected from FEMA-P695 (2009) and an existing literature (Medina and Krawinkler 2004). They are all recorded GMs from different earthquake events (5.8M to 7.6M) and with different fault mechanisms such as reverse and strike-slip. The response spectra of the selected 102 ground motions are shown in Figure 5.2(a). The 102 ground motions need to be scaled firstly that their spectral acceleration values equal to $S_{a0}(T_1)$ in the following analysis on bilinear SDOF systems to constrain the intensity component in the similarity index of the vector-valued DPI. Then scaling the ground motion into different intensity levels (λ) can investigate its influence on the determination of optimal period band. Figure 5.2(b) illustrates an example of the 5% damped response spectra scaled to the $S_{a0}(T_1)$ level that makes the bilinear system with T_1=0.5s and C_y=0.2 yield.

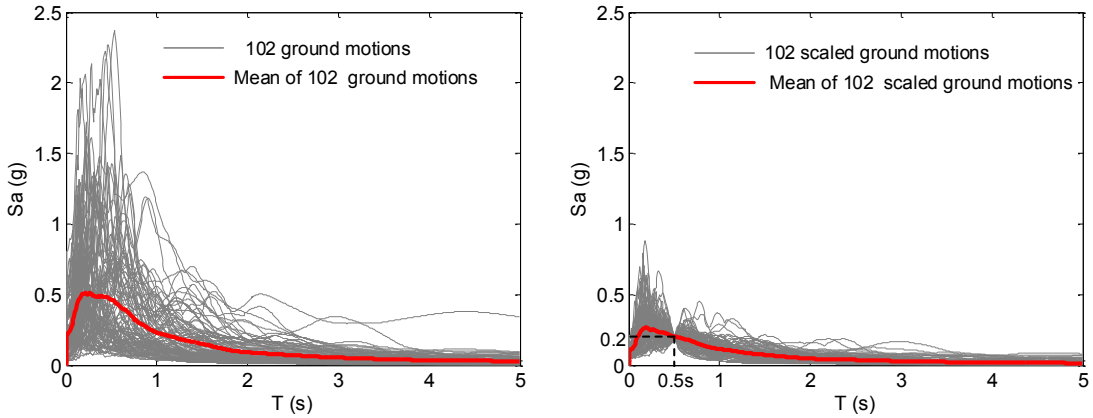

(a) (b)

Figure 5.2 5% damped response spectra of (a) original ground motions and (b) scaled ground motions.

5.8 Maximizing Damage Correlations for Bilinear SDOF Systems

It can be hypothesized that when the two ground motions match well at p_1 and p_2 ($SI_{DPI}\approx 0$), the damages of the structure caused by the two ground motions will be similar ($\Delta_{DD}\approx 0$). Even they do not match, a correlation between SI_{DPI} and Δ_{DD} can be found out through determining the optimal period band in their response spectra. The DPI vector inserted in SI_{DPI} is apparently structure-dependent. Firstly the intensity component is defined by the natural frequency of the structure, as well as the yielding intensity (in case of bilinear SDOF system, it is actually equal to the structural parameter C_y). Secondly, the starting and ending period values in the optimal period band to calculate the shape component is related to structural system parameters. Applying this on the comparison of two GMs to predict structural damage difference, we hypothesized that for a given bilinear system, there is an underling rule to derive optimal period band so that good correlation between SI_{DPI} and Δ_{DD} can be achieved. This hypothesis was investigated in the following sections.

5.8.1 Circle Rule of Optimal Period Band

Optimal period band for the shape component can be sought using data generated from the GM suite described above. Note that this was done for different intensity levels by scaling

the GM suite to different λ values. The coefficient of determination (R^2) was adopted to describe how well a linear relationship is fitted between the SI_{DPI} and Δ_{DD}. As the rule will also depend on structural parameters, different bilinear SDOF systems with ξ=5%, α=0.2, C_y=0.2 and T_1=0.5s, 1.0s, 1.5s were selected to investigate the correlation trends. The 102 ground motions with an intensity level λ can construct 5151 sets of two ground motions and thus produce the corresponding 5151 pairs of damage differences for a given bilinear system. The value of R^2 were obtained through the correlation analysis between these 5151 data points for different structural parameters, values of λ, and a varying period band [T_s, T_e]. Figure 5.3 shows the contour plots of R^2 for different situations against a T_s-T_e space, in which one point represents a unique starting period and ending period for the period band as long as the point is above the T_s= T_e line. From the contours, it can be observed that by change the value of [T_s, T_e] (moving the point within the T_s-T_e space), there exists an area on the T_s-T_e plot where R^2 is maximized. This period band is considered as the optimal period band for the given structural parameters and λ value (intensity level). It should be noted that there is a fairly large area on the T_s-T_e plot that R^2 is generally very close to the maximum value (i.e., the difference < 0.1,). Therefore, instead of locating the absolute maximum correlation, any point in this area can be regarded as a satisfactory period band (namely, optimal period band) for constructing the DPI shape component. Based on this observation, the trends in the location of this optimal period region were investigated as the value of intensity level λ and structural parameters change.

In Figure 5.3, one can see that the area with the largest R^2 (the points in the largest R^2 area value has less-than 0.1 difference relative to maximum R^2) is moving up towards to the point [T_p, T_p] as intensity level λ is increasing for a given system with T_1. It indicates that the response of the bilinear SDOF system becomes increasingly dominated by its post-yield stiffness (k_p) as the intensity level gradually increases. In the area with the largest R^2, a point closer to the diagonal line indicates a narrower optimal period band. For the engineering

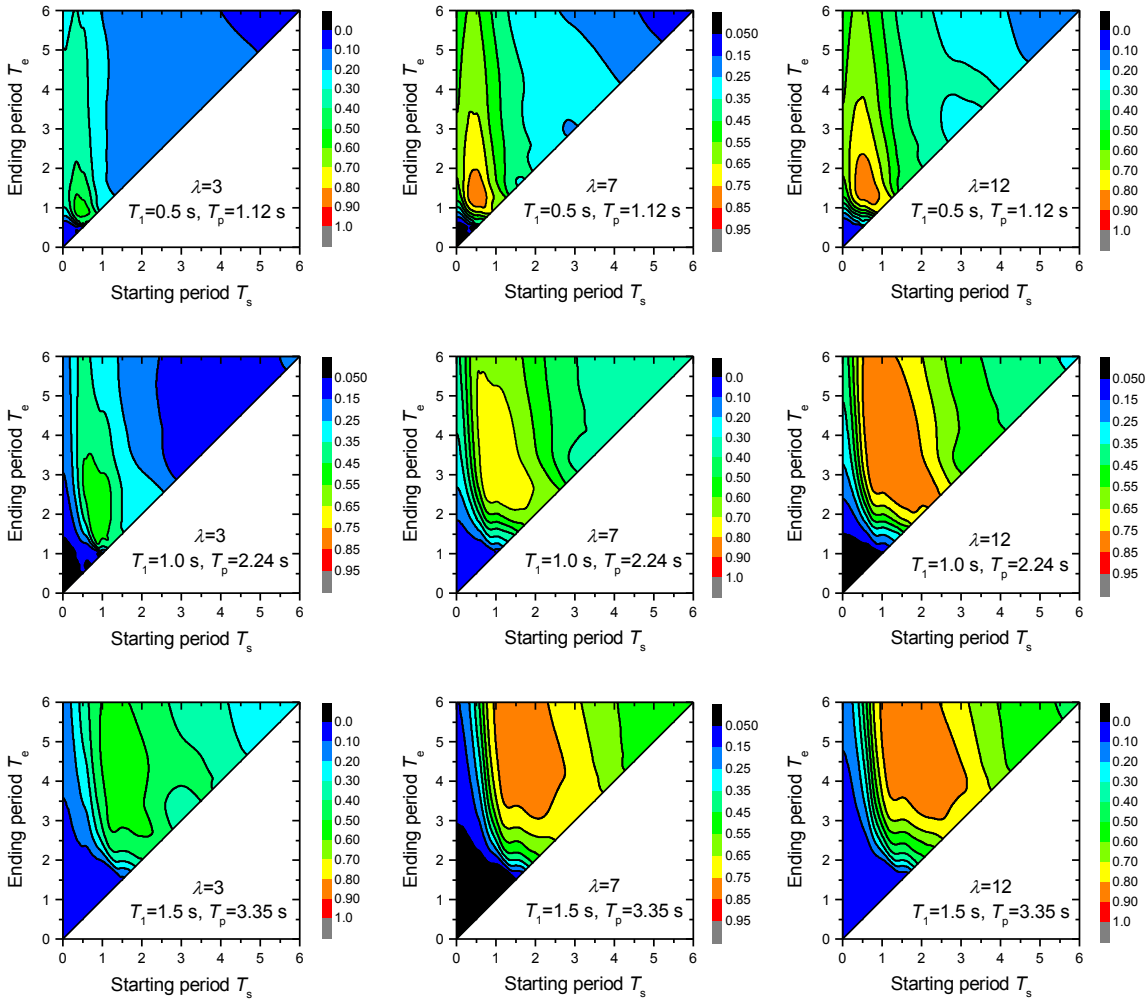

Figure 5.3 R^2 contour results for the bilinear SDOF system with T_1=0.5 s, 1.0 s and 1.5 s.

applications, a narrower period band is more preferable as the need for response spectrum comparing. These points for different intensity levels were selected and shown in Figure 5.4. It can be observed that the distribution of these points roughly follows the curve of a circle which has the origin [T_p, T_1] and the radius T_p-T_1. These points also move towards [T_p, T_p] when the intensity level λ gradually increases. Therefore, it was proposed that the optimal period band for a bilinear SDOF system follows a "circle rule" on the T_s-T_e plot. The location of the optimal period band can be found on the circle curve. With its location dictated by the intensity level λ, if λ=1, the system behaves linearly and the optimal period band point locates at the start point of the circle (T_1, T_1), which is resulted from that the linear system response can be perfectly matched using just one point on the spectrum. As λ increases, the system

response is increasingly dominated by the nonlinear response and the optimal period band point gradually approaches the end point of the circle (T_p, T_p). The circle can trace the variation of the optimal period band points with different intensity levels λ, and this phenomena is defined herein as the circle rule. This circle rule can be mathematically formulated as:

$$\left(T_s - T_p\right)^2 + \left(T_e - T_1\right)^2 = \left(T_p - T_1\right)^2 \quad T_1 \le T_s, T_e \le T_p \tag{5-12}$$

$$T_p = \alpha^{-0.5} T_1 \tag{5-13}$$

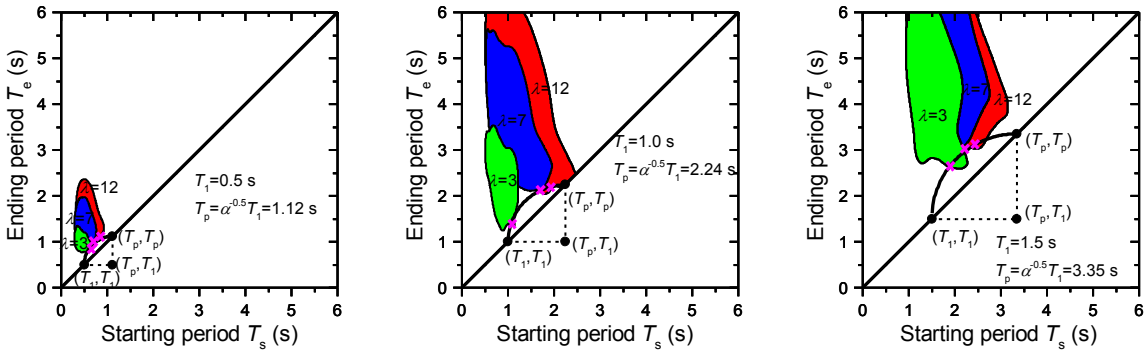

Figure 5.4 Illustration of the circle rule of optimal period band

5.8.2 Influence of λ on Optimal Period Band

Given the circle rule mentioned above, the relation between the λ and the location of optimal period band point on the circle is sought through regression analysis. As discussed above, the optimal period band point is moving along with the circle curve from the point [T_1, T_1] to [T_p, T_p] with the intensity level λ increasing. Once the starting period T_s is determined, the ending period T_e of the optimal period region can be calculated according to Eqs. (5-12) and (5-13). According to the proposed circle rule and basic structural dynamics, the extreme cases for the relationship between T_s and λ can be expressed as:

$$T_s = T_1 \quad for\ \lambda = 1 \tag{5-14}$$

$$T_s \to T_p \quad for \lambda \to \text{infinite} \tag{5-15}$$

Considering the constraints of the two extreme cases, the relationship between T_s and λ can be formulated as:

$$T_s = T_p - \left(T_p - T_1\right)\beta^{\lambda-1} \tag{5-16}$$

where β is a variable smaller than 1 and assumed to be related with structural parameters T_1, α and C_y. Damping ratio is considered as 5% in this study.

When T_1 and α remain unchanged, C_y is positively proportional to the displacement demands for a given intensity level λ as following (Deng et al. 2017):

$$\frac{D_2}{C_{y2}} = \frac{D_1}{C_{y1}} \tag{5-17}$$

where D_2 is the displacement demand for the system with C_{y2} while D_1 is the displacement demand for the system with C_{y1} for a given intensity level λ. Since C_y is positively proportional to the yield displacement with other structural parameters unchanged (Eq. (5-10)), Eq. (5-17) implies that the ductility demands are independent of C_y. Thus one can learn that the structural parameter C_y will not affect the value of R^2 when doing the damage correlation analysis between SI_{DPI} and Δ_{DD} as well as the variable β in Eq. (5-16). In order to validate the conclusion about C_y, contours of R^2 on the T_s-T_e plot for different bilinear SDOF systems (α=0.2, ξ=5%, T_1=0.5 s, and C_y=0.1, 0.2, 0.3) are showed in Figure 5.5, which illustrates that the contours of R^2 remain unchanged for different C_y values.

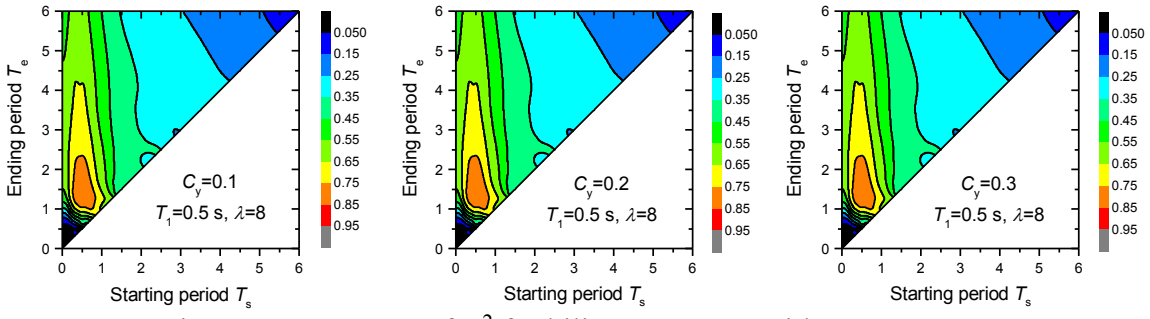

Figure 5.5 Contours of R^2 for bilinear systems with C_y=0.1, 0.2, 0.3.

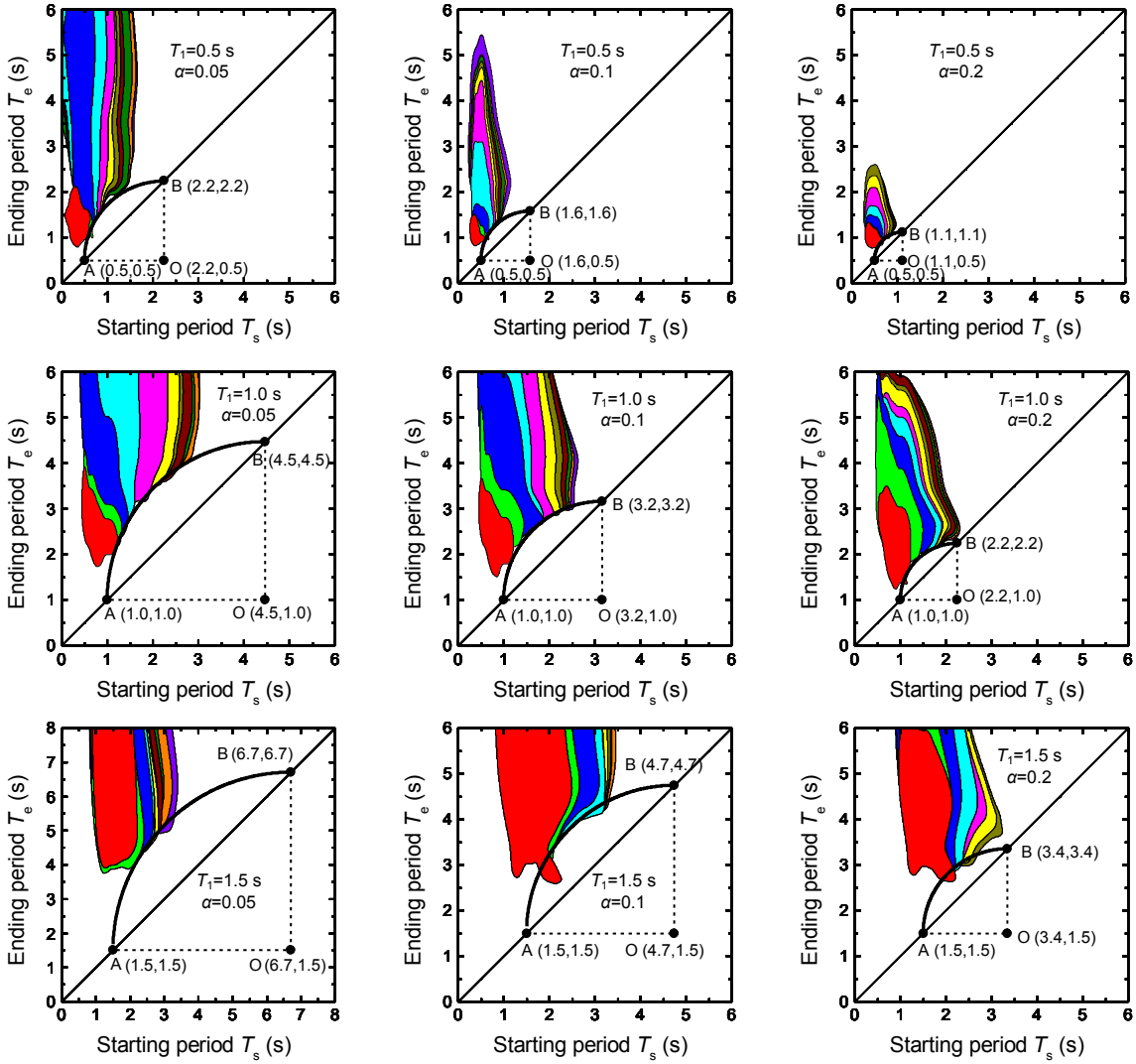

Figure 5.6 Circle rule illustration of bilinear SDOF systems with different structural parameters.

Through the analysis above, one can eliminate the dependence of β on C_y and can now focus on remaining structural parameters T_1 and α. In order to investigate how the value of β is related with T_1 and α, the 5% damped bilinear SDOF systems with T_1=0.5 s, 1.0 s and 1.5 s, and α=0.05, 0.1, 0.2 were selected. Figure 5.6 illustrates that all the optimal period bands for bilinear SDOF systems with different intensity levels λ are qualified to the circle rule. The colored areas for each case present the largest R^2 area under the intensity level λ=3, 4…13. Through selecting the intersection points of the areas and the circle, a regression analysis about Eq. (5-16) was conducted to determine the relationship between λ and the optimal starting

period (showed in Figure 5.7). Figure 5.7 illustrates that the effects brought by the difference of structural parameters will be enlarged with the intensity level λ increasing. For the systems with short natural periods such as T_1=0.5 s, the influence of hardening ratio on the relationship can be ignored for the intensity level λ<15. Additionally, the value of β is proportional of the hardening ratio α (e.g., negatively proportional for the system with T_1=0.5 s, but positively proportional for the systems with T_1=1.0 s and 1.5 s). As to the systems with other values of structural parameters, a linear interpolation can be adopted to compare the damages caused by different ground motions.

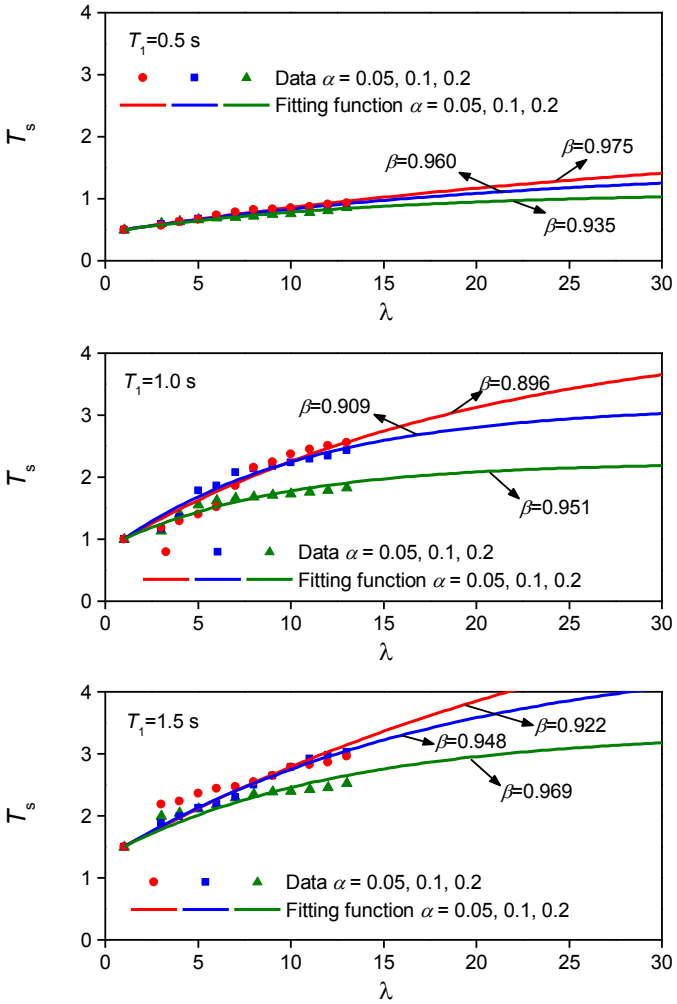

Figure 5.7 Relationship between λ and the optimal starting period.

To sum up, the proposed circle rule for constructing the DPI vector in similarity index to achieve the maximum damage correlation for a given bilinear SDOF system can be summarized mathematically as:

$$\begin{aligned} T_{\mathrm{p}} &= \alpha^{-0.5} T_{\mathrm{I}} \\ T_{\mathrm{s}} &= T_{\mathrm{p}} - \left(T_{\mathrm{p}} - T_{\mathrm{I}}\right)\beta^{\lambda-1} \\ \left(T_{\mathrm{s}} - T_{\mathrm{p}}\right)^2 + \left(T_{\mathrm{e}} - T_{\mathrm{I}}\right)^2 &= \left(T_{\mathrm{p}} - T_{\mathrm{I}}\right)^2 \quad T_{\mathrm{I}} \le T_{\mathrm{s}}, T_{\mathrm{e}} \le T_{\mathrm{p}} \end{aligned} \tag{5-18}$$

According to the above summarized equations, all the parameters needed in the vector-valued DPI can be calculated for a given bilinear system under a ground motion, in which the value of β can be obtained by the linear interpolation using Figure 5.7. If one wants to investigate whether there is another ground motion generating the almost same damage for the given system under a ground motion, the component p_1 and p_2 in the vector-valued DPI can be the criteria. That is, if the two ground motions have similar values in p_1 and p_2, the structural damages are expected to be similar.

5.9 Numerical Validation

Generally, if the intensity component is used to predict the responses of structures, which can accurately capture the linear responses but has large scatter for the nonlinear responses because the effective period of the subjecting structure is lengthened when it vibrates nonlinearly. Thus, the spectral shape component (with longer-than elastic periods) was introduced to help reduce the prediction scatter when the values of intensity component p_1 of ground motions are almost identical. In order to validate the effectiveness of the p_2 as a complement of p_1, the investigation on the relation between p_2 quantity and ductility quantity for the ground motions with same p_1 values was carried on.

1600 earthquake ground motions, with magnitude 4~7 and different mechanisms such as strike slip, reverse and normal, were downloaded from PEER strong ground motion database

(Chiou et al. 2008). Every two ground motions in the 1600 ground motions gathered into a ground motion pair (totally 1600*1599/2=1279200 pairs) and then every ground motion pair with less-than 5% difference on p_1 values for the two ground motions was selected (termed it as same-p_1 ground motion pairs). When the bilinear systems are subjected to the same- p_1 ground motion pairs, their ductility demands for each ground motion pair tend to be different (that is the prediction scatter brought by p_1). The spectral shape component p_2 values of the same-p_1 ground motion pairs were calculated based on the aforementioned circle rule. The subjecting bilinear systems with T_1=0.5 s, 0.7 s, 1.2 s and 1.5 s were selected. Figure 5.8 shows that the similarity index of p_2 (SI_{DPI}) for each of same-p_1 ground motion pairs is linearly correlated with normalized ductility difference. The similarity index of p_2 for each pair was calculated by Eq. (5-8) while normalized ductility difference under each GM pair means that

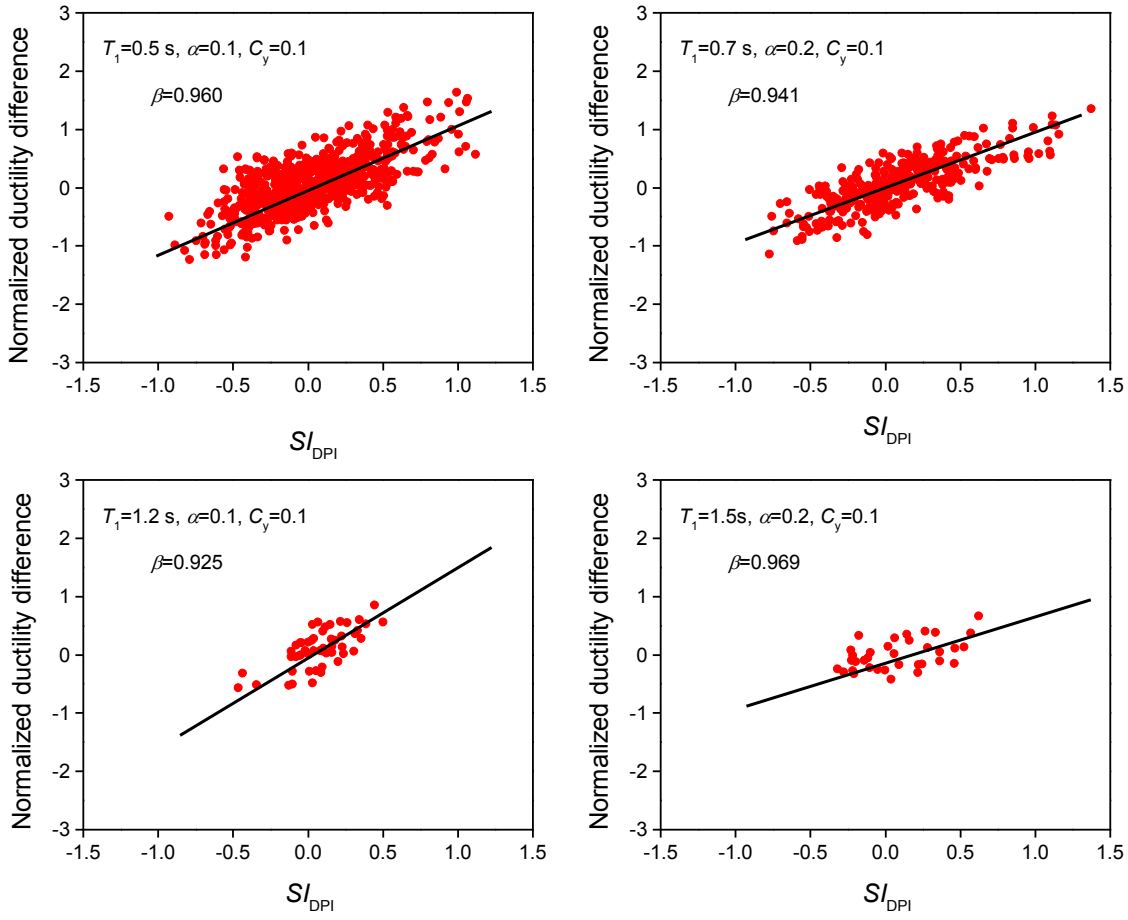

Figure 5.8 Relationship between SI_{DPI} and normalized ductility difference.

one ductility in the pair is subtracted from the other ductility then divided by the mean of the two ductilities. The normalizing (that is to be divided by the mean of the two ductilities) is to get rid of the effects of different intensity values for the same- p_1 ground motion pairs. The linear correlation in Figure 5.8 validates that the spectral shape component in the vector-valued DPI calculated from the circle rule can provide additional information on the damage prediction when compared to using p1 only.

5.10 Summary and Conclusions

In this study, a vector-valued DPI was formulated based on the ground motion response spectrum for structural damage prediction. This DPI vector has an intensity component and a shape component. By applying a circle rule to this DPI vector, strong correlation between a generalized bilinear system damage and the DPI vector can be established. The circle rule proposed is to identify the optimal period band for the spectral shape component. Once the bilinear SDOF system is given, the circle curve location in the T_s-T_e plot is determined regardless of the subjected ground motions. The ground motions are affecting the location of the optimal period band point in the circle curve. The vector-valued DPI added a spectral shape component to as a complement of generally-used intensity component to reduce the prediction scatter. Through the validation, it can be seen that the shape component values have a linear correlation with the damage quantity when the intensity component values for each GM pair are significantly close, which demonstrates that the combination of the intensity component and the shape component can be a good DPI to predict structural damages.

CHAPTER 6

CONCLUSIONS AND FUTURE WORK

6.1 Major Observations and Conclusion

1. An uncertainty quantification framework of linear systems and simple nonlinear systems through IDA curves was proposed. For SDOF and first-mode dominated MDOF linear systems, the uncertainty of peak structural responses (represented by coefficient of variation, COV) is a constant (regardless of seismic intensity) which is determined by the GM suite's COV spectrum at the first-mode period and a given damping ratio. For elastoplastic and bilinear SDOF systems, IDA curves were introduced to describe the relationship between their peak responses and seismic intensity. The main benefit of IDA curves is to decouple the seismic intensity from ground motion characteristics and investigate the change of response uncertainty with seismic intensity. Regarding the shape features of IDA curves of elastoplastic acceleration and bilinear displacement quantities, IDA curve quantification formulas as a function of seismic intensity, structural parameters and ground motion parameters have been proposed (e.g., Eq. (2-19) is for elastoplastic acceleration and Eq. (3-15) is for bilinear displacement). According to the quantified IDA curves, the COV or standard deviation of the responses at a given seismic intensity can be calculated as response uncertainty.

2. During the uncertainty quantification framework, the normalized ground motion parameters (independent of seismic intensity) used to define ground motion uncertainty have been identified. For example, $I_0/S_a(T,\xi)$and PGV/EPV are the dominated ground motion parameters that can present the effects of ground motion suite on elastoplastic peak acceleration while k_1, α_{sq}/v_{sq}, and PGA/PGV are the identified ground motion parameters for bilinear peak displacement. The selected three ground motion parameters can be used to almost present the ground motion suite characteristics for doing the comparisons between different ground motion

suites. Once the statistical distributions of the three selected ground motion parameters are similar for two ground motion suites, the corresponding response uncertainty with seismic intensity should be similar as well, which can be seen in Figure 2.13 for the elastoplastic acceleration quantity and Figure 3.9 for the bilinear displacement quantity. The two ground motion suites can be reckoned as be equivalent.

3. Response uncertainty quantification framework is built upon the concept of IDA curve parameterization, through which one can explicitly evaluate the effects of ground motion uncertainty and structural parameter uncertainty on response uncertainty without conducting NLTHA. This framework also implies that the contribution of GM uncertainty and structural parameter uncertainty will vary with seismic intensity. This varying can be reflected by the response uncertainty values with seismic intensity in Figures 2.11 and 3.8 for theoretical methods and in Figure 4.13 for experimental data. Furthermore, the relative contribution of two uncertainty sources on response uncertainty are decoupled in the shake table tests. The individual contribution of two uncertainty sources is changing with seismic intensity (in Figures 4.10 and 4.11). Through the shake table tests, the effectiveness of SRSS method which is commonly used in the engineering community is validated. The uncertainty ranges recommended by FEMA P695 for the SRSS method can provide a reasonable and conservative estimation of the actual response uncertainty for the specimens tested, as long as one does not use the lower bound values of the recommended ranges of input uncertainties.

4. In the engineering community, response spectrum is generally used to predict structural damages. The use of response spectrum in damage prediction is typically quite simple and not optimized. In this study, a vector-valued DPI considering the spectral amplitude (seismic intensity) and shape information of GMs was proposed. Through correlation analyses, a circle rule was proposed to determine the optimal period band in spectral shape component for a given spectral amplitude value. The vector-valued DPI with two components also can

improve the damage prediction ability and reduce the prediction scatter than only intensity component used, which is validated in Figure 5.8.

6.2 Future Work

The overarching theme of this study is to develop quantitative methods for PBEE applications with a focus on ground motion impact. With the increasing availability of more computational power, it is beneficial to utilize NLTHA in PBEE. Because, it is one of the most robust methods currently available when combined with Monte Carlo simulations. However, the earthquake engineering community must also be aware of the negative impact of allowing NLTHA to dominate PBEE. Firstly, it can harm technical transfer of the seismic engineering research to practice. Secondly it can undermine a deeper understanding of the seismic response phenomenon, as most of the conclusions reached through NLTHA are case-specific and empirical. This study explored some potential pathways to assess a number of core concepts of PBEE (such as fragility) without relying on NLTHA. Some benefits are immediately shown and could potentially influence research in the future. Bypassing NLTHA in PBEE is a very wide topic that can have many specific applications. This study only scratched the surface and provided verifications on the possibility using simple cases. There are numerous future works in this area that can be carried out in order to establish a family of methodologies that will not necessarily replace NLTHA-based approaches but serve as a nice compliment. There are three directions that the future work should follow:

1. Keep building on the uncertainty propagation framework developed here towards a full reliability based design/assessment framework for building structures under seismic hazard loading. With a mechanism in this framework to quantitatively consider GM uncertainty and accurately predict its impact at different intensity levels, a uniform base line for using NLTHA to assess or design structures with GM suites can be established and a rational treatment can be given to specific cases.

2. Further study can be focused on more realistic structural systems followed by the concept of IDA parameterization. For complex systems, the IDA curve quantification formula will be more complex but can still be obtained. It is also expected that for complicated systems, the role of modeling uncertainty might have to be considered. It is likely not possible to conduct experimental validation of realistic building structures following the probabilistic shake table test method employed here, but the IDA curve models may be validated through a variety of data sources including actual earthquake damaged buildings and limited data from large-scale shake table tests.

3. The link between the semi-closed form solutions to PBEE problems and performance based seismic design needs to be established. This could potentially change how PBSD is conducted currently (primarily through an experienced trail-and-error) because iterative NLTHA can be eliminated. It is potentially beneficial to instruct a final design check with NLTHA. But the actual design process may be able to return to a much simpler format that can be used by average structural engineers.

REFERENCE

Akkar, S., and Özen, Ö. (2005). "Effect of peak ground velocity on deformation demands for SDOF systems." *Earthquake engineering & structural dynamics*, 34(13), 1551-1571.

Arias, A. (1970). "MEASURE OF EARTHQUAKE INTENSITY." Massachusetts Inst. of Tech., Cambridge. Univ. of Chile, Santiago de Chile.

ASCE7-10 (2010). *Minimum design loads for buildings and other structures*, American Society of Civil Engineers.

Aydinoğlu, M. N. (2003). "An incremental response spectrum analysis procedure based on inelastic spectral displacements for multi-mode seismic performance evaluation." *Bulletin of Earthquake Engineering*, 1(1), 3-36.

Baker, J. W. (2011). "Conditional mean spectrum: Tool for ground-motion selection." *Journal of Structural Engineering*, 137(3), 322-331.

Baker, J. W. (2015). "Efficient analytical fragility function fitting using dynamic structural analysis." *Earthquake Spectra*, 31(1), 579-599.

Baker, J. W., and Allin Cornell, C. (2005). "A vector-valued ground motion intensity measure consisting of spectral acceleration and epsilon." *Earthquake Engineering & Structural Dynamics*, 34(10), 1193-1217.

Baker, J. W., and Allin Cornell, C. (2006). "Spectral shape, epsilon and record selection." *Earthquake Engineering & Structural Dynamics*, 35(9), 1077-1095.

Baker, J. W., and Cornell, C. A. (2008). "Uncertainty propagation in probabilistic seismic loss estimation." *Structural Safety*, 30(3), 236-252.

Baker, J. W., and Cornell, C. A. (2003). *Uncertainty specification and propagation for loss estimation using FOSM methods*.

Bianchini, M., Diotallevi, P., and Baker, J. "Prediction of inelastic structural response using an average of spectral accelerations." *Proc., Proc. of the 10th International Conference on Structural Safety and Reliability (ICOSSAR09), Osaka, Japan*, 13-17.

Bojorquez, E., and Iervolino, I. (2011). "Spectral shape proxies and nonlinear structural response." *Soil Dynamics and Earthquake Engineering*, 31(7), 996-1008.

Bradley, B. A. (2010). "Epistemic uncertainties in component fragility functions." *Earthquake Spectra*, 26(1), 41-62.

Bradley, B. A. (2010). "A generalized conditional intensity measure approach and holistic ground-motion selection." *Earthquake Engineering & Structural Dynamics*, 39(12), 1321-1342.

Bradley, B. A. (2012). "A ground motion selection algorithm based on the generalized conditional intensity measure approach." *Soil Dynamics & Earthquake Engineering*, 40, 48-61.

Bradley, B. A. (2013). "A critical examination of seismic response uncertainty analysis in earthquake engineering." *Earthquake Engineering & Structural Dynamics*, 42(11), 1717-1729.

Bradley, B. A., and Lee, D. S. (2010). "Accuracy of approximate methods of uncertainty propagation in seismic loss estimation." *Structural Safety*, 32(1), 13-24.

Celik, O. C., and Ellingwood, B. R. (2010). "Seismic fragilities for non-ductile reinforced concrete frames - Role of aleatoric and epistemic uncertainties." *Structural Safety*, 32(1), 1-12.

Chiou, B., Darragh, R., Gregor, N., and Silva, W. (2008). "NGA project strong-motion database." *Earthq Spectra*, 24(1), 23-44.

Chopra, A. K. (2012). *Dynamics of structures*, Prentice Hall New Jersey.

Christovasilis, I. P., Filiatrault, A., Constantinou, M. C., and Wanitkorkul, A. (2009). "Incremental dynamic analysis of woodframe buildings." *Earthquake Engineering & Structural Dynamics*, 38(4), 477-496.

Cordova, P. P., Deierlein, G. G., Mehanny, S. S., and Cornell, C. A. "Development of a two-parameter seismic intensity measure and probabilistic assessment procedure." *Proc., The Second US-Japan Workshop on Performance-Based Earthquake Engineering Methodology for Reinforced Concrete Building Structures*, 187-206.

Cornell, C. A., Jalayer, F., Hamburger, R. O., and Foutch, D. A. (2002). "Probabilistic basis for 2000 SAC federal emergency management agency steel moment frame guidelines." *Journal of Structural Engineering*, 128(4), 526-533.

Deng, P., Pei, S., van de Lindt, J. W., Liu, H., and Zhang, C. (2017). "An approach to quantify the influence of ground motion uncertainty on elastoplastic system acceleration in incremental dynamic analysis." *Advance in Structural Engineering*, Accepted.

Deng, P., Pei, S., van de Lindt, J. W., and Zhang, C. (2017). "Uncertainty quantification for seismic responses of bilinear SDOF systems: A semi-closed-form estimation." *Soil Dynamics and Earthquake Engineering*, 93, 18-28.

Dolsek, M. (2009). "Incremental dynamic analysis with consideration of modeling uncertainties." *Earthquake Engineering & Structural Dynamics*, 38(6), 805-825.

Ellingwood, B. R., Celik, O. C., and Kinali, K. (2007). "Fragility assessment of building structural systems in Mid-America." *Earthquake Engineering & Structural Dynamics*, 36(13), 1935-1952.

Ellingwood, B. R., and Kinali, K. (2009). "Quantifying and communicating uncertainty in seismic risk assessment." *Structural Safety*, 31(2), 179-187.

Fajfar, P., Vidic, T., and Fischinger, M. (1990). "A measure of earthquake motion capacity to damage medium-period structures." *Soil Dynamics and Earthquake Engineering*, 9(5), 236-242.

FEMA356 (2000). *Pre-Standard and Commentary for the Seismic Rehabilitation of Buildings*, Federal Emergency Management Agency, Washington, D.C.

FEMA-P695 (2009). *Quantification of building seismic performance factors*, Federal Emergency Management Agency, Washington(DC).

Fragiadakis, M., and Vamvatsikos, D. (2010). "Fast performance uncertainty estimation via pushover and approximate IDA." *Earthquake Engineering & Structural Dynamics*, 39(6), 683-703.

Ghobarah, A. (2001). "Performance-based design in earthquake engineering: state of development." *Engineering structures*, 23(8), 878-884.

Gokkaya, B. U., Baker, J. W., and Deierlein, G. G. (2016). "Quantifying the impacts of modeling uncertainties on the seismic drift demands and collapse risk of buildings with implications on seismic design checks." *Earthquake Engineering & Structural Dynamics*, 45(10), 1661-1683.

Günay, S., and Mosalam, K. M. (2013). "PEER performance-based earthquake engineering methodology, revisited." *Journal of Earthquake Engineering*, 17(6), 829-858.

Hadjian, A. (1982). "A re-evaluation of equivalent linear models for simple yielding systems." *Earthquake Engineering & Structural Dynamics*, 10(6), 759-767.

Hamburger, R. O., Foutch, D. A., and Cornell, C. A. (2003). "Translating research to practice: FEMA/SAC performance-based design procedures." *Earthq Spectra*, 19(2), 255-267.

Housner, G. "Measures of severity of earthquake ground shaking." *Proc., Proceedings of the US National Conference on Earthquake Engineering*, 25-33.

Huo, Y., and Zhang, J. (2013). "Effects of pounding and skewness on seismic responses of typical multispan highway bridges using the fragility function method." *Journal of Bridge Engineering*, 18(6), 499-515.

Iervolino, I., Manfredi, G., and Cosenza, E. (2006). "Ground motion duration effects on nonlinear seismic response." *Earthquake engineering & structural dynamics*, 35(1), 21-38.

Iwan, W. (1980). "Estimating inelastic response spectra from elastic spectra." *Earthquake Engineering & Structural Dynamics*, 8(4), 375-388.

Ji, X., Kajiwara, K., Nagae, T., Enokida, R., and Nakashima, M. (2009). "A substructure shaking table test for reproduction of earthquake responses of high-rise buildings." *Earthquake Engineering & Structural Dynamics*, 38(12), 1381-1399.

Katsanos, E., Sextos, A., and Elnashai, A. (2014). "Prediction of inelastic response periods of buildings based on intensity measures and analytical model parameters." *Engineering Structures*, 71, 161-177.

Kim, J. H., and Rosowsky, D. V. (2005). "Fragility analysis for performance-based seismic design of engineered wood shearwalls." *J Struct Eng ASCE*, 131(11), 1764-1773.

Krawinkler, H., Parisi, F., Ibarra, L., Ayoub, A., and Medina, R. (2001). *Development of a testing protocol for woodframe structures*, CUREE Richmond, CA.

Kwon, O.-S., and Elnashai, A. (2006). "The effect of material and ground motion uncertainty on the seismic vulnerability curves of RC structure." *Engineering Structures*, 28(2), 289-303.

Lee, T. H., and Mosalam, K. M. (2005). "Seismic demand sensitivity of reinforced concrete shear-wall building using FOSM method." *Earthquake Engineering & Structural Dynamics*, 34(14), 1719-1736.

Li, Y., and Ellingwood, B. R. (2007). "Reliability of woodframe residential construction subjected to earthquakes." *Structural Safety*, 29(4), 294-307.

Li, Y., and Ellingwood, B. R. (2009). "Framework for multihazard risk assessment and mitigation for wood-frame residential construction." *Journal of structural engineering*, 135(2), 159-168.

Liel, A. B., Haselton, C. B., Deierlein, G. G., and Baker, J. W. (2009). "Incorporating modeling uncertainties in the assessment of seismic collapse risk of buildings." *Struct Safety*, 31(2), 197-211.

Loth, C., and Baker, J. W. (2015). "Rational design spectra for structural reliability assessment using the response spectrum method." *Earthquake Spectra*, 31(4), 2007-2026.

Makris, N., and Black, C. J. (2004). "Evaluation of peak ground velocity as a “good” intensity measure for near-source ground motions." *Journal of Engineering Mechanics*, 130(9), 1032-1044.

Martinelli, P., and Filippou, F. C. (2009). "Simulation of the shaking table test of a seven-story shear wall building." *Earthquake Engineering & Structural Dynamics*, 38(5), 587-607.

Medina, R. A., and Krawinkler, H. (2004). "Seismic demands for nondeteriorating frame structures and their dependence on ground motions." Pacific Earthquake Engineering Research Center.

Mehanny, S. S. (2009). "A broad-range power-law form scalar-based seismic intensity measure." *Engineering Structures*, 31(7), 1354-1368.

Nielson, B., and Pang, W. "Effect of ground motion suite size on uncertainty estimation in seismic bridge fragility modeling." *Proc., Structures congress*.

Padgett, J. E., and DesRoches, R. (2007). "Sensitivity of seismic response and fragility to parameter uncertainty." *Journal of Structural Engineering-Asce*, 133(12), 1710-1718.

Pang, W. C., Rosowsky, D. V., Pei, S. L., and van de Lindt, J. W. (2010). "Simplified direct displacement design of six-story woodframe building and pretest seismic performance assessment." *J Struct Eng ASCE*, 136(7), 813-825.

Park, Y. J., Ang, A. H. S., and Wen, Y. K. (1985). "Seismic damage analysis of reinforced concrete buildings." *Journal of Structural Engineering*.

Pei, S., and van de Lindt, J. W. (2011). "Seismic Numerical Modeling of a Six-Story Light-Frame Wood Building: Comparison with Experiments." *Journal of Earthquake Engineering*, 15(6), 924-941.

Porter, K. A. "An overview of PEER's performance-based earthquake engineering methodology." *Proc., Proceedings of Ninth International Conference on Applications of Statistics and Probability in Civil Engineering*.

Ramanathan K., W. T., Desroches R., and Padgett J.E. (2010). "Effect of ground motion suites on the seismic fragility of a three-span continuous steel girder bridge." *9th US National and 10th Canadian Conference on Earthquake Engineering,including Papers from the 4th International Tsunami Symposium*, 7426-7435.

Riddell, R. (2007). "On ground motion intensity indices." *Earthq Spectra*, 23(1), 147-173.

Riddell, R. (2008). "Inelastic response spectrum: Early history." *Earthquake Engineering & Structural Dynamics*, 37(8), 1175-1183.

Riddell, R., and Garcia, J. E. (2001). "Hysteretic energy spectrum and damage control." *Earthquake Engineering & Structural Dynamics*, 30(12), 1791-1816.

Sfahani, M., Guan, H., and Loo, Y.-C. (2015). "Seismic Reliability and Risk Assessment of Structures Based on Fragility Analysis–A Review." *Advances in Structural Engineering*, 18(10), 1653-1669.

Vamvatsikos, D. (2014). "Seismic performance uncertainty estimation via IDA with progressive accelerogram-wise Latin Hypercube Sampling." *Journal of Structural Engineering*, 140(8), A4014015.

Vamvatsikos, D., and Cornell, C. A. (2002). "Incremental dynamic analysis." *Earthq Eng Struct Dyn*, 31(3), 491-514.

Vamvatsikos, D., and Cornell, C. A. (2004). "Applied incremental dynamic analysis." *Earthquake Spectra*, 20(2), 523-553.

Vamvatsikos, D., and Cornell, C. A. (2005). "Developing efficient scalar and vector intensity measures for IDA capacity estimation by incorporating elastic spectral shape information." *Earthquake engineering & structural dynamics*, 34(13), 1573-1600.

Vamvatsikos, D., and Fragiadakis, M. (2010). "Incremental dynamic analysis for estimating seismic performance sensitivity and uncertainty." *Earthquake Engineering & Structural Dynamics*, 39(2), 141-163.

Van de Lindt, J. W., Pei, S., Pryor, S. E., Shimizu, H., and Isoda, H. (2010). "Experimental seismic response of a full-scale six-story light-frame wood building." *Journal of Structural Engineering*, 136(10), 1262-1272.

Wang, G. (2011). "A ground motion selection and modification method capturing response spectrum characteristics and variability of scenario earthquakes." *Soil Dynamics and Earthquake Engineering*, 31(4), 611-625.

Wang, G., Youngs, R., Power, M., and Li, Z. (2015). "Design ground motion library: an interactive tool for selecting earthquake ground motions." *Earthquake Spectra*, 31(2), 617-635.

Wong, K. K. F., and Harris, J. L. (2012). "Seismic damage and fragility analysis of structures with tuned mass dampers based on plastic energy." *Structural Design of Tall and Special Buildings*, 21(4), 296-310.

Yang, D. X., Pan, J. W., and Li, G. (2009). "Non-structure-specific intensity measure parameters and characteristic period of near-fault ground motions." *Earthq Eng Struct Dyn*, 38(11), 1257-1280.

Yin, Y.-J., and Li, Y. (2010). "Seismic collapse risk of light-frame wood construction considering aleatoric and epistemic uncertainties." *Structural Safety*, 32(4), 250-261.

Yun, S.-Y., Hamburger, R. O., Cornell, C. A., and Foutch, D. A. (2002). "Seismic performance evaluation for steel moment frames." *Journal of Structural Engineering*, 128(4), 534-545.